NO. ST5
SEPTEMBER 1956

JOURNAL of the

Structural Division

PROCEEDINGS OF THE

AMERICAN SOCIETY OF CIVIL ENGINEERS

VOLUME 82

BASIC REQUIREMENTS FOR MANUSCRIPTS

This Journal represents an effort by the Society to deliver information to the reader with the greatest possible speed. To this end the material herein has none of the usual editing required in more formal publications.

Original papers and discussions of current papers should be submitted to the Manager of Technical Publications, ASCE. The final date on which a discussion should reach the Society is given as a footnote with each paper. Those who are planning to submit material will expedite the review and publication procedures by complying with the following basic requirements:

1. Titles should have a length not exceeding 50 characters and spaces.

2. A 50-word summary should accompany the paper.

3. The manuscript (a ribbon copy and two copies) should be double-spaced on one side of 8½-in. by 11-in. paper. Papers that were originally prepared for oral presentation must be rewritten into the third person before being submitted.

4. The author's full name, Society membership grade, and footnote reference stating present employment should appear on the first page of the paper.

5. Mathematics are reproduced directly from the copy that is submitted. Because of this, it is necessary that capital letters be drawn, in black ink, 3/16-in. high (with all other symbols and characters in the proportions dictated by standard drafting practice) and that no line of mathematics be longer than 6½-in. Ribbon copies of typed equations may be used but they will be proportionately smaller in the printed version.

6. Tables should be typed (ribbon copies) on one side of 8½-in. by 11-in. paper within a 6½-in. by 10½-in. invisible frame. Small tables should be grouped within this frame. Specific reference and explanation should be made in the text for each table.

7. Illustrations should be drawn in black ink on one side of 8½-in. by 11-in. paper within an invisible frame that measures 6½-in. by 10½-in.; the caption should also be included within the frame. Because illustrations will be reduced to 69% of the original size, the capital letters should be 3/16-in. high. Photographs should be submitted as glossy prints in a size that is less than 6½-in. by 10½-in. Explanations and descriptions should be made within the text for each illustration.

8. Papers should average about 12,000 words in length and should be no longer than 18,000 words. As an approximation, each full page of typed text, table, or illustration is the equivalent of 300 words.

Further information concerning the preparation of technical papers is contained in "Publication Procedure for Technical Papers" (Proc. Paper 290) which can be obtained from the Society.

This Journal is published bi-monthly by the American Society of Civil Engineers. Publication office is at 2500 South State Street, Ann Arbor, Michigan. Editorial and General Offices are at 33 West 39 Street, New York 18, New York. $4.00 of a member's dues are applied as a subscription to this Journal. Second-class mail privileges are authorized at Ann Arbor, Michigan.

HY,PO,SA,ST.

JOURNAL
STRUCTURAL DIVISION
Proceedings of the American Society of Civil Engineers

CONTENTS

September, 1956

Papers

DIVISION ACTIVITES

Paper 1054 ST 5

Journal of the
STRUCTURAL DIVISION
Proceedings of the American Society of Civil Engineers

STRESSES IN PRESSURE PIPELINES AND PROTECTIVE CASING PIPES[a]

M. G. Spangler,* M. ASCE
(Proc. Paper 1054)

The tremendous growth of the pipeline industry in the United States since World War II has resulted not only in increased mileage of gas transmission lines and petroleum products pipelines, but in larger diameter pipes and increased operating pressures as well. As pipe diameters and operating pressures have increased, the problem of secondary stresses in the pipe wall, due to earth cover and surface traffic, has become more prominent. Increased mileage of pipelines has necessitated the construction of many more railway, highway and airfield runway crossings and questions relative to stresses in the pipe wall when the pipes are uncased, and deflections in protective casing pipes, due to both earth loads and super-imposed traffic loads, have increased many fold.

The purpose of this paper is to review the stress situation in buried pressure pipelines and the deflections of casing pipes, when installed under several postulated conditions which are believed to be typical of many actual conditions encountered in pipeline design and construction. The basis for this study is the Marston Theory of Loads on Underground Conduits which was developed through many years of basic and applied research at Iowa State College under the active inspiration and leadership of the late Anson Marston, Past President and Hon. M. ASCE. Marston's theory was originally developed with reference to the loads and supporting strengths of both rigid and flexible types of conduits used in sewerage and drainage practice, but many of the principles therein are believed to be adaptable to problems in connection with the structural design of pipelines.

The adaptation of the Marston Theory to the structural design of pipelines involves the employment of three major theories of mechanics, viz; loads on buried conduits, the Boussinesq solution for stresses in an elastic solid, and the elastic theory applied to thin rings. These theories will be discussed in the order named, after which their application to several arbitrarily chosen problems in pipeline design will be demonstrated.

Note: Discussion open until February 1, 1957. Paper 1054 is part of the copyrighted Journal of the Structural Division of the American Society of Civil Engineers, Vol. 82, No. ST 5, September, 1956.

a. Prepared for presentation before the Committee on Pipelines, Constr. Div., ASCE Convention, St. Louis, Mo., June 17, 1955.

* Research Prof. of Civ. Eng., Iowa State College, Ames, Iowa.

Marston's Load Theory

Pipelines are usually constructed in relatively narrow ditches or trenches and then backfilled with soil up to the ground surface. This backfill soil has a tendency to settle downward in relation to the undisturbed sides of the ditch, thereby generating upward shearing forces which act on the prism of backfill soil. These upward shearing forces partially support the weight of the backfill, and thus influence the load on the conduit. Marston's development of a load formula for pipes buried in ditches follows.

Notation (see Fig. 1)

W_c = load on conduit, in pounds per unit length

w = unit weight (wet density) of filling material, in pounds per cubic foot;

V = vertical pressure on any horizontal plane in backfill, in pounds per linear foot of ditch;

B_c = horizontal breadth (outside) of conduit, in feet;

B_d = horizontal width of ditch at top of conduit, in feet;

H = height of fill above top of conduit, in feet;

h = distance from ground surface down to any horizontal plane in backfill, in feet;

C_d = load coefficient for ditch conduits;

μ = $\tan \phi$ = coefficient of internal friction of fill material;

μ' = $\tan \phi'$ = coefficient of friction between fill material and sides of ditch

K = ratio of active lateral unit pressure to vertical unit pressure;

e = base of natural logarithms.

The coefficient μ' may be equal to or less than μ, but cannot be greater than μ. The value of K will be taken as Rankine's ratio and may be found by equation

$$K = \frac{\sqrt{\mu^2+1}-\mu}{\sqrt{\mu^2+1}+\mu} = \frac{1-\sin\phi}{1+\sin\phi} = \tan^2\left(45^\circ - \frac{\phi}{2}\right)$$

Let Fig. 1 represent a section of a ditch and ditch conduit 1 unit in length; and consider a thin horizontal element of the fill material of height dh located at any depth h below the ground surface. The forces acting on this element at equilibrium are: V, the vertical pressure on the top of the element; V + dV, the vertical pressure on the bottom of the element; $wB_d dh$, the weight of the element; and $K \frac{V}{B_d}$, the lateral unit pressure on each side of the element, it being assumed that the vertical pressure on the element is uniformly distributed over the width B. Since the element has a tendency to move downward in relation to the sides of the ditch, these lateral unit pressures induce upward

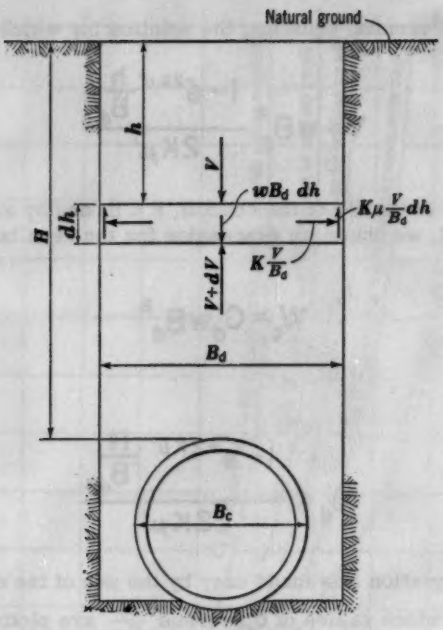

Fig. 1 –Free-Body Diagram for Ditch Conduit

shearing forces equal to $K\mu' \frac{V}{B_d}$ dh. Equating the upward and downward vertical forces on the element, we obtain:

$$V + dV + 2K\mu' \frac{V}{B_d} dh = V + wB_d dh \qquad (1)$$

This is a linear differential equation, the solution for which is

$$V = wB_d^2 \frac{1 - e^{-2K\mu' \frac{h}{B_d}}}{2K\mu'} \qquad (2)$$

At the elevation of the top of the conduit, h = H; and by substituting this value in Equation 2, we obtain an expression for the resultant vertical load at the top of the pipe.

$$W_c = C_d w B_d^2 \qquad (3)$$

in which

$$C_d = \frac{1 - e^{-2K\mu' \frac{H}{B_d}}}{2K\mu'} \qquad (4)$$

Evaluation of Equation 3 is made easy by the use of the computation diagram in Fig. 2, in which values of C_d versus $\frac{H}{B_d}$ are plotted for several kinds of filling materials having different coefficients of internal friction.

Attention is directed to the fact that Equation 3 applies only to the case of a pipe buried in a relatively narrow ditch. If the pipe is installed in a sloping sided ditch, the load may be calculated by considering B_d equal to the width of the ditch at the level of the top of the pipe. If the pipe is installed in a ditch which is more than two or three times wider than the pipe, or if it is installed at or near the ground surface and then covered with an embankment, the ditch conduit analysis does not apply. In these situations, loads may be determined by the projecting conduit phase of Marston's Theory. Since pipelines are rarely installed as projecting conduits, this phase of the theory will not be presented here.

Boussinesq Theory

The Boussinesq Theory of stress distribution in a semi-infinite elastic solid, due to a point load applied at the surface, was published in 1885. The expression for vertical unit stress in the elastic mass due to a point load applied at the surface is

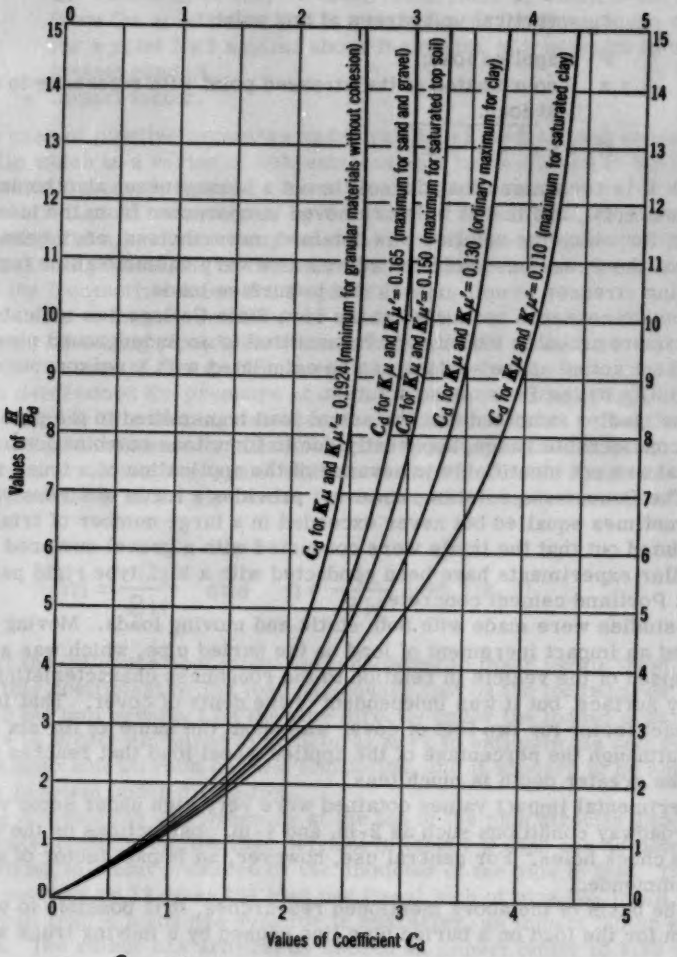

Fig. 2 Diagram for Coefficient C_d for Ditch Conduits

$$\sigma_z = \frac{3P}{2\pi R^5} \qquad (5)$$

in which

σ_z = vertical unit stress at any point;

P = applied load;

x,y,z = coordinates of the stressed point with reference to origin at load.

$R = \sqrt{x^2 + y^2 + z^2}$

Although it is recognized that the soil is not a homogeneous, isotropic and elastic material, and that it is far removed in character from the idealized material for which the solution was obtained, nevertheless, engineers have found that the Boussinesq solution serves as a very valuable guide for estimating stresses in soil masses due to surface loads.

Extensive research conducted at the Iowa State College has indicated that the maximum probable load that is transmitted to an underground pipe from a truck wheel acting at the surface can be calculated with a reasonable degree of reliability by the Boussinesq solution.

These studies indicated that the actual load transmitted to the pipe varies over a considerable range, apparently due to fortuitous combinations of conditions that are not identifiable in advance of the application of a truck wheel load. The Boussinesq solution, however, provides a locus of stress value that was sometimes equalled but never exceeded in a large number of trials. Also, it is pointed out that the trials were conducted with a gravel surfaced roadway. No similar experiments have been conducted with a high type rigid pavement such as Portland cement concrete.

The studies were made with both static and moving loads. Moving loads produced an impact increment of load on the buried pipe, which was a function of the speed of the vehicle in relation to the roughness characteristics of the roadway surface, but it was independent of the depth of cover. That is to say, the impact factor for two feet of cover was about the same as for six feet of cover, although the percentage of the applied wheel load that reaches the pipe under the greater depth is much less.

Experimental impact values obtained were very high under some very adverse roadway conditions such as 2-in. and 4-in. obstructions on the surface or deep chuck holes. For general use, however, an impact factor of about 1.5 is recommended.

On the basis of the above mentioned researches, it is possible to write an equation for the load on a buried pipe line caused by a moving truck wheel, as follows:

$$W_t = \frac{C_t P F}{12 L} \qquad (6)$$

in which

W_t = load on pipe due to truck wheel, lb per lin in.

P = truck wheel load, lb
L = effective length of pipe, ft. The length over which the average load produces the same stress as the actual load which varies in intensity from point to point along the pipe.
C_t = a load coefficient which depends on the diameter of the pipe, D; the effective length, L; and the height of fill above the top of pipe, H. Values of C_t may be taken from Table 2, which is derived from the solution of Holl's integration of the Boussinesq equation for a point load applied above the center of a segment of underground conduit.
F = impact factor.

In the case of pipeline crossings under railways, the live load consists of rail traffic which is a series of concentrated axle loads applied to the rails. It is assumed, however, that the concentrated loads are distributed longitudinally by the rails and transversely by the ties and ballast to such an extent that the weight of a locomotive can be considered as a uniformly distributed load applied at the elevation of the base of ties over an area equal to the length of the locomotive times the length of ties.

On the basis of this assumption, the unit pressure at a point on the top of the line pipe or casing pipe directly beneath the center of the area may be estimated by means of Newmark's integration of the Boussinesq equation. Newmark determined the pressure at a point in the undersoil at any elevation below one corner of a rectangular area over which unit loads are uniformly applied, and gave influence coefficients corresponding to the ratios of: length of the loaded area over depth, and width over depth. To determine the unit pressure on the top of the pipe under the center of the loaded area, calculate the ratios

$$m = \frac{D}{2H} \quad \text{and} \quad n = \frac{L}{2H} \quad \text{(see Fig. 3)},$$

and select the influence coefficient corresponding to these ratios from Table 1. Multiply this coefficient by the load per square foot on the loaded area. This product is the unit pressure on the pipe directly under the loaded area. This procedure is widely employed in structural work to estimate the unit pressure on a deep soil stratum below a foundation, and it appears to be appropriate to the problem under discussion.

Having obtained the unit pressure at the top of the pipe directly under the center of the loaded area, the load per foot of length of pipe can be determined by multiplying this unit pressure by the diameter of the pipe in feet. Dividing this load per foot by 12 gives the load per lineal inch of pipe (W_t in Eq. 6).

Since rail traffic loads are dynamic in character, an impact factor is appropriate. The author has arbitrarily chosen an impact factor of 1.75 when studying stresses in pipelines and casing pipes under railways.

Elastic Theory of Thin Rings

Practically all transmission lines and products pipelines are constructed of steel of various kinds and grades. Therefore, stresses and deflections in the pipe wall can be analyzed by the elastic theory applied to thin rings.

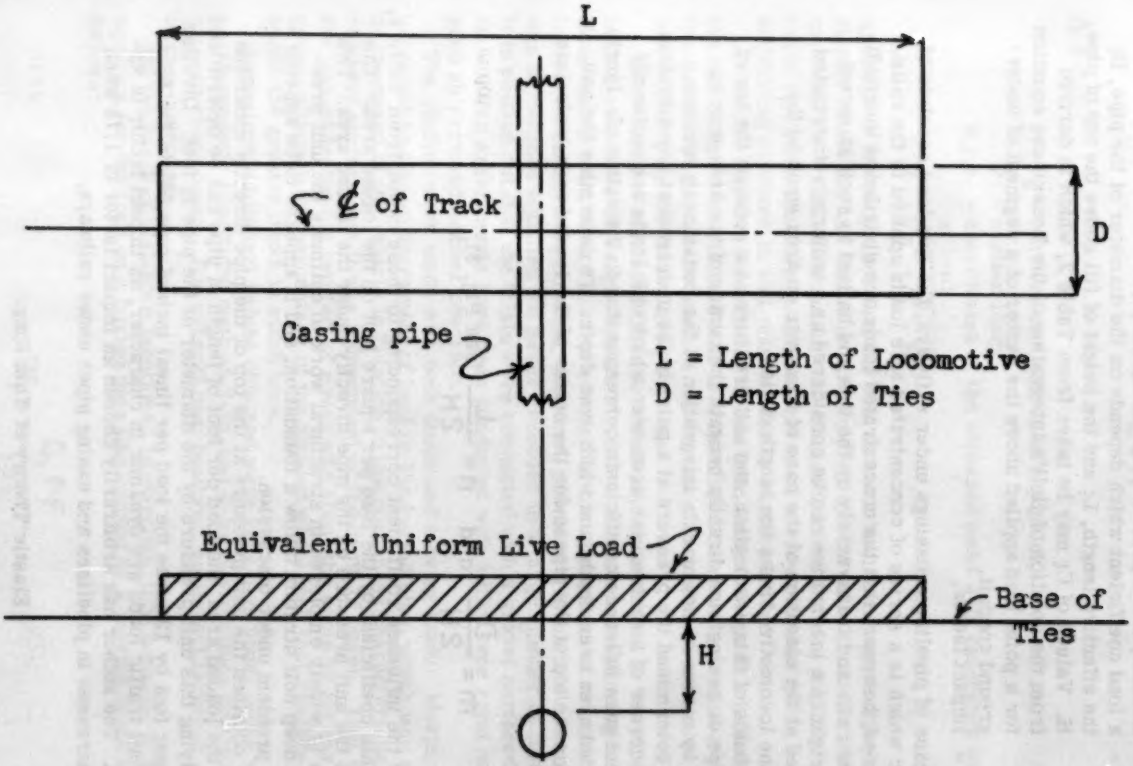

Fig. 3 Area Over Which Weight of Locomotive is Assumed Uniformly Distributed.

One question which arises in connection with the application of the elastic theory to pipeline problems is whether to assume a condition of plane strain or plane stress. In the state of plane strain, it is assumed that the pipe is infinitely long and contains identical forces in every transverse cross section. It is also assumed that no deformation occurs in the direction normal to a cross section and, consequently, stresses and deflections, which depend upon Poisson's ratio, act upon every cross section.

In the case of plane stress, it is assumed that the pipe metal is free to deform in the direction normal to a cross section and, consequently, no stresses, due to Poisson's ratio, act upon either end of a short segment of the pipe.

Theoretically, it would appear that a pipeline more nearly conforms to the condition of plane strain, since the pipe is very long. However, initial longitudinal stresses in the pipe due to slack laying and unevenness in the bottom of the ditch may modify this condition to the extent that it is impossible to say definitely which of the conditions most nearly applies. Therefore in this analysis, and until research indicates which assumption is most nearly applicable, the condition of plane stress will be employed, since the resulting expressions are somewhat simpler when Poisson's ratio does not enter into the analysis.

Moments and deflections in a loaded thin ring can be determined in the following manner.

Let:

r = radius of unloaded ring.
ρ = radius of loaded ring at any point.
M = bending moment at any point on the ring.
E = modulus of elasticity of ring material.
I = moment of inertia of cross section of the ring.

Then:

$$\frac{1}{\rho} - \frac{1}{r} = \frac{M}{EI} \tag{7}$$

Where:

$\left(\frac{1}{\rho} - \frac{1}{r}\right)$ = the change in curvature between the unloaded and loaded state.

Also:

$$\frac{1}{\rho} - \frac{1}{r} = \frac{d\theta}{ds} \tag{8}$$

Where:

$d\theta$ = angle through which a plane section normal to the curve of the elastic ring rotates as the ring is loaded.
ds = length of arc within which $d\theta$ occurs.

Substituting equation 8 in equation 7:

Table 1. Influence Coefficients for Solution of Holl's and Newmark's Integration of the Boussinesq Equation for Vertical Stress.

$\frac{D}{2H}$	$\frac{L}{2H}$													
	.1	.2	.3	.4	.5	.6	.7	.8	.9	1.0	1.2	1.5	2.0	5.0
.1	.019	.037	.053	.067	.079	.089	.097	.103	.108	.112	.117	.121	.124	.128
.2	.037	.072	.103	.131	.155	.174	.189	.202	.211	.219	.229	.238	.244	.248
.3	.053	.103	.149	.190	.224	.252	.274	.292	.306	.318	.333	.345	.355	.360
.4	.067	.131	.190	.241	.284	.320	.349	.373	.391	.405	.425	.440	.454	.460
.5	.079	.155	.224	.284	.336	.379	.414	.441	.463	.481	.505	.525	.540	.548
.6	.089	.174	.252	.320	.379	.428	.467	.499	.524	.544	.572	.596	.613	.624
.7	.097	.189	.274	.349	.414	.467	.511	.546	.574	.597	.628	.650	.674	.688
.8	.103	.202	.292	.373	.441	.499	.546	.584	.615	.639	.674	.703	.725	.740
.9	.108	.211	.306	.391	.463	.524	.574	.615	.647	.673	.711	.742	.766	.784
1.0	.112	.219	.318	.405	.481	.544	.597	.639	.673	.701	.740	.774	.800	.816
1.2	.117	.229	.333	.425	.505	.572	.628	.674	.711	.740	.783	.820	.849	.868
1.5	.121	.238	.345	.440	.525	.596	.650	.703	.742	.774	.820	.861	.894	.916
2.0	.124	.244	.355	.454	.540	.613	.674	.725	.766	.800	.849	.894	.930	.956

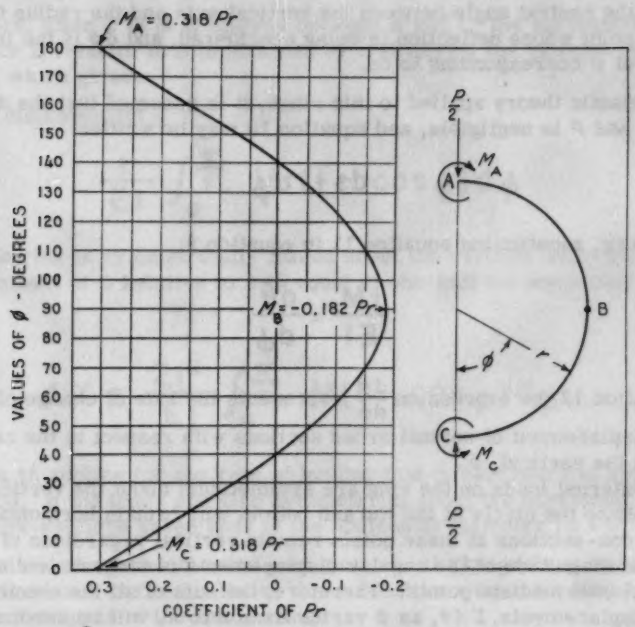

FIGURE 4.—VARIATION IN MOMENT AROUND A PIPE RING RESULTING FROM LOADS AT DIAMETRICALLY OPPOSITE POINTS.

$$\frac{d\theta}{ds} = \frac{M}{EI} \tag{9}$$

Also $$ds = \rho d\phi \tag{10}$$

Where:

ϕ = the central angle between the vertical axis and the radius to the point whose deflection is being considered, and $d\phi$ is the increment of ϕ corresponding to ds.

In the elastic theory applied to thin rings, it is assumed that the difference between r and ρ is negligible, and equation 10 may be written:

$$ds = r d\phi \tag{11}$$

Therefore, substituting equation 11 in equation 9:

$$\frac{rM}{EI} = \frac{d\theta}{d\phi} \tag{12}$$

In equation 12 the expression $\frac{d\theta}{d\phi}$ represents the rate of change of the angular displacement of normal cross sections with respect to the central angle with the vertical, ϕ.

When external loads on the ring are symmetrical about the vertical axis, the tangents to the circle at the top and bottom will remain horizontal, and the normal cross-sections at these points remain vertical regardless of the direction and magnitude of the angular displacements of tangents and normal sections at intermediate points. Therefore, the sum of all the elementary angular displacements, $\Sigma d\theta$, as ϕ varies from 0 to π, will be zero; and, when the left side of equation 12 is integrated between these limits, we obtain:

$$\frac{r}{EI} \int_0^{\pi} M d\phi = 0 \tag{13}$$

Or simply:

$$\int_0^{\pi} M d\phi = 0 \tag{14}$$

The moment and thrust resulting from any system of loads that is symmetrical about the vertical axis may be obtained from equation 14, for either the top or bottom point on a ring, by substituting a general expression for moment of the actual loads for M. From the moment and thrust at either of these points, the moment, tangential thrust, and radial shear may be obtained at any point of the ring by the equations of equilibrium.

The vertical and horizontal deflections of the ring may be derived by the displacement theory of arches. In this theory the origin is taken at a point on the ring that is assumed to be free to move with respect to any other point.

The displacement of any intermediate point is the product of the moment at that point multiplied by its ordinate measured perpendicularly to the supposed displacement. Thus if A in Fig. 4 is regarded as the fixed point and C the free point, the ordinate in question in the case of horizontal movement of any intermediate point D is the vertical distance from C to D, or:

$$r(1 - \cos\phi)$$

Therefore, when D is at B midway between A and C, the horizontal displacement of B relative to A is obtained by multiplying the moment at B by $r(1-\cos\phi)$, which gives:

Horizontal displacement =

$$\frac{r}{EI}\int_0^{\frac{\pi}{2}} Mr(1 - \cos\phi)d\phi \qquad (15)$$

When the ring is symmetrically loaded about the vertical axis, the horizontal displacement of B relative to A is equal to one-half the horizontal deflection.
Therefore:

$$\Delta X = \frac{2r^2}{EI}\int_0^{\frac{\pi}{2}} M(1 - \cos\phi)d\phi \qquad (16)$$

Equation 16 applies for any type of loading that is symmetrical about the vertical axis. If the loads are also symmetrical about the horizontal axis, the normal cross-sections at the ends of the horizontal diameter ($\phi = \frac{\pi}{2}$) will not rotate in relation to their unloaded positions, and the tangents at the sides of the ring will remain vertical. Under these conditions equation 16 may be simplified by substitution of the relationship:

$$\int_0^{\frac{\pi}{2}} Md\phi = 0$$

Which gives:

$$\Delta X = \frac{2r^2}{EI}\int_0^{\frac{\pi}{2}} M\cos\phi d\phi \qquad (17)$$

Similarly, the vertical displacement of C relative to A, i.e., the vertical deflection of the ring, may be shown to be:

$$\Delta Y = \frac{r^2}{EI}\int_0^{\pi} M\sin\phi d\phi \qquad (18)$$

For vertical loads and reactions on an elastic ring, the above procedure leads to the following equations for moments and deflections.

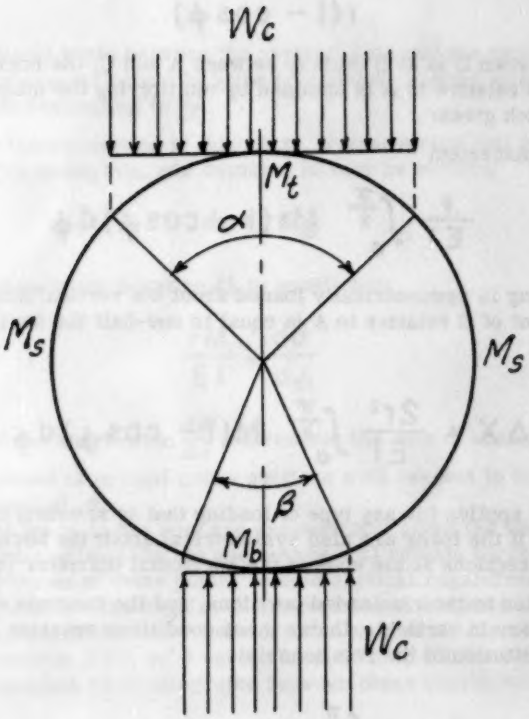

Fig. 5

Table 2. Coefficients for Bending Moments and Deflections of an Elastic Ring under Uniformly Distributed Vertical Load and Reaction.

α Deg.	B Deg.	K_b	K_t	K_s	K_x	K_y
0	0	0.318	0.318	0.182	0.149	0.137
	30	0.259	0.317	0.180	0.146	0.135
	60	0.213	0.312	0.175	0.138	0.130
	90	0.182	0.305	0.168	0.129	0.122
	120	0.162	0.299	0.161	0.122	0.116
	150	0.153	0.295	0.156	0.117	0.111
	180	0.150	0.294	0.153	0.116	0.110
30	0	0.317	0.259	0.180	0.146	0.135
	30	0.257	0.257	0.178	0.143	0.133
	60	0.211	0.252	0.173	0.135	0.127
	90	0.180	0.246	0.166	0.127	0.120
	120	0.160	0.240	0.159	0.119	0.114
	150	0.151	0.236	0.154	0.115	0.109
	180	0.148	0.235	0.152	0.113	0.108
60	0	0.312	0.213	0.175	0.138	0.129
	30	0.252	0.211	0.173	0.135	0.127
	60	0.207	0.207	0.168	0.122	0.127
	90	0.175	0.201	0.161	0.118	0.115
	120	0.156	0.194	0.154	0.111	0.109
	150	0.146	0.190	0.149	0.107	0.104
	180	0.143	0.189	0.147	0.105	0.103
90	0	0.306	0.182	0.168	0.129	0.122
	30	0.246	0.180	0.166	0.127	0.120
	60	0.201	0.175	0.161	0.118	0.115
	90	0.169	0.169	0.154	0.110	0.108
	120	0.150	0.163	0.147	0.103	0.101
	150	0.140	0.158	0.142	0.098	0.097
	180	0.137	0.157	0.140	0.096	0.096
120	0	0.299	0.162	0.161	0.122	0.116
	30	0.240	0.160	0.159	0.119	0.114
	60	0.194	0.156	0.154	0.111	0.109
	90	0.163	0.150	0.147	0.103	0.101
	120	0.143	0.143	0.140	0.096	0.095
	150	0.134	0.139	0.135	0.091	0.091
	180	0.131	0.138	0.133	0.089	0.089
150	0	0.295	0.153	0.156	0.117	0.111
	30	0.236	0.151	0.154	0.115	0.109
	60	0.190	0.146	0.149	0.107	0.104
	90	0.158	0.140	0.142	0.098	0.097
	120	0.139	0.134	0.135	0.091	0.091
	150	0.129	0.129	0.129	0.086	0.086
	180	0.126	0.128	0.128	0.085	0.085
180	0	0.294	0.150	0.153	0.116	0.110
	30	0.235	0.148	0.152	0.113	0.108
	60	0.189	0.143	0.147	0.105	0.103
	90	0.157	0.137	0.140	0.096	0.096
	120	0.138	0.131	0.133	0.089	0.089
	150	0.128	0.126	0.127	0.085	0.085
	180	0.125	0.125	0.125	0.083	0.083

Moments $M = KWr$ (19)

Deflections $\Delta = K\frac{Wr^3}{EI}$ (20)

Table 2 gives values of the parameter K in Equations 19 and 20 for loads and reactions distributed over various widths. In this table (see Fig. 5)

Use: K_b for moment at bottom
K_t for moment at top
K_s for moment at sides

Use: K_x for horizontal deflection
K_y for vertical deflection

Supporting Strength of Buried Pipes

In general, buried pipes may be divided into two classes on the basis of the amount of deformation which they can withstand without structural damage. These classes are: 1, rigid pipes, such as those made of concrete and burned clay; and, 2, flexible pipes, such as those made of relatively thin corrugated metal sheets or steel line pipe.

Rigid pipes fail under external loading by rupture of the pipe wall when the outer fiber stresses at points of maximum bending moment exceed the strength of the material of which the pipes are made. These failure stresses occur when the deflection of the pipe ring is relatively small; hence the term "rigid." As an illustration, the deflection, i.e., the shortening of the vertical diameter and the lengthening of the horizontal diameter of a heavy-walled concrete pipe at the time of rupture of the material, is measurable only in hundredths of an inch.

In contrast, the flexible pipes are capable of withstanding relatively very large deflections without rupture of the pipe wall or other evidence of structural damage. When a flexible pipe is installed as an underground conduit, the external loads and pressures to which it is subjected cause the pipe to deflect in a manner somewhat as shown in Fig. 6. The first increments of load cause the initially circular ring to assume an elliptical shape. As the loading increases, this tendency continues until the top of the pipe is essentially flat for a considerable distance. Further increases in load may causes the top of the pipe to reverse its curvature and become concave upward, while the sides of the pipe pull inward as the pipe proceeds toward complete collapse. The whole action is one of large deflection change unaccompanied by rupture or buckling of the metal ring, although the material in certain parts of the ring may be stressed well beyond its elastic limit.

Buried pipes derive their ability to support the vertical loads to which they are subjected from the inherent strength of the pipe and from lateral earth pressures acting against the sides. These lateral pressures produce stresses in the pipe ring that act in the opposite direction to those caused by the vertical loads, thereby augmenting the inherent load-carrying capacity of the pipe. Soil is neither a fluid nor a solid, but it possesses some of the properties of each of these states of matter. One characteristic that is similar

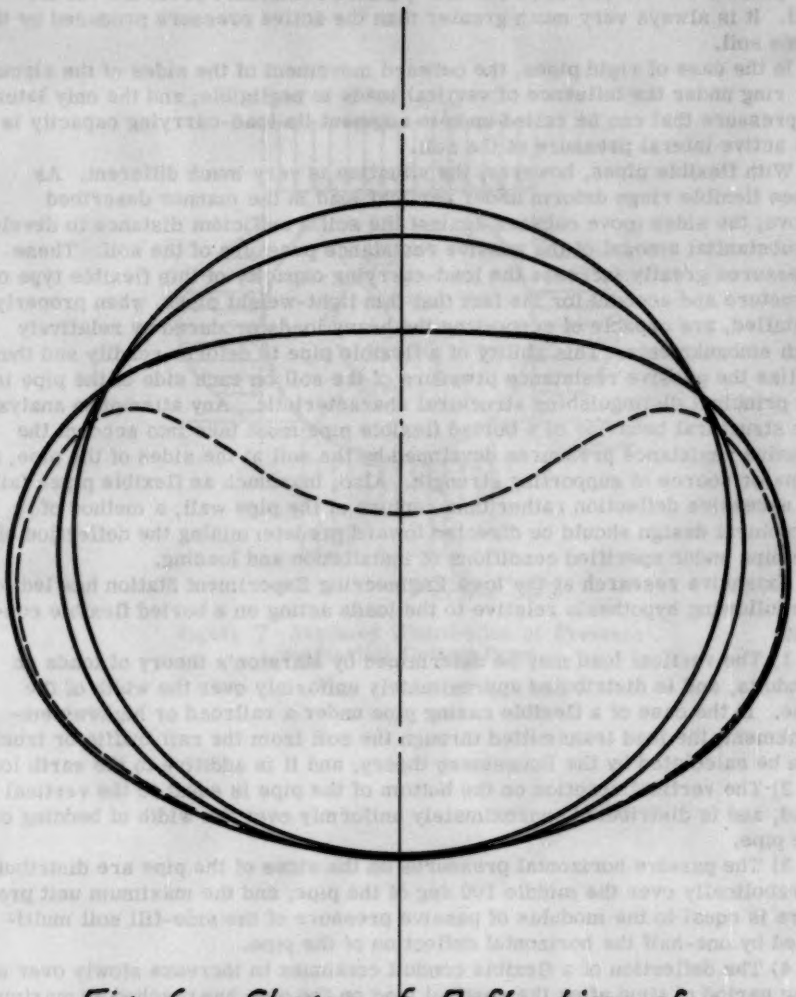

Fig. 6 Stages of Deflection of a Flexible Pipe Culvert

to that of a fluid is its ability to exert lateral pressure against a structure with which it comes in contact. If the structure against which the soil impinges is essentially stationary, the pressure developed is called "active lateral pressure." On the other hand, if the structure moves toward the soil, the pressure developed is called the "passive resistance pressure" of the soil. It is always very much greater than the active pressure produced by the same soil.

In the case of rigid pipes, the outward movement of the sides of the circular ring under the influence of vertical loads is negligible, and the only lateral pressure that can be relied upon to augment its load-carrying capacity is the active lateral pressure of the soil.

With flexible pipes, however, the situation is very much different. As these flexible rings deform under vertical load in the manner described above, the sides move outward against the soil a sufficient distance to develop a substantial amount of the passive resistance pressure of the soil. These pressures greatly increase the load-carrying capacity of this flexible type of structure and account for the fact that thin light-weight pipes, when properly installed, are capable of supporting the heavy loads produced by relatively high embankments. This ability of a flexible pipe to deform readily and thus utilize the passive resistance pressure of the soil on each side of the pipe is its principal distinguishing structural characteristic. Any attempt to analyze the structural behavior of a buried flexible pipe must take into account the passive resistance pressures developed by the soil at the sides of the pipe, as a major source of supporting strength. Also, inasmuch as flexible pipes fail by excessive deflection rather than rupture of the pipe wall, a method of structural design should be directed toward predetermining the deflection of the pipe under specified conditions of installation and loading.

Extensive research at the Iowa Engineering Experiment Station has led to the following hypothesis relative to the loads acting on a buried flexible conduit.

1) The vertical load may be determined by Marston's theory of loads on conduits, and is distributed approximately uniformly over the width of the pipe. In the case of a flexible casing pipe under a railroad or highway embankment, the load transmitted through the soil from the rail traffic or truck can be calculated by the Boussinesq theory, and it is additive to the earth load.

2) The vertical reaction on the bottom of the pipe is equal to the vertical load, and is distributed approximately uniformly over the width of bedding of the pipe.

3) The passive horizontal pressures on the sides of the pipe are distributed parabolically over the middle 100 deg of the pipe, and the maximum unit pressure is equal to the modulus of passive pressure of the side-fill soil multiplied by one-half the horizontal deflection of the pipe.

4) The deflection of a flexible conduit continues to increase slowly over a long period of time after the vertical load on the pipe has reached its maximum value, due to a gradual yielding of the soil at the sides.

The distribution of pressures around a flexible pipe under an embankment, determined in accordance with the foregoing load hypothesis, is shown graphically in Fig. 7.

With a load hypothesis established, it is possible, by substituting the actual moment equations in equation 17, to develop a mathematical expression for the horizontal deflection of a flexible pipe in terms of the load, the properties of the pipe, and the properties of the soil at the sides of the pipe. This

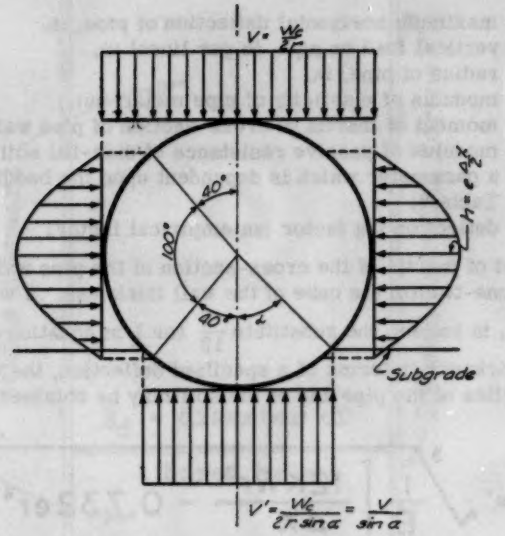

Figure 7 Assumed Distribution of Pressure on Flexible Culvert Pipes

expression is:

$$\Delta X_1 = \frac{D_e K W_c r^3}{EI + 0.061er^4} \qquad (21)$$

Where:

ΔX_1 = maximum horizontal deflection of pipe, in.
W_c = vertical load on pipe, lb per lineal in.
r = radius of pipe, in.
E = modulus of elasticity of pipe metal, psi.
I = moment of inertia of cross-section of pipe wall, $in.^4$ per in.
e = modulus of passive resistance of side-fill soil, psi per in.
K = a parameter which is dependent upon the bedding angle. (see Table 2)
D_e = deflection lag factor (an empirical factor)

The moment of inertia of the cross-section of the pipe wall per unit length of the pipe is one-twelfth the cube of the wall thickness. If we let t equal the wall thickness, in inches, the substitute $\frac{t3}{12}$ for I in equation 21, an expression for the wall thickness in terms of a specified deflection, the vertical loads, and the properties of the pipe and of the soil may be obtained:

$$t = \sqrt[3]{\frac{1}{E}\left[\frac{12KWr^3}{\Delta X} - 0.732er^4\right]} \qquad (22)$$

Casing Pipe under a Railroad

Casing pipes are usually installed by tunneling under the railroad road bed at relatively shallow depths, say from 5 ft. to 8 ft. below the base of rail. This method of installation creates a very uncertain situation relative to the earth load which will actually develop on the pipe. It is conceivable that the bored hole in which the pipe is placed might retain its shape as a circular opening slightly larger than the casing, in which case there would be no load on the pipe either from the earth above it or the traffic on the rails. However, it seems more probable that the traffic loads and vibrations, climatic fluctuations, and moisture changes will cause the prism of soil above the bored hole to move downward until it rests on the casing—thus producing vertical load and acting as a medium through which the traffic loads may be transmitted to the casing pipe, as indicated in Fig. 7. This action would induce upward vertical shearing stresses along the vertical planes extending upward from the sides of the bored hole, and the load situation would be typical of the class of conduits described by Marston as "ditch conduits." The maximum probable earth load on the casing pipe may be estimated by Equation 3.

The maximum probable load, due to rail traffic, may be estimated by Newmark's integration of the Boussinesq equation.

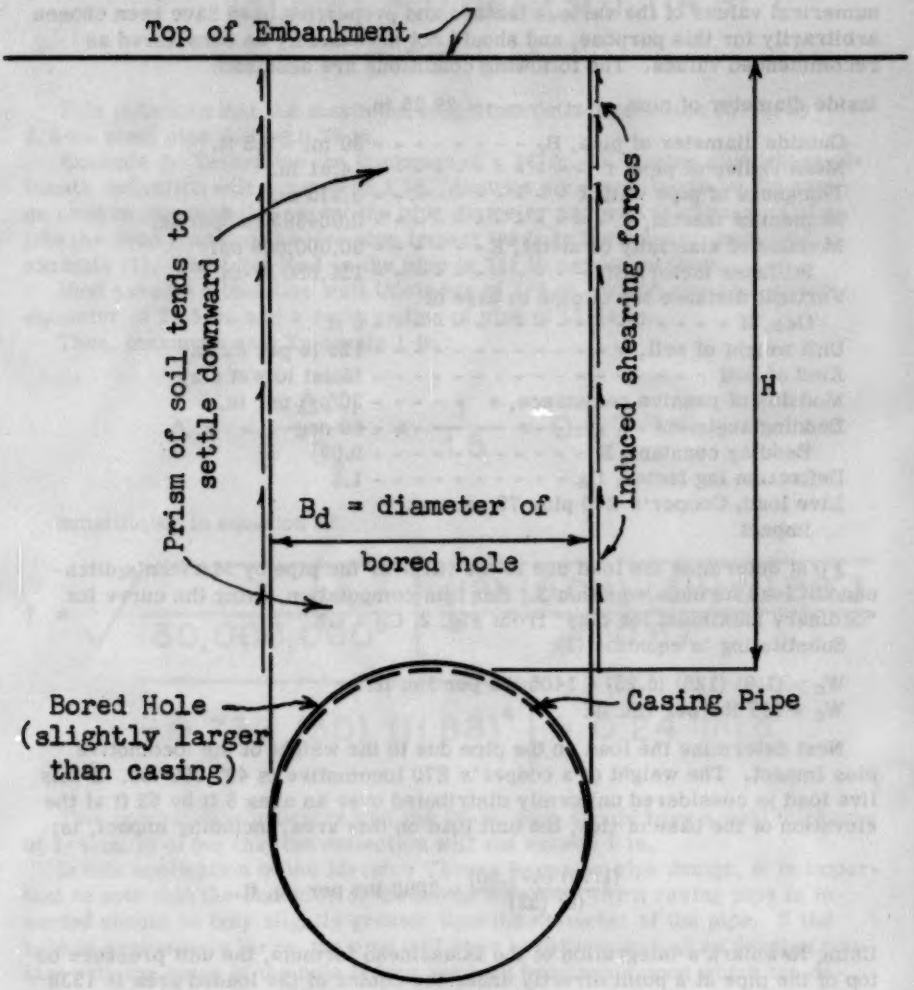

Fig. 8 Settlements which Influence Loads on Casing Pipe.

Example 1: A complete example of a procedure for determining the deflection of a smooth steel protective casing pipe under a railroad embankment, based upon the aforedescribed researches, will now be presented. It is emphasized that the purpose of this example is to illustrate a method. The numerical values of the various factors and properties used have been chosen arbitrarily for this purpose, and should not necessarily be considered as recommended values. The following conditions are assumed:

Inside diameter of pipe - - - - - - - - 29.25 in.

Outside diameter of pipe, B_c - - - - - - - - 30 in. = 2.5 ft.
Mean radius of pipe, r - - - - - - - - - - - - 14.81 in.
Thickness of pipe wall, t - - - - - - - - - - - 0.375 in.
Moment of inertia, I - - - - - - - - - - - - - 0.004395 $in.^4$ per in.
Modulus of elasticity of metal, E - - - - - - 30,000,000 psi
Stiffness factor, EI - - - - - - - - - - - - 131,850 lb-in.
Vertical distance top of pipe to base of ties, H - - - - - - - - - - - - - - - - - - 6 ft.
Unit weight of soil, w - - - - - - - - - - - - 125 lb per cu ft.
Kind of soil - - - - - - - - - - - - - - - - - Moist to wet clay
Modulus of passive resistance, e - - - - - 30 psi per in.
Bedding angle - - - - - - - - - - - - - - - - 60 deg
Bedding constant, K - - - - - - - - - - - - 0.09
Deflection lag factor, D_e - - - - - - - - - - 1.5
Live load, Cooper's E70 plus 75 percent impact

First determine the load due to the fill over the pipe by Marston's ditch-conduit load formula equation 3. For this computation, using the curve for "ordinary maximum for clay" from Fig. 2, $C_d = 1.8$.
Substituting in equation (3):

$W_c = (1.8)\ (125)\ (6.25) = 1405$ lbs per lin. ft. or
$W_c = 117$ lbs per lin. in.

Next determine the load on the pipe due to the weight of the locomotive plus impact. The weight of a cooper's E70 locomotive is 497,000 lbs. If this live load is considered uniformly distributed over an area 8 ft by 52 ft at the elevation of the base of ties, the unit load on this area, including impact, is:

$$\frac{(1.75)\ (497.00)}{(8)\ (52)} = 2090 \text{ lbs per sq. ft.}$$

Using Newmark's integration of the Boussinesq formula, the unit pressure on top of the pipe at a point directly under the center of the loaded area is 1338 lbs per sq ft. Assuming this pressure is uniformly distributed over the top of the pipe, the load per lineal inch is:

$$W_e = \frac{(1338)\ (2.5)}{12} = 279 \text{ lbs per lineal inch}$$

The total load on the pipe is:

Earth load, $W_c = 117$ lbs per lineal inch.
Live load plus impact, $W_e = 279$ lbs per lineal inch.
Total load, W = 396 lbs per lineal inch.

The computation for ultimate deflection by equation 21 is:

$$\Delta X_1 = \frac{(1.5)\ (0.09)\ (396)\ (14.81^3)}{131{,}850 + 0.061\ (30)\ (14.81^4)}$$

$$= 0.79 \text{ inch}$$

This indicates that the maximum long-time deflection of the 30-in. by 3/8-in. steel pipe will be 0.79 in.

Example 2: Determine the thickness of a 24-in.-OD casing pipe whose ultimate deflection will not exceed 1 in. Assume all quantities to be the same as used in example (1), except the pipe diameter and wall thickness. Calculate the dead load and the live plus impact loads in the manner employed in example (1). The total load on the pipe is 311 lb per lineal inch.

Next assume a tentative wall thickness of 1/4-in., which gives an inside diameter of 23.5 in. and a mean radius of pipe of 11.88 in.

Then, inasmuch as ΔX_1 equals 1 in.:

$$\Delta X = \frac{\Delta X_1}{D_e} = \frac{1}{1.5} = 0.67 \text{ inch}$$

Substituting in equation 22:

$$t = \sqrt[3]{\frac{1}{30{,}000{,}000}\left[\frac{(12)\ (0.09)\ (311)\ (11.88^3)}{0.67} - 0.732\ (30)\ (11.88)^4\right]} = 0.24 \text{ inch}$$

This computation indicates that the 24-in. pipe should have a wall thickness of 1/4-in. in order that the deflection will not exceed 1 in.

In this application of the Marston Theory to casing pipe design, it is important to note that the diameter of the bored hole into which casing pipe is inserted should be only slightly greater than the diameter of the pipe. If the hole is excessively large, the pipe will have to deform enough to develop contact with the sides of the hole before the load hypothesis upon which the deflection formula is based becomes effective.

Also, it is pointed out that if the casing pipe is installed in an open ditch, the width factor to use in the expression for earth load (Equation 3) should be the width of the ditch at the elevation of the top of pipe. In order for passive resistance pressures to be effective in this case, it is necessary that the soil at the sides of the pipe be compacted thoroughly.

The above discussion was first presented in a paper before the Division of Transportation of the American Petroleum Institute on November 6, 1951. Later, Mr. Ernest A. Slade of the Service Pipeline Co. of Tulsa, Oklahoma,

demonstrated the use of an electronic calculator for mass production of solutions for the various equations, in a paper before the same organization on November 10, 1953.

Stresses in Uncased Line Pipe

The primary stress in an uncased pipeline is the bursting or hoop stress. Secondary stresses may be induced in the pipe wall by earth fill loads and by surface traffic loads, such as truck wheels, railroad traffic or airplane wheel loads.

When steel line pipe is assembled and laid prior to being covered with earth, it is nominally in a circular shape. After covering, the vertical load on the pipe from the earth backfill causes it to deflect to an elliptical shape with the major axis horizontal and the minor axis vertical. When internal pressure is introduced into the pipe, the resultant of vertical components of this pressure will be greater than the resultant of horizontal components because of the elliptical shape. This excess vertical internal pressure against the upper half of the pipe acts in opposition to the vertical external load and combines with the resilience or stored energy in the deflected pipe to resist the external load.

Under these conditions, equilibrium of forces on the pipe will prevail when the sum of the vertical excess pressure plus the resilience in the deflected pipe is equal to the external load. This means that when internal pressure is introduced into a pipe, which has been deflected by external load, the deflection will decrease to some equilibrium value and the shape of the pipe will be stabilized as an ellipse intermediate between a circle and the deflected shape under external load alone.

The bending stresses in the pipe wall corresponding to this equilibrium deflection, which are less than the stresses due to external load without internal pressure, are assumed to be algebraically additive to the tensile hoop stress due to internal pressure. The deflections of a pipe under various load and pressure situations are shown in Fig. 9.

The above hypothesis can be expressed in mathematical formulas that facilitate the calculation of combined primary and secondary stresses in the pipe wall.

The primary bursting or hoop stress in the pipe can be computed by the formula:

$$S_1 = \frac{p(D - 2t)}{2t} \qquad (23)$$

in which

S_1 = circumferential tensile stress in pipe wall due to internal pressure, psi
p = internal fluid pressure, psi
D = outside diameter of pipe, in.
t = thickness of pipe wall, in.

Underground pipe lines may be installed under a wide variety of environmental conditions that influence the amount of load produced by the earth

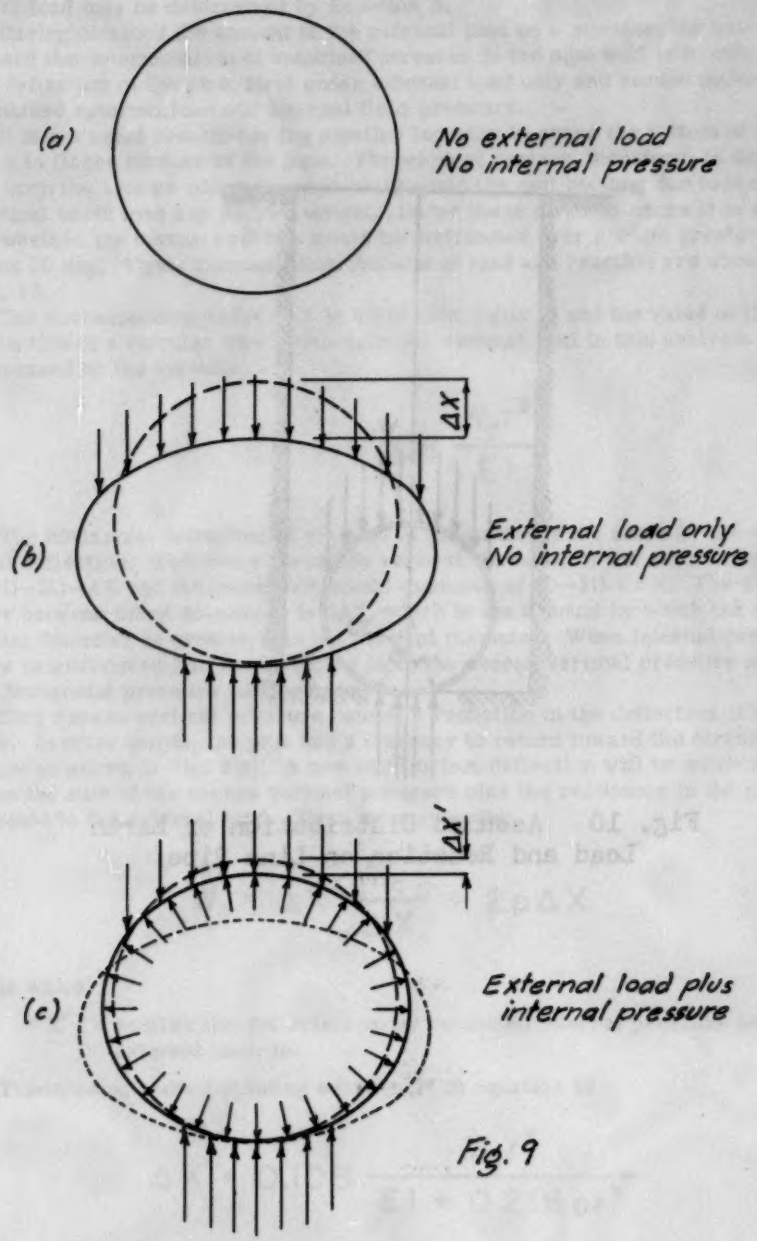
(a)
No external load
No internal pressure
Δx
(b)
External load only
No internal pressure
Δx'
(c)
External load plus
internal pressure

Fig. 9

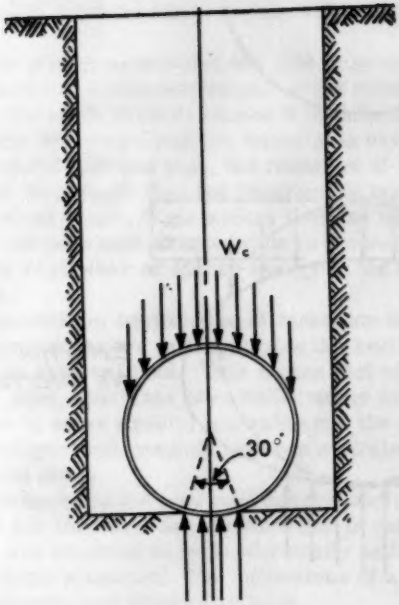

Fig. 10 Assumed Distribution of Earth Load and Reaction on Line Pipe.

cover. However, since most pipelines are installed as ditch conduits, the earth load may be determined by Equation 3.

Having obtained the amount of the external load on a pipeline, the next step toward the determination of combined stresses in the pipe wall is to calculate the deflection of the pipe, first under external load only and second under combined external load and internal fluid pressure.

It is not usual practice in the pipeline industry to shape the bottom of the ditch to fit the contour of the pipe. The width of contact, therefore, is dependent upon the amount which the pipe pushes into the soil bedding due to the vertical earth load and its own weight. Under these circumstances it is doubtful whether the bottom reaction would be distributed over a width greater than about 30 deg. These assumed distributions of load and reaction are shown in Fig. 10.

The corresponding value of $\underline{K}$ is 0.108 (see Table 2) and the value of the deflection of a circular pipe under external vertical load in this analysis is expressed by the formula:

$$\Delta X = 0.108 \frac{W_c r^3}{EI} \tag{24}$$

The horizontal deflection of the pipe is substantially the same as the vertical deflection. Therefore the inside vertical diameter of the deflected pipe is $(D-2t)-\Delta X$ and the inside horizontal diameter of $(D-2t)+\Delta X$. The difference between these diameters is $2\Delta X$, which is the a mount by which the horizontal diameter is greater than the vertical diameter. When internal pressure is introduced into the deflected pipe, the excess vertical pressure over the horizontal pressure will be $2p\Delta X$.

This excess vertical pressure causes a reduction in the deflection of the pipe. In other words, the pipe has a tendency to return toward the circular shape as shown in Fig. 9(c). A new equilibrium deflection will be established when the sum of the excess vertical pressure plus the resilience in the pipe is equal to the external load. Thus, we may write:

$$W_c = \Delta X' \frac{W_c}{\Delta X} + 2p\Delta X \tag{25}$$

in which

$\Delta X'$ = equilibrium deflection under combined internal pressure and external load, in.

Transposing and substituting equation 24 in equation 25

$$\Delta X' = 0.108 \frac{W_c r^3}{EI + 0.216 pr^3} \tag{26}$$

The external load bending moment is maximum at the bottom of the pipe and at the equilibrium deflection is:

$$M'_b = 2.170 \frac{\Delta X' E I}{r^2} \qquad (27)$$

Substituting equation 26 in equation 27:

$$M'_b = 0.234 \frac{W_c r E I}{E I + 0.216 p r^3} \qquad (28)$$

Then the tensile stress at the bottom of the pipe due to bending is, by the flexure formula:

$$S_2 = \frac{M'_b}{2 I} t \qquad (29)$$

Substituting equation 29 and equation 2 and $I = \frac{t3}{12}$ in equation 28:

$$S_2 = 0.117 \frac{C_d w B_d^2 E t r}{E t^3 + 2.592 p r^3} \qquad (30)$$

Equation 30 is an expression for the maximum bending moment stress at the bottom of a pipe subjected to both external fill load and internal fluid pressure. The maximum combined stress may be obtained by adding equation 23 and equation 30:

$$S = S_1 + S_2 = \frac{p(D - 2t)}{2t} + 0.117 \frac{C_d w B_d^2 E t r}{E t^3 + 2.592 p r^3} \qquad (31)$$

If highway, railway or airplane traffic vehicles cause loads on the pipeline, the magnitude of load may be determined by use of the Boussinesq theory, as discussed earlier in this paper.

If it is assumed that the distribution of the load and reaction on the pipe due to a truck wheel load applied at the roadway surface is essentially the same as that of the fill load (see Fig. 10), then an equation for the bending moment stress at the bottom of the pipe can be written:

$$S_3 = 0.117 \frac{C_t \frac{P}{L} F E t r}{E t^3 + 2.592 p r^3} \qquad (32)$$

in which

S_3 = bending moment stress at bottom of pipe due to truck and impact loads, psi

Other symbols are as previously defined.

An example of stress computation which may be of some interest is that of an airfield runway designed for 120,000 lb. aircraft (60,000 lb. on one dual wheel). An 18-in. by 11/32-in. pipeline operating at 900 psi internal pressure passed beneath the runway with the top of pipe 4 ft. below the runway surface, which was paved with bituminous concrete on a crushed rock and gravel base course.

Data for this problem is as follows:

Diameter of pipe	18 in.
Thickness of pipe wall	0.34375 in.
Internal pressure	900 psi
Depth of cover	4 ft.
Width of trench	2.5 ft.
Unit weight of soil	120 pcf
Modulus of elasticity of steel	30×10^6 psi
Width of pipe bedding	30 deg.
Effective length of pipe	3 ft.
Airplane wheel load (considered as point load)	60,000 lb.
Impact factor	None

Using the above data, the hoop stress in the pipe wall,

By Equation 23 $S_1 = 22650$ psi

The maximum bending moment stress due to earth fill is,

By Equation 30 $S_2 = 3730$ psi

The maximum bending moment stress due to one airplane wheel is,

By Equation 32 $S_3 = 9040$ psi

The total stress in the pipe wall is: $S_1 + S_2 + S_3 = 35{,}390$ psi.

Figures 11, 12 and 13 show the results of stress calculations for several assumed pipeline problems. In Fig. 11, the hoop stress, fill load stress and truck load (plus 50% impact) stress are shown for a 30 x 3/8-in. pipe at 800 psi pressure, subject to external earth loads and a 10,000 lb. truck wheel load.

Fig. 12 shows the fill load stress in a 30 x 3/8-in. pipe at various internal pressures and under various depths of cover.

Fig. 13 shows the hoop stress, fill load stress, and Cooper's E-70 (plus 75% impact) stress for a 30 x 3/8-in. pipe at 800 psi pressure. In this case, it was assumed that the pipe was placed in a bored hole of essentially the same diameter as that of the pipe.

SELECTED BIBLIOGRAPHY

1. G. M. Braune, William Cain, and H. F. Janda, "Earth-Pressure Experiments on Culvert Pipe," Public Roads 10:153-69, (1929).

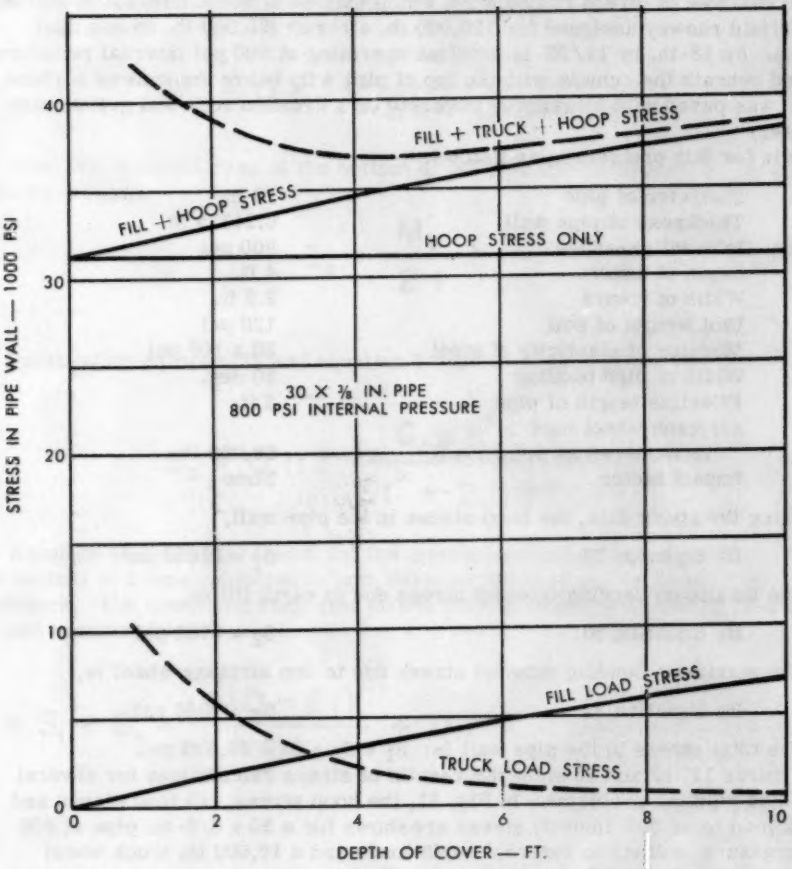

Fig. 11 Combined Stress in 30 x 3/8 in. Pipe at 800 psi Internal Pressure plus Earth and Highway Truck Load.

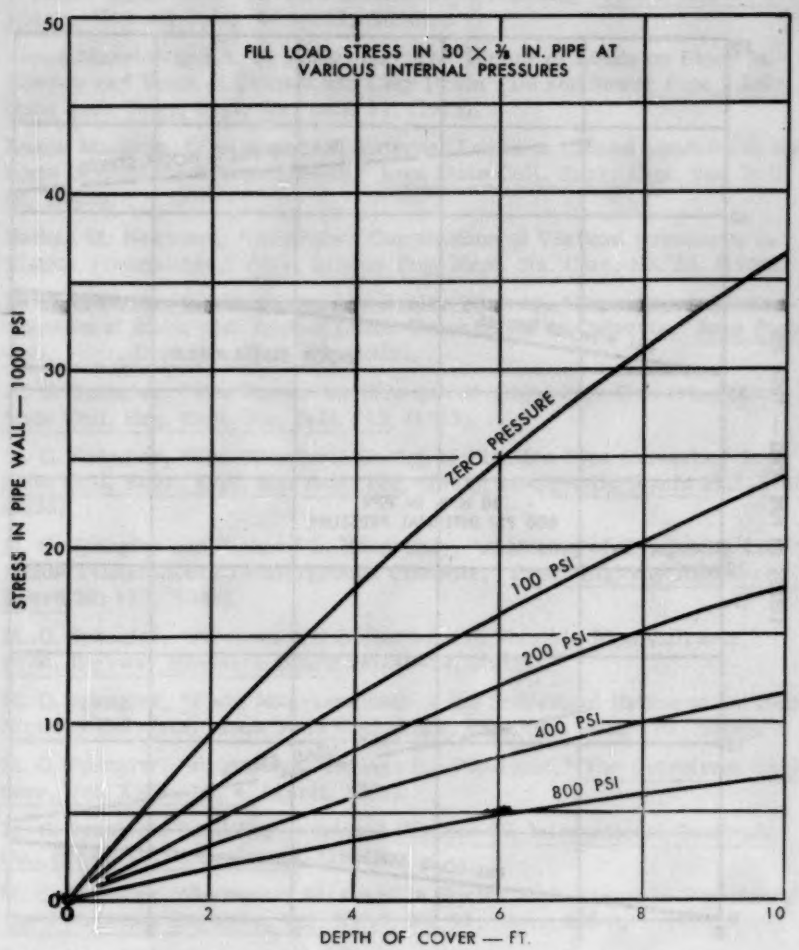

Fig. 12 Earth Load Stress in 30 x 3/8 in. Pipe at Various Internal Pressures.

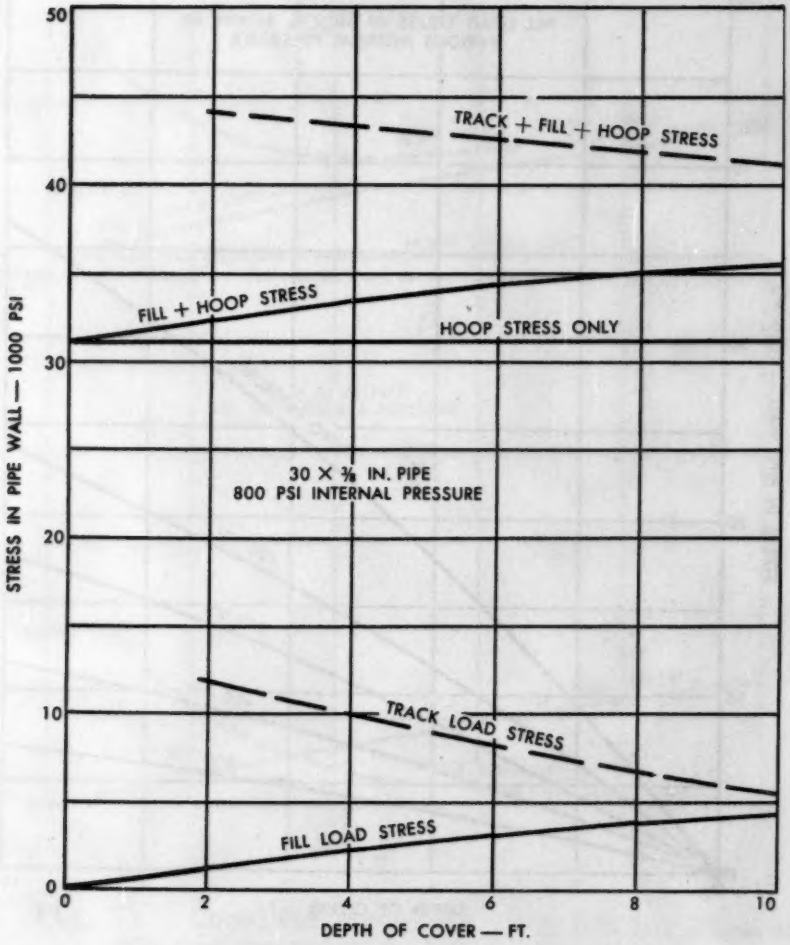

Fig. 13 Combined Stress in 30 x 3/8 in. Pipe at 800 psi Internal Pressure plus Earth and Railway Track Load.

2. William Cain, "Stresses and Deflections of Pipe Culverts," Public Roads 10: 169-76, (1929).

3. Claude W. L. Filkins and Edwin J. Fort, "Stresses and Deflections in Circular Rings under Various Conditions of Loading," Trans. Assoc. Civil Engrs., Cornell Univ. 4:99-112, (1896).

4. Anson Marston and A. O. Anderson, "The Theory of Loads on Pipes in Ditches and Tests of Cement and Clay Drain Tile and Sewer Pipe," Iowa State Coll. Engr. Expt. Sta. Bull. 31, (1913).

5. Anson Marston, "The Theory of External Loads on Closed Conduits in the Light of the Latest Experiments," Iowa State Coll. Engr. Expt. Sta. Bull. 96, (1930).

6. Nathan M. Newmark, "Simplified Computation of Vertical Pressures in Elastic Foundations," Univ. Illinois Eng. Expt. Sta. Circ. No. 24, (1935).

7. M. G. Spangler, Clyde Mason, and Robley Winfrey, "Experimental Determination of Static and Impact Loads Transmitted to Culverts," Iowa State Coll. Engr. Expt. Sta. Bull. 79, (1926).

8. M. G. Spangler, "The Supporting Strength of Rigid Pipe Culverts," Iowa State Coll. Eng. Expt. Sta. Bull. 112, (1933).

9. M. G. Spangler, "The Structural Design of Flexible Pipe Culverts," Iowa State Coll. Engr. Expt. Sta. Bull. 153, (1941); also Public Roads 18:217-31, (1938).

10. M. G. Spangler and Richard L. Hennessay, "A Method of Computing Live Loads Transmitted to Underground Conduits," Proc. Highway Research Board 26: 179, (1946).

11. M. G. Spangler, "Stresses and Deflections in Flexible Pipe Culverts," Proc. Highway Research Board 28:249-59, (1948).

12. M. G. Spangler, "Field Measurements of the Settlement Ratios of Various Highway Culverts," Iowa State Coll. Engr. Expt. Sta. Bull. 170, (1950).

13. M. G. Spangler, "Protective Casings for Pipelines," The Petroleum Engineer, Vol. XXIV, No. 4, (April, 1952).

14. M. G. Spangler, "Soil Engineering," Chapter 25, International Textbook Co., Scranton, Pennsylvania, (1951).

15. M. G. Spangler, "Secondary Stresses in Buried High Pressure Pipelines," The Petroleum Engineer, Vol. XXVI, No. 11, (Nov., 1954).

16. Ernest A. Slade, "Solution of a Pipeline Problem Using an Electronic Calculator," Pipeline Symposium, Division of Transportation, 33rd Annual Meeting, American Petroleum Institute, (Nov., 1953).

17. Arthur N. Talbot, "Tests of Cast-Iron and Reinforced-Concrete Culvert Pipe," Univ. Illinois Engr. Expt. Sta. Bull. 22, (reprinted, (1926).

Paper 1055 ST 5

Journal of the
STRUCTURAL DIVISION
Proceedings of the American Society of Civil Engineers

PRESTRESSED CONTINUOUS BEAMS AND FRAMES

P. B. Morice[1] and H. E. Lewis[1]
(Proc. Paper 1055)

SUMMARY

The paper describes methods of design for continuous prestressed concrete beams and frames, in particular those of uniform section. Methods for determining suitable tendon profiles are discussed and it is shown that certain displacements of these profiles are possible without affecting the stress conditions. In the case of frames consideration is given to the effects of varying direct forces on section design. The methods of allowing for transom shortening due to prestress are discussed.

A comparison is made between simply supported and continuous beam construction, it being shown that the use of continuity becomes advantageous only when large dead loads occur.

It is also shown that the adoption of alternating long and short spans, as has sometimes been suggested, does not lead to economy.

INTRODUCTION

The design of any statically indeterminate structure presents a problem of greater complexity than that of designing a similar structure of statically determinate form. In the latter case bending moments, shearing forces and reactions for any system of loading are determined by simple statics. However, when the structure is statically indeterminate, there are insufficient equations of equilibrium to determine the external restraints acting on the structure. This deficiency is overcome by considering the elastic and geometric properties of the members which form the structure. Thus a preliminary estimate has to be made of the relative sizes of the members, which may have to be adjusted when the analysis has been completed if the structure is to be economical. Should the members of the structure be of non-uniform section their elastic properties may not easily be determined in a general form, and the work becomes more laborious since numerical methods will often have to be used.

Note: Discussion open until February 1, 1957. Paper 1055 is part of the copyrighted Journal of the Structural Division of the American Society of Civil Engineers, Vol. 82, No. ST 5, September, 1956.

1. Cement & Concrete Assn., London, England.

In the design of prestressed indeterminate structures, the deformations due to prestress have also to be considered, which naturally increases the labour required. That these additional relationships must be included is at once obvious if the action of a prestressed tendon is thought of as being equivalent to an axial compression together with a transverse load whose value is proportional at all positions to the curvature of the prestressing tendon. The bending moments and shear forces due to this equivalent load are equally as indeterminate as those due to dead load and superimposed load.

Characteristics of Tendon Profiles

Concordant Profiles

It is readily seen that in a beam where there exists a centroidal prestressing force H the effects of a moment M upon the beam may be considered as the application of an eccentricity e to the centre of the prestressing force, where $e = \frac{M}{H}$.

Suppose some form of statically indeterminate beam is loaded and that the application of the load introduces no movement of the supports A, B, C and D (Figure 1); i.e. there is no vertical deflexion at any support and in addition no rotation at an encastered support. Normal methods of analysis enable the bending moment diagram to be determined from the known values of the loads and the properties of the beam (Figure 1).

From the previous statements it is evident that this bending moment, together with a uniform compression, could be produced in the unloaded beam by a prestressing tendon with an eccentricity e given by $e = \frac{M}{H}$ provided that there is no restraint to the longitudinal compressive strain at the points of support. Since the bending moments occurred with the beam undeflected at the supports, the introduction of the prestressing tendon in the shape of the bending moment profile would produce no tendency to deflect at A, B, C and D, and thus would introduce no support reactions in the otherwise unloaded beam. Such a tendon profile is called a "concordant" profile.

No particular load has been specified and it is thus evident that the argument applies to all loads and may be stated generally as follows:

> "A tendon profile corresponding to the bending moment diagram due to any possible loading on a rigidly supported statically indeterminate beam is a concordant tendon profile and a tendon laid to that profile will produce no support reactions provided there is no restraint to longitudinal compression."

It is to be noted that the term loading in this context applies to local bending couples acting on the beam as well as the more familiar transverse loading.

Concordant profiles developed from external loading conditions of the structure are not the only possible kind but they represent a very useful set for practical design purposes.

The name "concordant profile" follows from the fact that the centre of pressure in the unloaded beam lies on the tendon profile when this is concordant. In the case of an arbitrary tendon profile in an unloaded beam the points of support would not remain relatively undeflected without the application of external support reactions, whose effect is to introduce additional moments

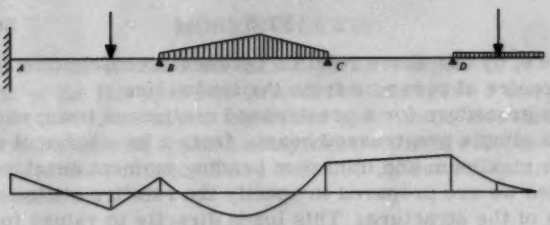

Figure 1: Loading and bending moment diagram of a continuous beam.

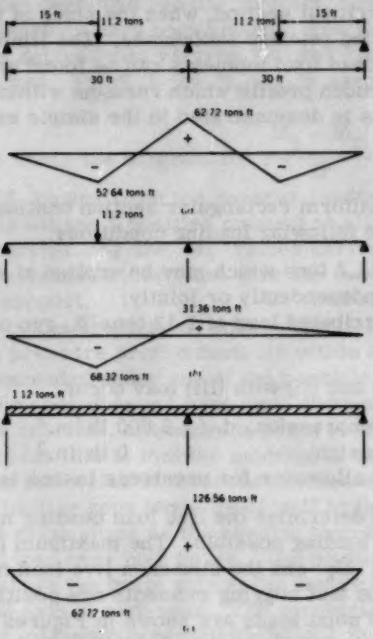

Figure 2: Loadings and bending moment diagram for a two-span continuous beam (example 1).

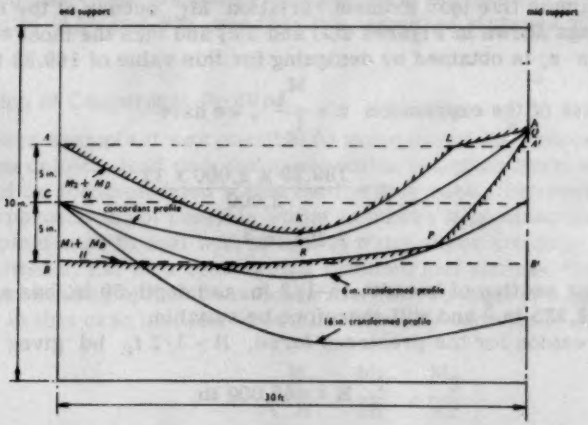

Figure 3: Zone limits and tendon profiles for one span of a two-span continuous beam (example 1).

which therefore, by our above relation between eccentricities and moments, displace the centre of pressure from the tendon line.

The design procedure for a prestressed continuous beam can thus follow from that of a simple prestressed beam: from a knowledge of all the loading conditions the maximum and minimum bending moment envelopes can be found, provided we are prepared to specify the relative stiffnesses of the various parts of the structure. This leads directly to values for the maximum live load moment variation in the various sections of the beam. With specified stress limits and a choice of section shape the minimum section size can be determined at the critical section, when the sizes of all other sections will follow from the specified relative stiffnesses. The limiting zone may now be determined since the dead load moments can be found and all that remains is to find a concordant tendon profile which remains within the limiting zone.

This design process is demonstrated in the simple example given below.

Example 1

Design a beam of uniform rectangular section continuous over two spans each 30 ft. long for the following loading conditions:

i) point loads of 11.2 tons which may be applied at either of the two mid-span sections independently or jointly;
ii) a uniformly distributed load of 1.12 tons/ft. run over both spans;
iii) dead load only.

Any combination of (i) and (ii) with (iii) may occur.

Design stress in compression, f_c, = 2,000 lb/in.^{2}
Design stress in tension = 0 lb/in.^{2}
(In this example no allowance for prestress losses is made.)

The first step is to determine the live load bending moment diagrams for the separate forms of loading possible. The maximum live load moment at any section is denoted M_1 and the minimum live load moment is denoted M_2 with the convention that hogging moments are positive. The bending moment diagrams for the point loads are shown in Figures 2(a) and 2(b) and the bending moment diagram for the uniformly distributed load is as shown in Figure 2(c).

The maximum live load moment variation M_L occurs at the mid support under loadings shown in Figures 2(a) and 2(c) and thus the most economic section modulus z, is obtained by designing for this value of 189.28 tons. ft.

Making use of the expression $z = \frac{M_L}{f_c}$, we have

$$z = \frac{189.28 \times 2{,}000 \times 12}{2{,}000}$$

$$= 2{,}271 \text{ in.}^3$$

A rectangular section of breadth 15-1/2 in. and depth 30 in. has a section modulus of 2,325 in.^{3} and will therefore be suitable.

The expression for the prestress force, $H = 1/2\, f_c\, bd$ gives

$$H = 465{,}000 \text{ lb.}$$

here b is the breadth of the beam and d is its depth.

An elevation of the left span has been drawn in Figure 3 where AA' and BB' are, respectively, the upper and lower core limits i.e. the distances from the centroid where an applied compressive force will just not introduce tensile stresses in the section. For a beam 30 in. deep they are both 5 in. from the centroidal axis.

On the upper limit, AA', the diagram for $\frac{M_2 + M_D}{H}$ has been drawn, the calculation of M_D, the dead load bending moment, now being possible since the beam section dimensions have been chosen. For the portion AKL of the curve the M_2 values derive from Figures 2(b) and 2(c), since these give the minimum moment values. From L to N, M_2 is zero, i.e. the loading is dead load only.

On BB' is drawn BPQ, the diagram for $\frac{M_1 + M_D}{H}$. The contribution of M_1 to the portion BP comes from the reverse loading to that shown in Figure 2(b), since this causes a positive moment at all sections of the left-hand span. For the portion PQ the M_1 values derive from the loadings of Figure 2(a) and 2(c) combined since these give the maximum δ values in the vicinity of the support.

The zone bounded by the two curves AKLN and PBQ is termed the limiting zone and the pressure profile must lie within it if the design stress limits are not to be exceeded under any of the possible forms of loading. It will be noticed that the zone does not have zero width at the mid support, i.e. N and Q do not quite coincide, although the beam section was economically designed. The reason for this is that the modulus of the beam section chosen is slightly larger than that which is theoretically necessary.

The shape of the limiting zone lends itself well to the introduction of a concordant profile of the same shape as the bending moment diagram due to a uniformly distributed load over both spans. The profile, CRN, is parabolic and the eccentricity above the beam axis at the centre support is twice the eccentricity below the axis at mid-span. The eccentricity at the centre support is -6.2 in. and at mid-span eccentricity is +3.1 in. where positive eccentricities are measured downwards. Application of any of the possible forms of loading will not cause the centre of pressure at any section to pass outside the core limits AA' and BB' and thus the permitted stresses will never be exceeded.

Determination of Concordant Profiles

In the above example it was possible to make use of the concordant profile derived from uniform load on a constant section two-span beam since this profile could be accommodated within the limiting zone. However, in some cases this approach is not possible whilst in others it is unnecessary.

The simplest case to deal with is that in which there are only two limiting loading conditions, i.e. on a beam with a symmetrical section, the maximum and minimum bending moment envelopes are derived from two loading conditions only. In this case the well-known eccentricity expression for simple beams

$$e = -\left\{\frac{M_D}{H} + \frac{M_1}{2H} + \frac{M_2}{2H}\right\}$$

may be used directly to determine the tendon eccentricity. Here, it will be remembered, eccentricities are measured position downwards, and M_D, M_1 and M_2 are respectively the dead load, maximum live load moments, hogging moments being considered positive. This profile will necessarily be concordant because $\frac{M_D}{H}$ is naturally concordant and the sum $\frac{M_1 + M_2}{H}$ is also concordant since it is derived from two actual bending moment diagrams. It must be noted here that the proposition is not generally true for sections which are not symmetrical.

The second method of determining concordant profiles is the one mentioned above whereby we may select a bending moment diagram due to an actual loading system on the structure—not the ones, however, for which the structures is designed—and introduce the tendon to this profile with any suitable absolute eccentricity magnitude required to fit the limiting zone.

A considerable body of tabulated and grouped information exists in the form of bending moments on statically indeterminate structures which is thus directly convertible to concordant profiles.

If neither of the previously mentioned methods of determining concordant profiles is applicable it becomes necessary to assume forms and analyse their effects until a suitable one is found. This process is admittedly a more laborious one and is to be avoided where possible. Nevertheless, it is practical in difficult cases. It is useful to recall the various theorems given below concerning bending moments which are equally applicable to tendon profiles.

1) The change of slope between two points in a beam is equal to the area of the $\frac{He}{EI}$ diagram between these points

$$\left[\frac{dy}{dx}\right]_{X_1}^{X_2} = \int_{X_1}^{X_2} \frac{He}{EI}\, dx$$

This expression is perfectly general and applies if H changes within the range under consideration, that is H can be a function of x.

2) The difference between the intercepts on the y axis of the tangents to the deflexion curve at the point x_1 and the point x_2 is equal to the moment of the $\frac{He}{EI}$ diagram about the origin.

$$\left[x\frac{dy}{dx} - y\right]_{X_1}^{X_2} = \int_{X_1}^{X_2} \frac{He}{EI}\, x\, dx$$

A useful corollary to this theorem is as follows.

The slope at the support of a beam is equal to the reaction at that support for an adjacent span considered as being simply supported and loaded with the $\frac{He}{EI}$ diagram,

$$\theta_o = \frac{1}{\iota} \int_o^{\iota} \frac{He\,(\iota - x)}{EI}\, dx$$

3) The tangents to the beam at x_1 and x_2 intersect on the vertical through the centre of area of the $\frac{He}{EI}$ diagram.

Linear Transformations

The above procedure, although theoretically satisfactory, may often lead to practical difficulties since the tendon profiles may include many sudden changes of direction which induce considerable tendon friction during stressing. This, in turn, results in tendons with very variable stress along their length and the impossibility of obtaining the full prestressing force in parts of the beam. Often this effect can be greatly reduced by the process of tendon transformation.

Let us consider again the beam shown in Figure 1, this time with all the loads and the intermediate supports removed (Figure 4). Now let us apply arbitrary concentrated loads to the points B and C. This will result in a bending moment diagram consisting of straight lines between these points (Figure 4).

A tendon placed in the beam with an eccentricity $e = -\frac{M}{H}$ would provide an exact balance to the transverse loads and the only stress which the material of the beam would experience would be a uniform longitudinal compression. Also by virtue of the balance of transverse forces the beam would remain undeflected. If the external loads at B and C are now replaced by the restraint of undeflecting supports the stresses and deflexions of the beam will be unaffected.

Thus we may generalize the above in the following proposition.

> "Any tendon profile consisting of straight lines between supports and having zero eccentricity at an end simple support will produce no bending in the beam but only a series of support reactions and a uniform longitudinal compression."

The above proposition also applies to the case in which the prestress force varies provided that the moment, $M = He$, consists of a series of straight lines which intersect at the support sections.

Any concordant profile may be combined with any transformation profile and by the principle of superposition we know that the bending stresses in the beam will be those due solely to the concordant profile and the support reactions due to the prestress only will be those due solely to the transformation profile.

The resulting profile will be the addition (or subtraction) of a straight line function to the concordant profile which is mathematically described as a linear transformation: hence the use of the word transformation.

The values of the support reactions are easily evaluated. Thus in the example of Figure 4 we have

$$\begin{aligned}
&\text{reaction at A} = H \cos \alpha \\
&\text{moment at A} = He \\
&\text{reaction at B} = -H (\cos \beta_1 + \cos \beta_2) \\
&\text{moment at B} = 0 \\
&\text{reaction at C} = H (\cos \gamma_1 + \cos \gamma_2) \\
&\text{moment at C} = 0 \\
&\text{reaction at D} = -H \cos \delta \\
&\text{moment at D} = 0
\end{aligned}$$

where a positive reaction is upwards.

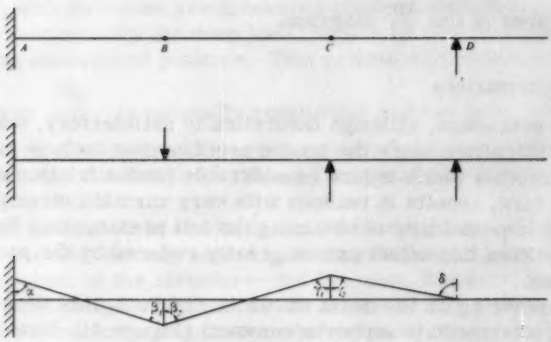

Figure 4: Transformation moments and support reactions in a continuous beam.

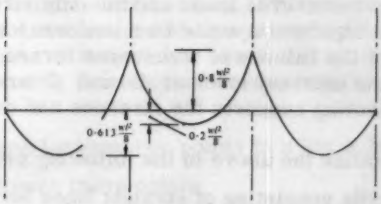

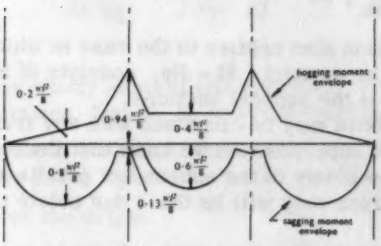

Figure 5: Moment ranges for two sets of loading conditions of a three-span continuous beam.

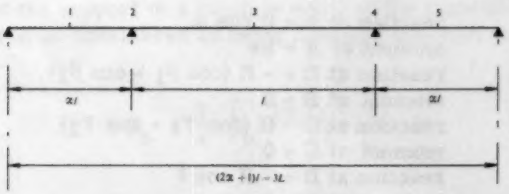

Figure 6: Symmetrical three-span continuous beam with unequal span lengths.

It is to be noted that a transformation will nearly always move the tendon profile outside the limiting zone. This is quite satisfactory provided the original concordant profile lay within the limiting zone, since the beam stresses remain those of the concordant profile.

The concordant profile determined for the beam in example 1 can be conveniently transformed by 6 in. downwards at the centre support (Figure 3) to reduce the angle change at that point. The support reactions will change by a reduction of 15,700 lb. at the centre which will cause an increase of 7,850 lb. at each outer support. This reduction at the centre support is equal to the reaction under dead load only. Therefore until the application of live load there will be no reaction at the centre support. The effect of such a transformation is that it is possible to lift the whole beam at its extremities without exceeding the permissible stresses.

The concordant tendon can in fact be transformed downwards by as much as 16 in. at the centre support which would give a reaction reduction of 40,500 lb. Since this exceeds the reaction due to dead load the support would have to be capable of exerting a downward reaction on the beam of 24,800 lb.

The Effects of Continuity on Live Load Moments

Significant economies result in normal design in reinforced concrete by using continuous beams since the absolute values of bending moments under the same loading conditions are less in the case of continuous beams than in the case of simple beams. This leads to the use of smaller sections. However, in prestressed concrete it is not absolute values of bending moments but ranges of bending moment which usually have to be considered.

Consider the case of a beam of constant section continuous over three equal spans. If the only cases of loading are those of a uniform load over the whole structure or zero load, then the maximum moment will also be the maximum moment variation. This occurs at the inner supports (Figure 5a) and is a positive moment of $0{\cdot}8\,\frac{w\ell^2}{8}$ where w is the rate of loading and ℓ is the span length. On the basis of this loading the continuous beam would lead to a saving since there is a 20 per cent reduction in the maximum moment variation over the comparable simple beam system. If, however, the loading may also include cases where not all of the spans are loaded there are several bending moments to be considered for each section of the beam and an envelope may be drawn (Figure 5b). Here we find that the maximum range of moment also occurs at an internal support and has limits $+0{\cdot}94\,\frac{w\ell^2}{8}$ δ to $-0{\cdot}13\,\frac{w\ell^2}{8}$ δ, giving a variation of $1{\cdot}07\,\frac{w\ell^2}{8}$. In this case continuity leads to larger moment variations than those in a similar statically determinate case.

As the number of spans increase the effect can be shown to increase and the range of moment reaches $1{\cdot}15\,\frac{w\ell^2}{8}$ for five or more spans (Table 1).

Table 1: Maximum bending moment variation, expressed as a coefficient of $\frac{w\ell^2}{8}$, at any support of a continuous beam having any number of equal spans

Spans to the right	Spans to the left: one	two	three	infinite
one	1	1·07	1·07	1·07
two	1·07	1·14	1·15	1·15
three	1·07	1·15	1·15	1·15
infinite	1·07	1·15	1·15	1·15

Variation in Span Length

Let us now consider the effect of variation of span length upon the moment conditions in continuous beams. A general treatment is very involved but recourse may be made to the three span example given in the previous section, making the internal span length ℓ and the external span lengths each $\alpha\ell$. Assuming that a uniform loading may occur on any or all of the spans the moment variations at the critical points 1 to 5, Figure 6 can be shown to be

$$M_{L_{(1,5)}} = \left(\frac{\alpha^3 + 3\alpha^2 + 1}{2\alpha + 3}\right) \frac{w\ell^2}{8}$$

$$M_{L_{(2,4)}} = 2\left(\frac{2\alpha^4 + 3\alpha^2 + 2\alpha + 1}{4\alpha^2 + 8\alpha + 3}\right) \frac{w\ell^2}{8}$$

$$M_{L_{(3)}} = \left(\frac{2\alpha^3 + 2\alpha + 1}{2\alpha + 3}\right) \frac{w\ell^2}{8}$$

In Figure 7 these expressions have been plotted against α.

In the case of equal spans, $\alpha = 1$, the values of the above expressions become $\frac{w\ell^2}{8}$, $1{\cdot}07\,\frac{w\ell^2}{8}$ and $\frac{w\ell^2}{8}$ respectively as obtained in section 6.

As α tends to zero the effect of the side spans is to give end fixity to the mid-span and thus, when $\alpha = 0$, we have

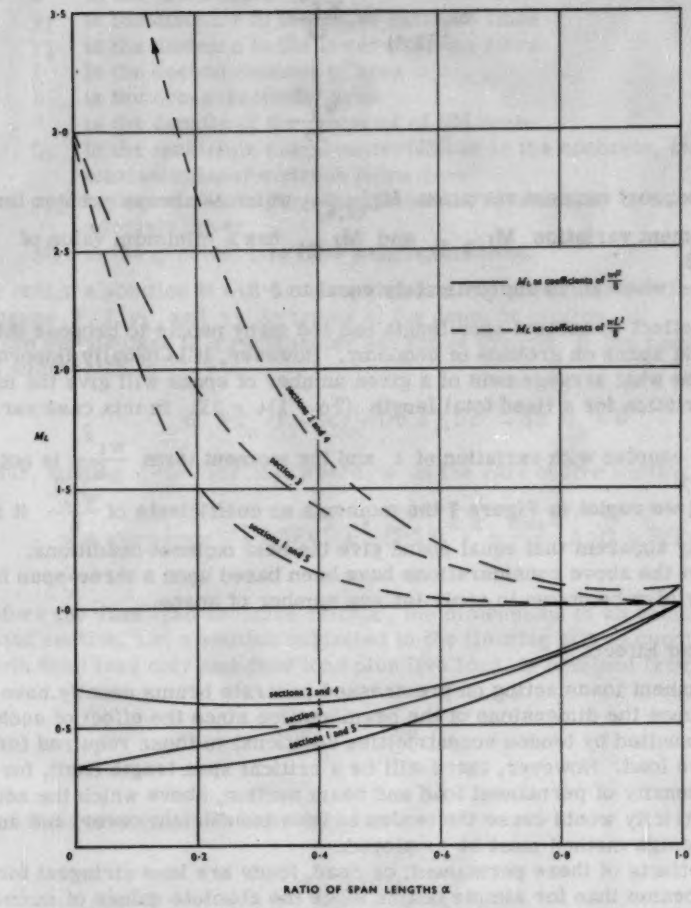

Figure 7: The effect of span length variations on the maximum live load moment ranges.

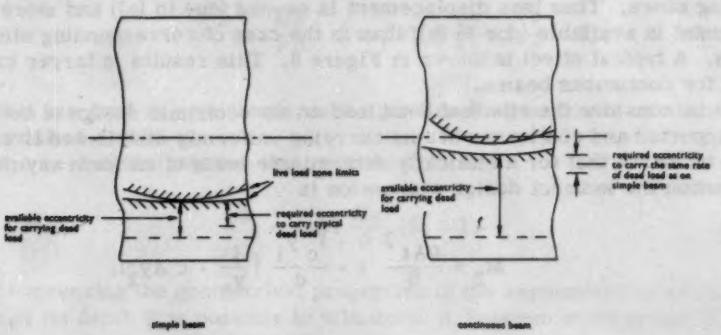

Figure 8: The available and required dead load tendon eccentricities in simple and continuous beams.

$$M_{L_{(2,4)}} = \frac{w\ell^2}{12}$$

$$M_{L_{(3)}} = \frac{w\ell^2}{24}$$

The support moment variation $M_{L_{(2,4)}}$, which is always greater than the span moment variation $M_{L_{(1,5)}}$ and $M_{L_{(3)}}$ has a minimum value of $0{\cdot}59\frac{w\ell^2}{8}$ when α is approximately equal to 0·3.

This effect in unequal span length has led many people to propose the use of unequal spans on grounds of economy. However, it is usually important to determine what arrangement of a given number of spans will give the minimum variation for a fixed total length $(2\alpha + 1)\ell = 3L$. In this case variation of α is coupled with variation of ℓ and the moment term $\frac{w\ell^2}{8}$ is not constant. If we replot in Figure 7 the moments as coefficients of $\frac{wL^2}{8}$ it is immediately apparent that equal spans give the best moment conditions.

Whilst the above considerations have been based upon a three-span beam they may also be shown to apply for any number of spans.

Dead Load Effects

Permanent loads acting on prestressed concrete beams usually have no influence upon the dimensions of the beam section since the effect of such loads can be annulled by tendon eccentricities additional to those required for carrying live load. However, there will be a critical span length limit, for a given intensity of permanent load and beam section, above which the additional eccentricity would cause the tendon to have insufficient cover, and an indirect design method must be employed.

The effects of these permanent, or dead, loads are less stringent for continuous beams than for simple beams since the absolute values of moments in continuous beams are less. This means that (a) the additional eccentricity required to carry a given dead load will be less and (b) the reduced absolute values of the live load moments will mean less eccentricity of the tendon limiting zones. Thus less displacement is needed (due to (a)) and more displacement is available (due to (b)) than in the case of corresponding simple beams. A typical effect is shown in Figure 8. This results in larger critical spans for continuous beams.

Let us consider the effect of dead load on the economic design of both simply supported and continuous beams carrying uniformly distributed live loads. It can be shown that for a statically determinate beam of uniform asymmetrical section the indirect design expression is

$$M_2 = \frac{\rho A \ell^2}{8} = -\frac{f_c y_1}{d}\left[\frac{I}{y_2} + c\,Ay_2\right] \qquad (1)$$

where d is the beam depth
y_1 is the distance to the upper extreme fibre
y_2 is the distance to the lower extreme fibre
I is the second moment of area
A is the cross-sectional area
ρ is the density of the material of the beam
f_c is the maximum compressive stress in the concrete, the maximum tensile stress being zero
cy_2 is the maximum permissible tendon eccentricity to allow adequate cover
and M_2 is the greatest live load sagging moment.

To obtain a solution it will be necessary for any particular section shape to express A, I, y_1 and y_2 in terms of the depth of section, d.

In the simple case of a rectangular section of breadth b the resulting reduced expression is

$$d^2 b f_c (1 + 3c) - 1{\cdot}5\, d \rho b \iota^2 + 12\, M_2 = 0$$

and thus, writing $-\frac{w\iota^2}{8}$ for M_2, where w is the rate of live loading,

$$d = \frac{1}{2(1 + 3c)f_c} \left[1{\cdot}5\rho\iota^2 + \sqrt{(1{\cdot}5\rho\iota^2)^2 + \frac{6w\iota^2}{b} f_c (1 + 3c)} \right] \quad (2)$$

Before the dead load becomes critical, the dimensions of an economically designed section, i.e. a section subjected to the limiting stress conditions under both dead load only and dead load plus live load, is obtained from

$$\frac{w\iota^2}{8} = \frac{If_c}{y_2} \quad (3)$$

which for a rectangular section reduces to

$$d = 0{\cdot}867\iota\sqrt{\frac{w}{bf_c}} \quad (4)$$

It can also be shown that the limit to the use of expression (3) is when

$$\iota^2 = \frac{8f_c}{\rho d} \left[cy_1 y_2 + \frac{Id}{Ay_2} \left(\frac{y_1}{d} - 1\right) \right] \quad (5)$$

i.e. when the dead moment requires the prestressing tendon to be at the lowest permitted depth.

For a rectangular section this reduces to

$$\iota^2 = 0{\cdot}67 \frac{df_c}{\rho} (3c - 1) \quad (6)$$

By expressing the geometrical properties of the asymmetrical section in terms of its depth it is possible to eliminate d between expressions (3) and

(5) and obtain a limiting value for the span length ℓ in terms of the permissible maximum stress, the applied load per unit area, $\frac{w}{b}$, the density of the concrete and the limiting depth factor, c.

Eliminating d between expressions (4) and (6) for a rectangular beam gives

$$\ell = \frac{0{\cdot}578\ (3c - 1)}{\rho} \sqrt{\frac{wf_c}{b}} \qquad (7)$$

Thus for any given loading and stress condition the required depth of a rectangular beam of span ℓ is given by expression (4) for span lengths up to that of expression (7) and thereafter by expression (2).

It is possible to obtain similar expressions for continuous beams and a comparison may be made on this basis between statically determinate and indeterminate construction.

To make this comparison under the most unfavourable conditions for continuity we will consider only the case where there are five or more continuous spans. It can be shown that the critical section for maximum cable eccentricity is at the first interior support. The maximum dead load moment occurs at this section and, in spite of M_L being only $1{\cdot}07\frac{w\ell^2}{8}$, M_1 is greater ($0{\cdot}96\frac{w\ell^2}{8}$) than it is at any other section, even where M_L has its maximum value of $1{\cdot}15\frac{w\ell^2}{8}$. Thus the maximum numerical bending moment due to both dead and live load occurs at the first interior support.

Figure 9 shows an elevation in the region of a first interior support of a beam, of more than five equal spans, having an asymmetrical section whose centre of area is nearer the upper than the lower face. On the upper and lower core limits are drawn diagrams of $\frac{M_2}{H}$ and $\frac{M_1}{H}$ respectively. A concordant pressure profile may be positioned within the zone bounded by these two lines and the addition of ordinates of $\frac{M_D}{H}$ will give the desired concordant tendon profile. This profile has an upper limit of $-c_1y_1$ and a lower limit of c_2y_2 outside which it must not lie if adequate cover is to be provided. If the centre of pressure is at the lower limit, 0, of the above mentioned zone at the support we can write the following expression for the maximum permissible value of M_D

$$\frac{M_D}{H} = c_1 y_1 + \frac{I}{Ay_1} - \frac{M_1}{H}$$

and since the dimensions of the section are calculated for $M_L = 1{\cdot}15\frac{w\ell^2}{8}$ we have

$$M_L = 1{\cdot}15\frac{w\ell^2}{8} = H\left[\frac{I}{Ay_1} + \frac{I}{Ay_2}\right]$$

and thus

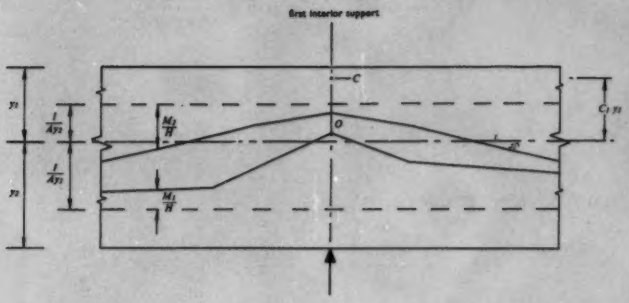

Figure 9: Available dead load eccentricity at the first interior support of a beam of more than five spans.

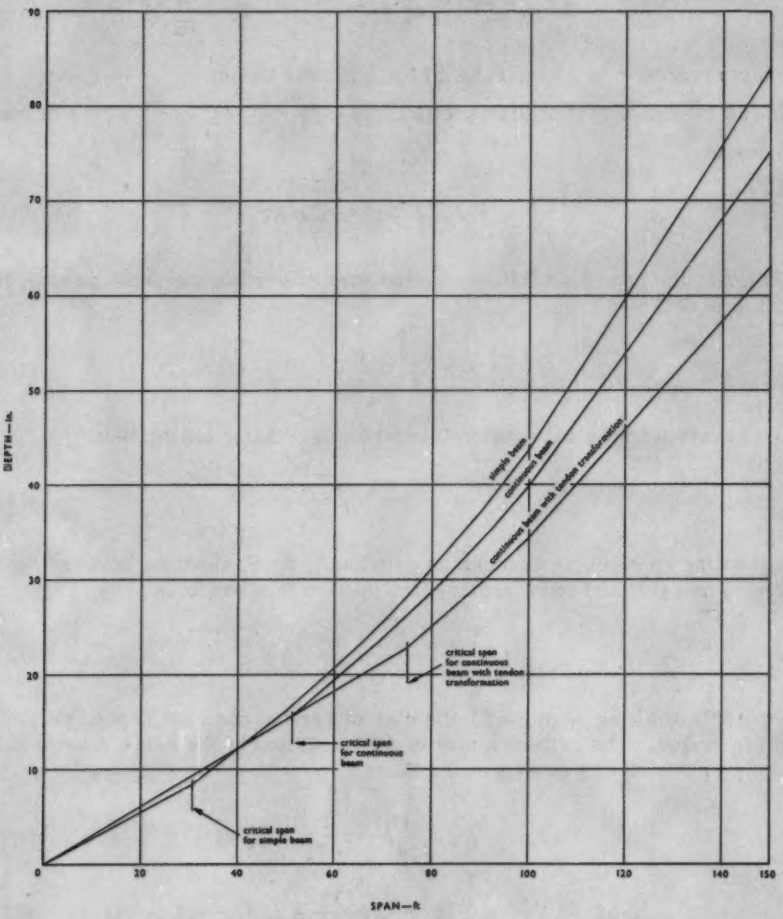

Figure 10: Depth to span relationships showing the critical values above which the dead load influences the section depth.

$$M_1 = 0{\cdot}96 \frac{w\iota^2}{8} = 0{\cdot}835 \frac{HId}{Ay_1 y_2}$$

Writing

$$H = \frac{y_1}{d} Af_c \quad (y_1 < y_2)$$

the expression for M_D reduces to

$$M_D = \frac{c_1 y_1^2}{d} Af_c + \frac{If_c}{d} \left[1 - 0{\cdot}835 \frac{d}{y_2}\right]$$

and since at the first interior support $M_D = 0{\cdot}85\ \rho A \frac{\iota 2}{8}$ we have

$$\iota 2 = \frac{9{\cdot}4 f_c}{\rho d} \left[c_1 y_1^2 + \frac{I}{A} (1 - 0{\cdot}83 \frac{d}{y_2}) \right] \qquad (8)$$

which corresponds to expression (5) for a simple beam.

In the case of a rectangular section, $y_1 = y_2 = \frac{d}{2}$, $c_1 = c_2 = c$ the above reduces to

$$\iota 2 = \frac{0{\cdot}785\ d f_c}{\rho} (3c - 0{\cdot}67) \qquad (9)$$

Prior to the dead load influencing the size of section the depth to span relationship is obtained from

$$1{\cdot}15 \frac{w\iota^2}{8} = \frac{If_c}{y_2} \qquad (10)$$

which corresponds to expression (3) and for a rectangular section

$$d = 0{\cdot}93\iota \sqrt{\frac{w}{bf_c}} \qquad (11)$$

The limiting span length is found as previously by eliminating between expressions (8) and (10) and for a rectangular section this becomes

$$\iota = \frac{0{\cdot}73 (3c - 0{\cdot}67)}{\rho} \sqrt{\frac{w}{b} f_c} \qquad (12)$$

Beyond this limiting span length the size of section does not depend only on the M_L value. The criterion now is the limitation of the cable eccentricity to $- c_1 y_1$ which can be expressed thus:

$$\frac{M_D}{H} + \frac{M_1}{H} = \frac{I}{Ay_1} + c_1 y_1$$

i.e. $$0{\cdot}85\ \rho A \frac{\iota^2}{8} + 0{\cdot}96\ w \frac{\iota^2}{8} = \frac{y_1}{d} A f_c \left[\frac{I}{Ay_1} + c_1 y_1 \right] \qquad (13)$$

In the case of a rectangular section this may be reduced to a quadratic in d giving

$$d = \frac{1}{2(1+3c)f_c}\left[1{\cdot}275\,\rho l^2 + \sqrt{(1{\cdot}275\rho l^2)^2 + 5{\cdot}76\,\frac{w}{b}\,l^2 f_c(1+3c)}\right] \quad (14)$$

It is now possible to compare how dead load affects the simple beam and the continuous beam of rectangular cross-section.

Expressions (4) and (11) show that, as previously appreciated, a greater depth is required for the continuous beam when dead load is not critical, while expressions (2) and (14) show the converse to be true when dead load is critical. Expressions (7) and (12) show that the dead load becomes critical at a shorter span length in the simple beam.

Thus it would appear that the longer the span the greater is the advantage to be gained from continuity, once the critical span has been exceeded.

Let us consider rectangular simple beams and infinitely continuous beams subjected to an applied surface load of 220 lb/ft^2. The permissible stress f_c = 2,000 lb/in.^{2}, ρ = 150 lb/ft^3, and $c = \frac{2}{3}$. Substituting these values in expressions (2), (4) and (7) for the simple beam and (11), (12) and (14) for the continuous beam, a graph (Figure 10) has been plotted relating the depths of section to the span length.

The limiting span lengths are 30 ft 5 in. and 51 ft 3 in. for the simple and continuous beams respectively. For spans longer than 30 ft 5 in. the rate of increase of depth of the simple beam is greater than that of the continuous beam. This results in the depth of the simple beam being greater than the depth of the continuous beam for spans longer than 41 ft 6 in. Between 55 ft span and 150 ft span the depth of the continuous beam section varies between 94 per cent and 90 per cent of the depth of the simple beam. Thus economy can be achieved by making use of continuity in the case of long spans where the dead load influences the size of the sections.

This economy may be extended even further by applying linear transformations to the tendon profile. For example a case may arise where, because of a large dead load, ordinary design on the basis of M_L would result in the tendon being outside the beam at the first interior support. The indirect design expression (14) would then have to be employed to determine the dimensions of a section which could accommodate the tendon. However, in the case of the first design, because of the excess depth available below the tendon at the mid-span section, a downward transformation could be applied. This would bring the tendon within the beam at the first interior support and yet would not cause it to have an excessive downward eccentricity at mid-span. Thus it may be seen that the limiting span length could be increased. When indirect design becomes necessary a smaller section than previously obtained is possible for any span length by application of a transformation.

Figure 11 shows the elevation of the end span of a continuous beam having an infinite number of spans. The asymmetrical beam section has $y_2 > y_1$. On the upper and lower core limits are drawn respectively the $\frac{M_2}{H}$ and $\frac{M_1}{H}$ diagrams. The limiting tendon eccentricities are $-c_1 y_1$ and $c_2 y_2$.

The eccentricity, e , at the support section is given by

$$e_1 = -\frac{M'_1}{H} - \frac{M'_D}{H} + \frac{I}{Ay_1} \qquad (15)$$

and the corresponding eccentricity at the mid-span is

$$e_2 = -\frac{M''_2}{H} - \frac{M''_D}{H} - \frac{I}{Ay_2} \qquad (16)$$

It has already been seen that when $e_1 = -c_1 y_1$ e_2 will generally be less than $c_2 y_2$. This depends on the value of c_2 but is generally true.

Substituting $M'_1 = 0{\cdot}96 \frac{w\iota^2}{8}$, $M'_D = 0{\cdot}85\rho A \frac{\iota^2}{8}$ and $H = \frac{y_1}{d} A f_c$ in expression (15) and remembering that $1{\cdot}15 \frac{w\iota^2}{8} = \frac{Hld}{Ay_1y_2}$ we have

$$e_1 = -\frac{I}{Ay_2}\left[\frac{0{\cdot}835d}{y_1} - \frac{y_2}{y_1}\right] - \frac{0{\cdot}85\rho\iota^2}{8} \cdot \frac{d}{y_1 f_c} \qquad (17)$$

and similarly with $M''_2 = -0{\cdot}789 \frac{w\iota^2}{8}$ and $M''_D = -0{\cdot}575\rho A \frac{\iota^2}{8}$ we have

$$e_2 = \frac{I}{Ay_2}\left[0{\cdot}685 \frac{d}{y_1} - 1\right] + 0{\cdot}575 \frac{\rho\iota^2}{8} \cdot \frac{d}{y_1 f_c} \qquad (18)$$

Now if $|e_1| > c_1 y_1$ but $e_2 < c_2 y_2$ a transformation of the tendon profile will be possible and the limiting condition will be when

$$-(e_1 + c_1 y_1) = 2(c_2 y_2 - e_2) \qquad (19)$$

i.e. when the depth available for transformation at mid-span is one half of the distance through which the cable has to be transformed downwards at the support to bring it to the limiting position. This follows since the transformation is linear and has zero value at the free support.

Substituting from expressions (17) and (18) in (19) gives an expression relating the section dimensions, to the span ι

$$\iota^2 = \left[2c_2y_2 + c_1y_1 - \frac{I}{Ay_2}\left(\frac{2{\cdot}205\,d - y_2}{y_1} - 2\right)\right] \frac{4\,y_1 f_c}{\rho d} \qquad (20)$$

and with $c_1 = c_2 = c$ this reduces for a rectangular section to

$$\iota^2 = \frac{df_c}{\rho}(3c - 0{\cdot}47) \qquad (21)$$

But expression (10) again holds and eliminating d between expressions (10) and (20) gives the limiting span length. For a rectangular section, using expressions (11) and (21), we have

$$\iota = \frac{0{\cdot}93\,(3c - 0{\cdot}47)}{\rho} \sqrt{\frac{w}{b} f_c} \qquad (22)$$

Beyond the above limiting span an indirect design method must be employed.

This requires that

$$\frac{M'_D}{H} + \frac{M'_1}{H} = c_1 y_1 + \frac{I}{Ay_1} + \delta \qquad (23)$$

where δ is the height of the centre of pressure above the limiting eccentricity - $c_1 y_1$. For the transformation of the tendon to be possible

$$\delta = 2\left[c_2 y_2 + \frac{I}{Ay_2} + \frac{M''_2 + M''_D}{H}\right] \qquad (24)$$

and substitution in expression (23) with the appropriate values for M'_1, M'_2, M'_D and M''_D gives on reduction

$$2{\cdot}0\,\rho A\frac{\iota^2}{8} + 2.538\,w\frac{\iota^2}{8} = \frac{y_1}{d}\,Af_c\left[c_1 y_1 + 2c_2 y_2 + \frac{I}{A}\left(\frac{1}{y_1} + \frac{2}{y_2}\right)\right] \qquad (25)$$

or for a rectangular section with $c_1 = c_2 = c$

$$d = \frac{1}{2f_c(1+3c)}\left[\rho\iota^2 + \sqrt{(\rho\iota^2)^2 + 5{\cdot}076\,\frac{w}{b}\,\iota^2 f_c(1+3c)}\right] \qquad (26)$$

which gives a smaller depth than expression (14).

Substituting the values for $\frac{w}{b}$, f_c, ρ and c used previously the variation of d with span length is shown in Figure 10. Expression (11) is used initially and the limitation to its use is given by expression (22). Thereafter the beam is indirectly designed and expression (26) is used. There is seen to be a large economy through the application of transformation. At 150 ft the required depth is only 75 per cent of the equivalent simple beam depth.

It should be noted that an approximation is used in the development of these transformation expressions. It has been assumed that the degree of transformation is governed by conditions at mid-span. This would be so if the absolute value of $M'_2 + M''_D$ was a maximum at this section, whereas it actually occurs slightly nearer the end support, its precise position depending on the relative magnitudes of M''_2 and M''_D. However the loss of accuracy is small especially since, at a point nearer the end support than the mid-span, the change in eccentricity due to the application of a linear transformation to the tendon profile would be less than one half of the change at the first interior support.

PORTAL FRAMES

Prestressed Portal Frames

In structures, such as portal frames, where the overall longitudinal contraction due to prestressing sets up support reactions and where loading affects the value of the prestressing force the usual simplifications of

prestressed beam design are not applicable and a more complex analysis may have to be used.

The data upon which the engineer will have to base his design will be the loading conditions and the overall shape of the structure. From these the first requirement will be the maximum and minimum live load bending moment diagrams. As is always the case in a statically indeterminate structure these will be dependent upon the stiffness ratios of the structure and a choice of the relative sizes of members, which may require later revision, will have to be made.

From the choice of stiffness ratios it is possible to obtain, by normal analysis, the diagrams of maximum and minimum bending moment at each section and the direct loads in the members which correspond with these moment conditions.

The maximum moment variation on each member may be found and the required size of sections determined such that all members are capable of withstanding their moment variations.

This latter procedure will not, in general, be as direct as in the case of beams because the value of the direct compression will vary for different loadings. The direct force in the members may be considered as made up of three parts: that due to the prestress alone, H_P, that due to the dead load, H_D, and that due to the live load, H_1 for maximum moment condition M_1, and H_2 for minimum moment condition M_2. We note that the worst moment conditions may be due to different loadings at different sections and thus the operative values of H_1 and H_2 may also vary from section to section.

Thus the total compression H in a member may be written for the loading $M_1 + M_D$

$$H = H_P + H_D + H_1 = H_A \text{ (say)} \tag{27}$$

and for $M_2 + M_D$

$$H = H_P + H_D + H_2 = H_B \text{ (say)} \tag{28}$$

Using the accepted stress limits of zero tension and a maximum compressive stress f_c, we assume that the limits will be reached when the compression is H_B (Figure 12(b)). A slightly lower compressive stress f_1 will be reached in the case of H_A (Figure 12(a)).

Thus the maximum moment variation ($M_1 = M_2$), or M_L, between the two diagrams in Figure 12 is equal to the difference between the moments of the compressive forces.

$$M_L = H_A \delta_A + H_B \delta_B \tag{29}$$

where δ_A and $-\delta_B$ are the core limits $\frac{I}{Ay_1}$ and $-\frac{I}{Ay_2}$ respectively. If we restrict our study to rectangular sections these are equal to $\frac{d}{6}$ and $-\frac{d}{6}$.

With this restriction using expression (27) and (28) we can rewrite expression (29) as

$$M_L = (H_P + H_D)\frac{d}{3} + (H_1 + H_2)\frac{d}{6} \tag{30}$$

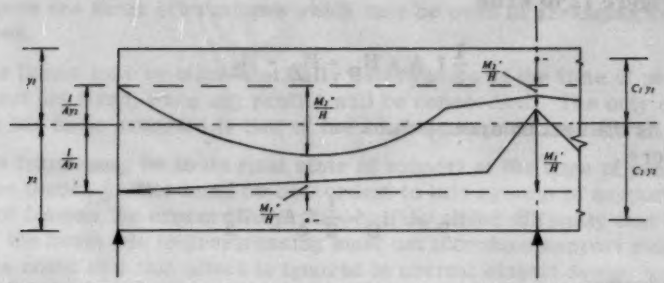

Figure 11: The end span of a continuous beam with an infinite number of spans.

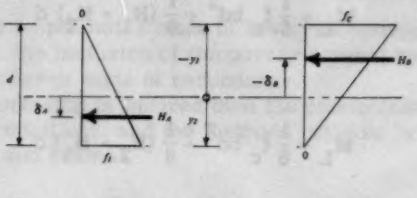

Figure 12: Limiting stress diagrams for frame sections.

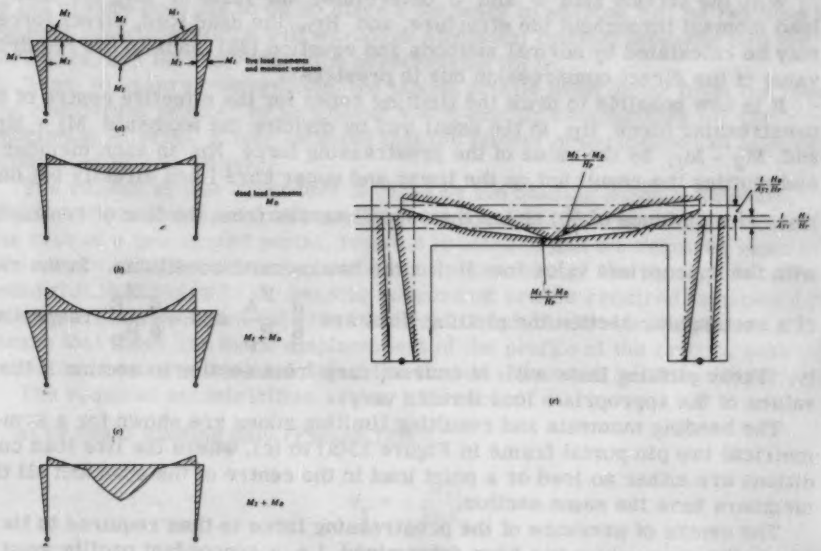

Figure 13: Moment diagrams and limiting zones for a two-pinned prestressed portal.

Further, since the assumed section shape is symmetrical (rectangular) we may use Figure 12 to write

$$\frac{1}{2} f_c A = H_P + H_D + H_2 \qquad (31)$$

where A is the section area (bd).

Therefore

$$H_P + H_D = \frac{1}{2} f_c A - H_2 \qquad (32)$$

and (30) becomes

$$M_L = \frac{1}{6} f_c \, bd^2 + \frac{1}{6} (H_1 - H_2) \, d$$

but if $H_A > H_B$ (33)

$$M_L = \frac{1}{6} f_c \, bd^2 + \frac{1}{6} (H_2 - H_1) \, d$$

It will be seen that the first term is the familiar result from beam theory and that the second term is always negative. Thus the section will be somewhat larger than that of a beam. All the quantities in equation (33) are known, with the exception of b and d. A choice of either gives the other.

With the section size b and d determined, the value of M_D, the dead load moment throughout the structure, and H_D, the dead load, direct forces may be calculated by normal methods and equation (32) leads to the required value of the direct compression due to prestress.

It is now possible to draw the limiting zones for the effective centre of the prestressing force H_P in the usual way by dividing the moments $M_1 + M_D$ and $M_2 + M_D$ by the value of the prestressing force H_P in each member and plotting the result not on the lower and upper core lines directly but on lines at a distance of $\frac{H}{H_P}$ times the core distances from the line of centroids with the appropriate value for H for the two moment conditions. In the case of a rectangular section the plotting lines are $\frac{d}{6} \frac{H_A}{H_P}$ and $-\frac{d}{6} \frac{H_B}{H_P}$ respectively. These plotting lines will, of course, vary from section to section if the values of the appropriate load thrusts vary.

The bending moments and resulting limiting zones are shown for a symmetrical two pin portal frame in Figure 13(a) to (c), where the live load conditions are either no load or a point load in the centre of the span and all the members have the same section.

The centre of pressure of the prestressing force is then required to lie within the zone which has been determined, i.e. a concordant profile must be found which lies within the given limiting zone. A concordant profile, it will be remembered, is a profile which allows a tendon to be stressed without introducing support reactions and the centre of pressure is therefore coincident with the tendon position.

Concordant Profiles

There are three alternatives which may be used in arranging concordant profiles.

a) The frame may be made statically determinate at the time of prestressing e.g. feet not fixed, when any profile will be concordant. The only condition which has to be satisfied is that of the zone limits, and no difficulty arises.

b) The frame may be in its final state of support at the time of prestressing and the tendon profile must be concordant to this system of support. In the case of frames the concordant profile has the added difficulty that the shortening of the beam due to prestressing must not introduce support reactions. (It may be noted that this effect is ignored in normal elastic design and has been ignored here in the cases of live loading since the effect is very small. The prestressing contractions must however not be ignored in general.)

c) The frame may be put into a state of lower redundancy for the operation of prestressing (e.g. the inclusion of temporary hinges) and the profile must be concordant to this lower state of redundancy.

If the beam shortening is ignored then the concordant profile has to satisfy only the pending conditions, and the methods outlined in section 4 apply equally well to frames and beams.

Total Concordance

When the members of a structure are prestressed they contract in resisting the average longitudinal compression. In the normal design of beams this effect is unimportant and need not be considered but in the case of frames it is not always possible to do so since a tendency to shorten will be resisted by support reactions, which will introduce additional bending stresses into the structure, and tend to reduce the prestressing force.

Thus, to ensure concordance, the tendon profile must differ from the "bending concordant profile" by an amount which exactly compensates for the shortening effects. It may be noted that the effects of shrinkage can also be eliminated in this manner.

The amount of this difference is given by the bending moment diagram, which will produce a separation at the feet equal to the beam shortening. In the case of a two-pinned portal, rotation is allowed and the required separation can be obtained either by bending of the beam or of the legs. It is to be noted that the change to the bending concordant profile required to produce the feet separation must not take the final profile outside the limiting zone. This means that there can be no displacement of the profile at the critical point or points and accounts for the form of the chosen separation profiles (Figure 14).

The required eccentricities are as follows:

a) by beam bending only (Figure 14(a))

$$e_1 = -\frac{\pi I_1}{2hA_1} \tag{34}$$

b) by leg bending only (Figure 14(b))

$$e_2 = -3\frac{H_1 I_2 L}{H_2 A_1 h^2} \tag{35}$$

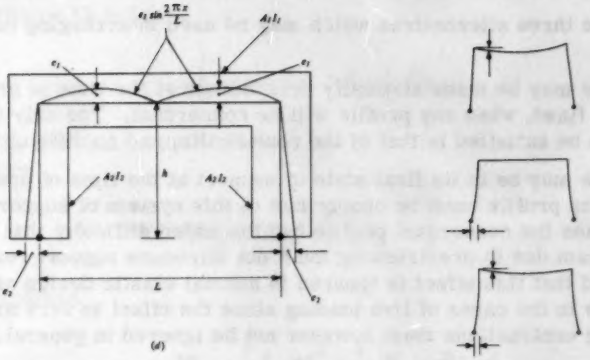

Figure 14: Separation profiles for two-pinned portals.

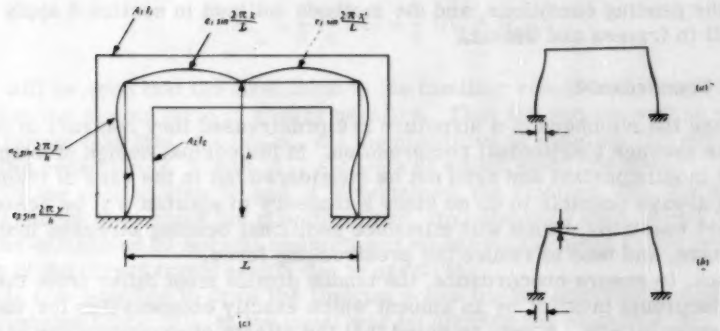

Figure 15: Separation profiles for fixed portals.

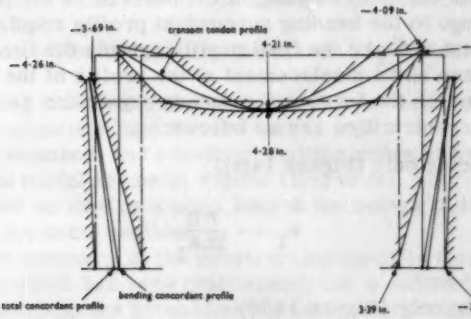

Figure 16: Limiting zones and tendon profiles for a two-pinned portal (example 2).

c) by combined beam and leg bending (Figure 14(c)) either

$$-e_1 = \frac{\pi I_1}{2hA_1}\left[1 + \frac{1}{3}\frac{A_1}{I_2}\frac{H_2}{H_1}\frac{h^2}{L}e_2\right] \quad (36)$$

or

$$-e_2 = \frac{3H_1I_2L}{H_2A_1h^2}\left[1 + \frac{2hA_1}{\pi I_1}e_1\right] \quad (37)$$

when the value of e_1 or e_2 can be chosen and the value of e_2 or e_1 will follow.

In the case of a frame with fixed feet the required separations must be accompanied by a state of no rotation at the feet. This means that there must be some leg bending whether beam bending takes place or not. These effects are covered by eccentricities as follows:

a) leg bending only (Figure 15(a))

in this case $e_3 = -e_2$

$$e_2 = -\pi\frac{H_1}{H_2}\frac{I_2}{A_1}\frac{L}{h^2} \quad (38)$$

b) combined leg and beam bending (Figure 15(b))

$$e_2 + 3e_3 = 2\pi\frac{H_1}{H_2}\frac{I_2}{A_1}\frac{L}{h^2}$$

and

$$e_1 = -\frac{h}{L}\frac{I1}{I_2}\frac{H_2}{H_1}(e_2 + e_3) \quad (39)$$

Here we may choose two eccentricities; the third will then follow from the above relationships.

The required true concordant profile is obtained by adding the "bending concordant profile" to the separation profile.

It is to be noted that it is not always possible to produce a true concordant profile so that it will often be necessary to reduce the redundancy of the structure.

Example 2

Let us consider a two-pinned portal frame with a span of 40 ft and a height of 25 ft which is to be designed to carry a load of 1,000 lb/ft on the beam with stress limits of 2,000 lb/in.^{2} in compression and zero tension. We shall assume that the beam and legs are to have the same section.

The moments and forces in the frame due to the applied loading can be determined by normal elastic analysis and are as follows:

vertical leg load	20,000 lb.
horizontal thrust	3,767 lb.
centre span beam moment	- 1,270,000 lb. in.
knee moment	1,130,000 lb. in.

The minimum section sizes for the beam and legs can be evaluated by using the expressions

$$M_L = \frac{1}{6} f_c\, bd^2 + \frac{1}{6} (H_1 - H_2)\, d$$

and

$$M_L = \frac{1}{6} f_c\, bd^2 + \frac{1}{6} (H_2 - H_1)\, d$$

For the beam we have M_L = 1,270,000 lb. in. and $H_1 - H_2$ = -3,767 lb. Assuming a section breadth of 12 in. the above expression leads to a value of the depth

$$d = 17{\cdot}9 \text{ in.} = 18 \text{ in.} \quad \text{(say)}$$

For the leg we have M_L = 1,130,000 lb. in. and $H_2 - H_1$ = -20,000 lb. This leads to a minimum depth of 17·25 in. Having assumed that the beam and leg sections will be the same we shall make these 18 in. by 12 in. throughout.

We are now in a position to determine the dead load moments and thrusts. The total dead weight of the beam can be taken as

$$18 \times 12 \times 40 = 8{,}640 \text{ lb.}$$

which gives a leg thrust of 4,320 lb. at the top of the leg and a beam thrust of 814 lb. It is to be noted that in this case the critical section for the leg is at the top and therefore the self-weight of the leg is not to be included. Had the critical section of the leg been at the foot the appropriate dead-weight leg thrust would be that including the weight of the leg.

The bending moments due to dead-weight loading are

centre span beam moment	- 270,000 lb. in.
knee moment	228,700 lb. in.

The prestressing forces required in the beam and the leg can now be calculated, the condition being that under maximum live and dead load thrusts the most highly stressed fibres in the section shall be under the maximum concrete stress, i.e.

$$H_P = \frac{1}{2} f_c\, bd - H_D - H_2$$

or

$$H_P = \frac{1}{2} f_c\, bd - H_D - H_1$$

for the beam

$$H_P = 211{,}419 \text{ lb.}$$

and for the legs

$$H_P = 191{,}680 \text{ lb.}$$

The permissible core limits can now be determined for each of the

members under their various load conditions. The core limits for a beam would be $\pm\frac{d}{6} = \pm 3$ in. but it will be remembered that in cases of applied loading thrusts these are modified by an amount $\frac{H}{H_p}$.

In the case of the beam we have

dead load only

$$\frac{H}{HP} = \frac{211,419 + 814}{211,419}$$

$$= 1{\cdot}004$$

live load plus dead load

$$\frac{H}{H_p} = \frac{216,000}{211,419}$$

$$= 1{\cdot}022$$

In the case of the top of the legs

dead load only

$$\frac{H}{H_p} = \frac{191,680 + 4,320}{191,680}$$

$$= 1{\cdot}022$$

live load plus dead load

$$\frac{H}{H_p} = \frac{216,000}{191,680}$$

$$= 1{\cdot}13$$

Evidently the effect of axial thrusts can be ignored in all but the last case, although we shall continue to include them in this example.

The limiting zones can now be drawn, these being the limiting bending moment diagrams plotted to a scale of $\frac{1}{H_p}$ on the corresponding core limits. These are indicated in Figure 16 but we may note the critical points.

a) Mid-span zone limits

Upper limit:

$$\frac{M_2 + M_D}{H_p} - \frac{I}{Ay_2} \cdot \frac{H}{H_p}$$

$$= \frac{1,540,000}{211,419} - 3 \,.\, 1{\cdot}022$$

$$= 4{\cdot}21 \text{ in.}$$

Lower limit:

$$\frac{M_1 + M_D}{H_p} + \frac{I}{Ay_1} \cdot \frac{H}{H_p}$$

$$= \frac{270,000}{211,419} + 3 \cdot 1{\cdot}004$$

$$= 4{\cdot}28 \text{ in.}$$

Here the limiting zones nearly touch, as should be the case for an economical design. The small width is due to our having increased the depth of the section from the theoretical minimum of 17·9 in. to a practical value of 18 in.

b) Beam end zone limits

Upper limit:

$$= -\frac{228,700}{211,419} - 3 \cdot 1{\cdot}004$$

$$= -4{\cdot}09 \text{ in.}$$

Lower limit:

$$= -\frac{1,358,700}{211,419} + 3 \cdot 1{\cdot}022$$

$$= -3{\cdot}35 \text{ in.}$$

Here the zone has a width of 0·74 in., the moment variation being less than at mid-span.

c) Leg top zone limits

Upper (outer) limit:

$$= -\frac{228,700}{191,680} - 3 \cdot 1{\cdot}022$$

$$= -4{\cdot}26 \text{ in.}$$

Lower (inner) limit:

$$= -\frac{1,358,700}{191,680} + 3 \cdot 1{\cdot}13$$

$$= -3{\cdot}69 \text{ in.}$$

Here the zone has a width of 0·57 in. which is less than the corresponding point in the beam due to the reduced prestressing force.

d) Leg foot zone limits

Ignoring the slight increase in direct thrust due to the weight of the leg the zone limits will be at the core limits since there are no moments under any loading conditions, i.e. upper limit = - 3·07 in.; lower limit = 3·39 in. A bending concordant profile can now be determined for the frame. In this case there are only two cases of loading so that the statically determinate eccentricity expression applies

$$e = -\left\{\frac{M_D}{H_p} + \frac{M_1 + M_2}{2H_p}\right\}$$

for the beam span centre

$$e = \frac{270,000}{211,419} + \frac{1,270,000}{422,838}$$

$$= 4{\cdot}28 \text{ in.}$$

and for the beam knee

$$e = -\frac{228,700}{211,419} - \frac{1,130,000}{422,838}$$

$$= -3{\cdot}75 \text{ in.}$$

and for the leg knee

$$e = -\frac{228,700}{191,680} - \frac{1,130,000}{383,360}$$

$$= -4{\cdot}09 \text{ in.}$$

The eccentricities in the beam and leg at the knee will be in the inverse ratios of the prestressing force values. For the foot of the leg the eccentricity will obviously be zero.

We must now investigate the additional eccentricity required to provide the feet separation equal to the contraction which will have occurred in the beam under prestress. Taking a form giving leg bending only, expression (35), we have

$$e_2 = -\frac{3H_1I_2L}{H_2A_1h^2}$$

$$= -\frac{3 \times 211,419 \times 18^2 \times 40}{191,680 \times 12 \times 25^2 \times 12}$$

$$= -0{\cdot}475 \text{ in.}$$

This is the maximum eccentricity of a transformation which is linear and equal to zero at the knee and - 0·475 in. at the foot. The final eccentricities of the tendon are shown in Figure 16.

Transformation

Linear transformation may be applied to portal frame tendon profiles in the same manner as has been discussed in section 5 for continuous beams. However some points must be noted. In the first place the beam thrust due to prestress represents a "support" reaction which will undergo a variation due to transformation in accordance with the relation given in section 5. This will, in turn, slightly affect the concrete stresses in the beam and may, in extreme circumstances, result in a re-determination of the section sizes having to be made.

A second point is that the change in beam thrust due to transformation must be the same at each end of the beam, otherwise parasitic moments will be introduced due to side sway and will inviolate the basic idea of tendon transformation.

Journal of the
STRUCTURAL DIVISION
Proceedings of the American Society of Civil Engineers

RESPONSE OF A RIGID FRAME TO A DISTRIBUTED TRANSIENT LOAD

R. C. DeHart,[1] M. ASCE
(Proc. Paper 1056)

SYNOPSIS

In this paper, a method for analyzing the response of a rigid frame structure subjected to a distributed lateral load of a transient nature is presented. The structure is studied from the standpoint that it is a continuous system having a distributed mass. Time dependent relations for deflection and moment are developed and these quantities are computed for one example.

INTRODUCTION

The determination of the response of structures subjected to transient loads is for the most part a rather difficult proposition even for the more simple cases. Most of the difficulty arises, however, from the numerical work involved. This difficulty can in a large measure be removed by making quantities available such as frequencies and the numerical factors required for energy computation.

The structure under consideration here is shown in Figure 1. The frame material is steel and the walls have a strength such that they do not fail under the applied load. Assumptions underlying the analytical treatment of this problem are as follows:

1) Each member of the frame is straight, has uniform mass and cross section.
2) The material obeys Hooke's law.
3) Damping is negligible.
4) Axial stresses do not influence the frequencies of vibration.
5) Effect of rotatory inertia is neglected.
6) Effect of shearing stress is neglected.

The method of attack for the problem under study here requires that the contribution of each vibratory mode be determined. Except for some extremely

Note: Discussion open until February 1, 1957. Paper 1056 is part of the copyrighted Journal of the Structural Division of the American Society of Civil Engineers, Vol. 82, No. ST 5, September, 1956.

1. Structural Research Analyst, Armed Forces Special Weapons Project, U. S. Dept. of Defense, Washington, D. C.

simple symmetrical cases, it is impossible to write the solution in a generalized form; thus each mode and its associated frequency will be examined individually. Within the elastic region only linear relations are involved; therefore, the principle of superposition applies which, of course, permits the addition of the contribution of each mode in order to obtain the total effect.

A procedure of this nature requires the determination of the mode shapes and their frequencies as a first step. The Lagrange equation of motion will be used; therefore, energy expressions are needed in addition to an expression for the generalized force.

Frequency Determination

As has been previously discussed, the method of attack to be used requires the summation of the contribution of each mode. This requires that the modes and frequencies of the modes be determined before a solution can be effected.

Considerable information concerning the determination of the frequencies of vibration of continuous beams is available. Some of these methods are also applicable to rigid frames, particularly those frames in which no sidesway is present.

In surveying the existing methods available for the determination of frequencies of vibration, several possibilities presented themselves. The work of Saibel(1) considers a continuous beam as an ordinary beam of the same length subject to constraints at the inner points of support. A so-called admittance method for obtaining frequencies has been published by Duncan(2) in which the term admittance is used to describe a dynamic flexibility that is analogous to flexibility under static conditions. Moment equations are written that allow the establishment of the frequency determinant.

A chart for obtaining the natural frequencies of continuous beams of uniform span length has been presented by Ayre et al(3) and Smith(4) has published a monogram for obtaining the frequencies of continuous systems. Tables have been made available by Darnley(5) that facilitate the solution of a frequency equation established by writing the differential equations describing the motion of each bar of the system and then using the proper boundary conditions at each bar end.

The author was able to locate three investigations devoted to the rigid frame. Masur(6) has shown how the fundamental frequency can be obtained by a dynamic moment balancing procedure. One of the other two methods was formulated by Prager and Hohenemser(7) and the other by Sezawa and Kanai.(8) In reference 7, tables may be found giving the value of the functions appearing in the frequency equation for a rigid frame with and without sidesway. It was therefore decided to use a procedure that would result in frequency equations having the same terms as those given by reference 7.

Symmetrical and unsymmetrical modes will be required. The structure to be considered is given in Figure 1; arrowheads indicate the assumed positive directions for the coordinate system.

The differential equation representing the free vibration of a straight bar is

$$\frac{\partial^2}{\partial x^2} EI \frac{\partial^2 Y}{\partial x^2} = -\mu \frac{\partial^2 Y}{\partial t^2} \qquad (1)$$

where E is the modulus of elasticity of the material,

I is the moment of inertia,

μ is the mass per unit length of bar.

Let $\alpha^2 = \frac{EI}{\mu}$ and rewrite equation (1) for bars having constant modulus of elasticity and moment of inertia.

$$\frac{\partial^2 Y}{\partial t^2} + \alpha^2 \frac{\partial^4 Y}{\partial x^4} = 0 \tag{2}$$

If Y_i is the lateral deflection of the neutral axis of any member of the frame resulting from the i^{th} vibratory mode then

$$Y_i = y_i(x)(A_i \sin \omega_i t + B_i \cos \omega_i t) \tag{3}$$

ω_i is the frequency of the i^{th} mode and t is the time variable. If equation (3) is substituted in (2), the following is obtained:

$$\frac{d^4 y_i(x)}{dx^4} = \frac{\omega_i^2}{\alpha^2} y_i(x) \tag{4}$$

The solution of equation (4) is

$$y_i(x) = a_i \cos k_i x + b_i \operatorname{ch} k_i x + c_i \sin k_i x + d_i \operatorname{sh} k_i x \tag{5}$$

where $$k_i^4 = \frac{\omega_i^2}{\alpha^2}$$

By superimposing all possible lateral vibrations, the general expression for the lateral deflection due to the free vibratory modes is

$$Y = \sum_{i=1}^{\infty} y_i(x)(A_i \cos \omega_i t + B_i \sin \omega_i t) \tag{6}$$

The frequencies corresponding to various end restraints can be obtained when use is made of the boundary conditions representing the end restraints. For the unsymmetrical modes and because of symmetry of the bent the moment and deflection at the center of the beam are both zero as shown in Figure 2. Items pertaining to the column are denoted by a u superscript. Items pertaining to the beam are denoted by a v superscript. At the column footing

$$y^u_{(x=0)} = 0 \tag{7}$$

$$EI^u(y^u)''_{(x=0)} = 0 \tag{8}$$

at the intersection of the beam and column

$$(y^u)'_{(x = L^u)} = (y^v)'_{(x = 0)} \tag{9}$$

$$EI^u(y^u)''_{(x = L^u)} = EI^v(y^v)''_{(x = 0)} \tag{10}$$

$$y^v_{(x = 0)} = 0 \tag{11}$$

at the center of the beam

$$y^v_{\left(x = \frac{L^v}{2}\right)} = 0 \tag{12}$$

$$EI^v(y^v)''_{\left(x = \frac{L^v}{2}\right)} = 0 \tag{13}$$

The eighth condition arises from the fact that the sum of the horizontal forces at the top of the column must be zero.

$$EI^u \frac{\partial^3 Y_1^u}{\partial x_1^3}_{(x = L^u)} - \frac{W^v}{2g} \frac{\partial^2 Y_1^u}{\partial t^2}_{(x = L^u)} = 0 \tag{14}$$

W^v is the total weight of the beam.

The set of eight conditions given above permits the writing of the frequency equation (15).

$$\frac{I^v}{I^u} \sqrt[4]{\frac{I^u}{I^v}\frac{\mu^v}{\mu^u}} \left[\frac{\frac{\mu^v}{\mu^u}\frac{L^v/2}{L^u} k^u L^u \eta_1^u - \eta_2^u}{\frac{\mu^v}{\mu^u}\frac{L^v/2}{L^u} k^u L^u \eta_3^u + \eta_1^u} \right] = -\frac{\eta_1^v}{\eta_3^v} \tag{15}$$

$$\eta_1^u = \sin k_1^u L^u \operatorname{ch} k_1^u L^u - \cos k_1^u L^u \operatorname{sh} k_1^u L^u$$

$$\eta_2^u = 2 \cos k_1^u L^u \operatorname{ch} k_1^u L^u$$

$$\eta_3^u = 2 \sin k_1^u L^u \operatorname{sh} k_1^u L^u$$

$$\eta_1^v = \sin k_1^v \frac{L^v}{2} \operatorname{ch} k_1^v \frac{L^v}{2} - \cos k_1^v \frac{L^v}{2} \operatorname{sh} k_1^v \frac{L^v}{2}$$

$$\eta_3^v = 2 \sin k_1^v \frac{L^v}{2} \operatorname{sh} k_1^v \frac{L^v}{2}$$

Numerical values for the terms given above are found in reference 7. Mode shape equations for the beam and column are as follows:

$$y_i^v = c_i^v \left[- \tan k_i^v \frac{L^v}{2} (\cos k_i^v x - \operatorname{ch} k_i^v x) + \sin k_i^v x - \frac{\tan k_i^v \frac{L^v}{2}}{\tanh k_i^v \frac{L^v}{2}} \operatorname{sh} k_i^v x \right] \tag{16}$$

$$y_i^u = c_i^u (\sin k_i^u x + D_i \operatorname{sh} k_i^u x) \tag{17}$$

$$c_i^u = 2c_i^v \sqrt{\frac{I^v}{I^u} \frac{\mu^v}{\mu^u}} \left[\frac{\tan k_i^v \frac{L^v}{2}}{- \sin k_i^u L^u + D_i \operatorname{sh} k_i^u L^u} \right] \tag{18}$$

where

$$D_i = \frac{- \cos k_i^u L^u + k_i^v \frac{L^v}{2} \sqrt[4]{\frac{I^v}{I^u} \frac{\mu^u}{\mu^v} \frac{\mu^v}{\mu^u}} \sin k_i^u L^u}{- k_i^v \frac{L^v}{2} \sqrt[4]{\frac{I^v}{I^u} \frac{\mu^u}{\mu^v} \frac{\mu^v}{\mu^u}} \operatorname{sh} k_i^u L^u - \operatorname{ch} k_i^u L^u}$$

For the symmetrical modes, no sidesway is present. In addition, the slope and shear at the center of the beam are both zero, and the problem reduces to that shown in Figure 3 with

$$(y^v)'_{(x = \frac{L^v}{2})} = 0 \tag{19}$$

$$(y^v)'''_{(x = \frac{L^v}{2})} = 0 \tag{20}$$

and the frequency equation for the symmetrical modes becomes

$$\frac{I^u}{I^v} \sqrt[4]{\frac{I^v}{I^u} \frac{\mu^u}{\mu^v}} \frac{\eta_3^u}{\eta_1^u} = - \frac{\eta_2^v}{\eta_4^v} \tag{21}$$

η_1^u, η_2^v, η_3^u are as given before, $\eta_2^v = 2 \cos k_i^v \frac{L^v}{2} \operatorname{ch} k_i^v \frac{L^v}{2}$, and

$\eta_4^v = \sin k_i^v \frac{L^v}{2} \operatorname{ch} k_i^v \frac{L^v}{2} + \cos k_i^v \frac{L^v}{2} \operatorname{sh} k_i^v \frac{L^v}{2}$

and the mode shape equations are

$$y_i^v = c_i^v \left[\cot k_i^v \frac{L^v}{2} (\cos k_i^v x - \operatorname{ch} k_i^v x) + \sin k_i^v x - \frac{\cot k_i^v \frac{L^v}{2}}{\operatorname{cth} k_i^v \frac{L^v}{2}} \operatorname{sh} k_i^v x \right] \tag{22}$$

$$y_i^u = c_i^u \left[\sin k_i^u x - \frac{\sin k_i^u L^u}{\operatorname{sh} k_i^u L^u} \operatorname{sh} k_i^u x \right] \tag{23}$$

where

$$c_i^u = c_i^v \sqrt{\frac{I^v}{I^u} \frac{\mu^v}{\mu^u}} \frac{\cot k_i^v \frac{L^v}{2}}{\sin k_i^u L^u} \tag{24}$$

Frequencies for the first two symmetrical and the first two unsymmetrical modes for various column-beam mass, length, and moment of inertia ratios are available in reference 9.

Determination of Kinetic Energy

The next quantity of importance once the frequencies and mode shapes for the system are known is the kinetic energy.

If the expression for the lateral deflection of the beam is written in terms of a generalized coordinate q_i, the following results:

$$Y^v = \sum_{i=1}^{\infty} q_i^v y_i^v \tag{25}$$

The expression for y_i^v for unsymmetrical modes is given by equation (17); therefore, (25) can be written:

$$Y_i^v = q_i^v \left[- \tan k_i^v \frac{L^v}{2} (\cos k_i^v x - \operatorname{ch} k_i^v x) + \sin k_i^v x - \frac{\tan k_i^v \frac{L^v}{2}}{\tanh k_i^v \frac{L^v}{2}} \operatorname{sh} k_i^v x \right] \tag{26}$$

The constant c_i^v appearing in y_i^v is incorporated into the expression for q_i^v. Since c_i^v and c_i^u influence only the amplitude and not the time dependency of the motion, these constants can be associated with either the generalized coordinate or the mode shape coordinate.

In order to obtain the contribution to the total flexural kinetic energy arising from the beam, equation (27) will be utilized. The symbol T_i^v is used to denote this quantity.

It can be demonstrated that when the entire structure is considered, the sum of all terms involving other than squares of the mode shape vanishes.

$$\frac{T_i^v}{2} = \frac{\mu^v}{2} \int_0^{\frac{L^v}{2}} \left(\frac{\partial Y_i^v}{\partial t} \right)^2 dx \tag{27}$$

Putting the value of Y_i^v into the integral, the expression for kinetic energy becomes:

$$\frac{T_i^v}{2} = \frac{\mu^v}{2} (\dot{q}_i^v)^2 \int_0^{\frac{L^v}{2}} \left[- \tan k_i^v \frac{L^v}{2} \cos k_i^v x + \tan k_i^v \frac{L^v}{2} \operatorname{ch} k_i^v x + \sin k_i^v x - \frac{\tan k_i^v \frac{L^v}{2}}{\tanh k_i^v \frac{L^v}{2}} \operatorname{sh} k_i^v x \right]^2 dx \tag{28}$$

The sum of the 10 terms that arise when the integration indicated in equation (28) is carried out is the following:

$$\frac{1}{k_i^v} \left\{ \tan k_i^v \frac{L^v}{2} \left[k_i^v \frac{L^v}{2} \left(1/2 - \frac{1}{2 \operatorname{sh}^2 k_i^v \frac{L^v}{2}} \right) + 1/2 \sin k_i^v \frac{L^v}{2} \cos k_i^v \frac{L^v}{2} - 1/2 \coth k_i^v \frac{L^v}{2} \right] + 1/2 k_i^v \frac{L^v}{2} + 1/2 \sin k_i^v \frac{L^v}{2} \cos k_i^v \frac{L^v}{2} \right\}$$

The translational kinetic energy of one half the beam is

$$1/2 \left[\frac{k_i^v L^v}{2} \frac{\mu^v}{k_i^v} (y_i^u)^2 (x = L^u) \right] (\dot{q}_i^u)^2$$

T_i^u is the contribution to the total flexural kinetic energy arising from both columns and is written as follows:

$$\frac{T_i^u}{2} = \frac{\mu^u}{2} (\dot{q}_i^u)^2 \int_0^{L^u} (\sin k_i^u x + D_i \operatorname{sh} k_i^u x)^2 dx \tag{29}$$

The quantity under the integral sign yields the following three terms:

$$\frac{1}{2k_i^u} (k_i^u L^u - \cos k_i^u L^u \sin k_i^u L^u)$$

$$\frac{1}{k_i^u} D_i (\operatorname{ch} k_i^u L^u \sin k_i^u L^u - \operatorname{sh} k_i^u L^u \cos k_i^u L^u)$$

$$-\frac{1}{2k_i^u} D_i^2 (\text{sh } k_i^u L^u \text{ ch } k_i^u L^u - k_i^u L^u)$$

The kinetic energy for the symmetrical modes is determined in same manner as that used for the symmetrical modes. In this case the evaluation of the integral appearing in the expression for beam kinetic energy yields:

$$\frac{1}{k_i^v}\left\{\cot^2 k_i^v \frac{L^v}{2}\left[k_i^v \frac{L^v}{2}\left(1/2 + \frac{1}{2\,\text{ch}^2 k_i^v \frac{L^v}{2}}\right) + 1/2 \sin k_i^v \frac{L^v}{2} \cos k_i^v \frac{L^v}{2} - 1/2 \tanh k_i^v \frac{L^v}{2}\right] + 1/2\, k_i^v \frac{L^v}{2} + 1/2 \sin k_i^v \frac{L^v}{2} \cos k_i^v \frac{L^v}{2} - \cot k_i^v \frac{L^v}{2}\right\}$$

For the column the same three terms arise from the evaluation of the integral for both symmetrical and unsymmetrical modes. The expression for D_i for the symmetrical modes is $-\dfrac{\sin k_i^u L^u}{\text{ch } k_i^u L^u}$.

Motion Due to an Arbitrary Transient Load

With the previously developed information, it is now possible to obtain the motion of the frame in question when it is subjected to a transient load. Lagrange's equation of motion written in the following form is utilized:

$$\frac{d}{dt}\left(\frac{\partial T_i}{\partial \dot{q}_i}\right) - \frac{\partial T_i}{\partial q_i} + \frac{\partial U_i}{\partial q_i} = Q_i \qquad (30)$$

T_i is kinetic energy

U_i is potential energy

Q_i is the generalized force.

Since T_i is a function of $\dot{q}_i$ only and does not contain q_i, equation (30) reduces to

$$\frac{d}{dt}\left(\frac{\partial T_i}{\partial \dot{q}_i}\right) + \frac{\partial U_i}{\partial q_i} = Q_i \qquad (31)$$

The kinetic energy of the entire structure for unsymmetrical modes can be written as

$$T_i = \bar{T}_i (\dot{q}_i^u)^2 \frac{\mu^u}{k_i^u}$$

where

$$\bar{T}_i = \bar{T}_i^u + \bar{T}_i^v + \bar{T}_i^r$$

$\bar{T}_i^u$ is the quantity obtained when the integral in equation (29) is evaluated for both columns and with the $\frac{1}{k_i^u}$ multiplier not included.

$\bar{T}_i^v$ is the quantity obtained when the integral in equation (28) is evaluated with the $\frac{1}{k_i^v}$ multiplier not included and a factor applied to convert from $\dot{q}_i^v$ to $\dot{q}_i^u$, μ^v to μ^u, and k_i^v to k_i^u.

$\bar{T}_i^r = \left[1/2\, k_i^v L^v \frac{\mu^v}{k_i^v} (Y_i^u)^2 \Big|_{x = L^u}\right]$ multiplied by a factor to convert from μ^v to μ^u and k_i^v to k_i^u.

The conversion of $\dot{q}_i^v$ to $\dot{q}_i^u$ is accomplished as follows:

$$\dot{q}_i^u = \frac{c_i^u}{c_i^v} \dot{q}_i^v$$

The relation between c_i^u and c_i^v is given by equation 19 for the unsymmetrical modes and by equation (24) for the symmetrical modes.

The kinetic energy for the symmetrical modes is obtained in a manner identical to that described above with the exception of the translatory kinetic energy term which does not exist in this case.

Similarly the potential energy for one mode is

$$U_i = \bar{U}_i (q_i^u)^2 (k_i^u)^3 EI^u$$

$\bar{U}_i$ is obtained from the potential energy expression

$$\frac{U_i}{2} = \frac{EI^v}{2} \int_0^{\frac{L^v}{2}} \left[\frac{\partial^2 Y_i^v}{\partial x^2}\right]^2 dx + \frac{EI^u}{2} \int_0^{L^u} \left[\frac{\partial^2 Y_i^u}{\partial x^2}\right]^2 dx$$

with q_i^v, k_i^v, and I^v converted to q_i^u, k_i^u, and I^u respectively.

Since

$$\frac{\partial T_i}{\partial \dot{q}_i} = 2\bar{T}_i q_i^u \frac{\mu^u}{k_i^u}$$

$$\frac{\partial U_i}{\partial q_i} = 2\bar{U}_i q_i^u (k_i^u)^3 EI^u$$

equation 30 becomes

$$2\bar{T}_i \ddot{q}_i^u \frac{\mu^u}{k_i^u} + 2\bar{U}_i q_i^u (k_i^u)^4 EI^u = Q_i$$

$$\ddot{q}_i^u + \frac{\bar{U}_i}{\bar{T}_i} \frac{(k_i^u)^4 EI^u}{\mu^u} q_i^u = \frac{Q_i}{2\bar{T}_i \frac{\mu^u}{k_i^u}}$$

$$\frac{\bar{U}_i}{\bar{T}_i} = 1 \text{ and } \frac{(k_i^u)^4 EI^u}{\mu^u} = \omega_i^2 \quad \text{thus}$$

$$\ddot{q}_i^u + \omega_i^2 q_i^u = \frac{Q_i}{2\bar{T}_i \frac{\mu^u}{k_i^u}} \tag{32}$$

Equation (32) is a non-homogeneous linear differential equation. The general solution may be written as

$$q_i^u = A_i \cos \omega_i t + B_i \sin \omega_i t + \frac{k_i^u}{2\omega_i \bar{T}_i \mu^u} \int_0^t Q_i(\tau) \sin \omega_i (t - \tau)\, d\tau \tag{33}$$

Motion Due to a Distributed Time Dependent Load

If one now considers the distributed transient force given in Figure 4, the generalized force Q_i is determined as follows:

$$\sum_{x=0}^{x=L^u} P\Delta y = P\Delta q_i^u \int_0^{L^u} (\sin k_i^u x + D_i \operatorname{sh} k_i^u x)\, dx$$

$$Q_i^u(\tau) = P_e \frac{(t_e - \tau)}{t_e} \int_0^{L^u} (\sin k_i^u x + D_i \operatorname{sh} k_i^u x)\, dx$$

$$Q_i^u(\tau) = P_e \frac{(t_e - \tau)}{t_e} \left[- \frac{\cos k_i^u x}{k_i^u} + \frac{D_i \operatorname{ch} k_i^u x}{k_i^u} \right]_0^{L^u}$$

$$Q_i^u(\tau) = \frac{P_e}{k_i^u t_e} (t_e - \tau) \left[- \cos k_i^u L^u + D_i \operatorname{ch} k_i^u L^u + 1 - D_i \right] \tag{34}$$

If no motion existed prior to load application time, equation (33) becomes

$$q_i^u = \frac{k_i^u}{2\omega_i \bar{T}_i \mu^u} \int_o^t \frac{P_e}{k_i^u t_e} (t_e - \tau) \cdot$$

$$\left[- \cos k_i^u L^u + D_i \operatorname{ch} k_i^u L^u + 1 - D_i \right] \sin \omega_i (t - \tau) \, d\tau, \text{ or}$$

$$q_i^u = \frac{1}{2t_e} \frac{P_e}{\bar{T}_i \mu^u \omega_i^2} \left[t_e (1 - \cos \omega_i t) - t + \frac{\sin \omega_i t}{\omega_i} \right]$$

$$\left[- \cos k_i^u L^u + D_i \operatorname{ch} k_i^u L^u + 1 - D_i \right] \tag{35}$$

$$Y_i^u = q_i^u \, y_i^u$$

$$EI^u \frac{\partial^2 Y_i^u}{\partial x^2} = - M_i$$

$$Y_i^u = (\sin k_i^u x + D_i \operatorname{sh} k_i^u x) \, q_i^u$$

$$\frac{\partial Y_i^u}{\partial x} = k_i^u (\cos k_i^u x + D_i \operatorname{ch} k_i^u x) \, q_i^u$$

$$\frac{\partial^2 Y_i^u}{\partial x^2} = (k_i^u)^2 (- \sin k_i^u x + D_i \operatorname{sh} k_i^u x) \, q_i^u$$

$$M_i = \frac{-P_e (k_i^u)^2 EI^u}{2\bar{T}_i \mu^u \omega_i t_e^2} \phi_i(x) \, \theta_i(t) \tag{36}$$

$$\phi_i(x) = (\sin k_i^u x + D_i \operatorname{sh} k_i^u x)$$

The equation for $\phi_i(x)$ given here is for the unsymmetric modes. It also applies to the symmetric modes if D_i is taken to be $- \dfrac{\sin k_i^u L^u}{\operatorname{sh} k_i^u L^u}$.

$$\theta_i(t) = \left[t_e (1 - \cos \omega_i t) - t + \frac{\sin \omega_i t}{\omega_i} \right]$$

$$\left[- \cos k_i^u L^u + D_i \operatorname{ch} k_i^u L^u + 1 - D_i \right]$$

substituting ω_i^2 for $\frac{k_i^{u\,4} EI^u}{\mu^u}$

$$\frac{M_1}{P_e(L^u)^2} = -\frac{\phi_1(x)\,\theta_1(t)}{2\bar{T}_1 t_e (k_1^u L^u)^2}$$

Response Determination

Consider the bent shown in Figure 5 which also gives the time dependency of the load.

$$\mu^u = 0.333 \ \frac{\text{lb. sec.}^2}{\text{in.}^2} = \mu^v$$

t_e = 0.5 sec.

P_e = 266 lb./in.

For the unsymmetrical modes

$k_1^v \frac{L^v}{2} = 1.03$	$k_1^u L^u = 1.05$	$\bar{T}_1 = 0.683$	$\omega_1 = 9.97$ rad/sec
$k_2^v \frac{L^v}{2} = 3.16$	$k_2^u L^u = 3.22$	$\bar{T}_2 = 5.82$	$\omega_2 = 94.1$ rad/sec
$k_3^v \frac{L^v}{2} = 3.98$	$k_3^u L^u = 4.07$	$\bar{T}_3 = 2.90$	$\omega_3 = 150$ rad/sec
$k_4^v \frac{L^v}{2} = 7.04$	$k_4^u L^u = 7.18$	$\bar{T}_4 = 5.47$	$\omega_4 = 468$ rad/sec

For the symmetrical modes

$k_1^v \frac{L^v}{2} = 1.83$	$k_1^u L^u = 1.87$	$\bar{T}_1 = 7.03$	$\omega_1 = 31.8$ rad/sec
$k_2^v \frac{L^v}{2} = 3.59$	$k_2^u L^u = 3.66$	$\bar{T}_2 = 2.10$	$\omega_2 = 122$ rad/sec
$k_3^v \frac{L^v}{2} = 4.97$	$k_3^u L^u = 5.07$	$\bar{T}_3 = 19.03$	$\omega_3 = 234$ rad/sec
$k_4^v \frac{L^v}{2} = 6.67$	$k_4^u L^u = 6.82$	$\bar{T}_4 = 3.91$	$\omega_4 = 422$ rad/sec

Moment diagrams determined from the consideration of eight modes are given in Figure 6 for several times. The moment diagrams are plotted on the tension side of the member in every case. It is of interest to note that at early times the moment at the top of the left-hand column has a direction such that tensile forces exist at the outside face of the column. At later times the direction of this moment reverses with a maximum value occurring after about 0.30 second has elapsed.

Sketches of the deflected structure accompany each moment diagram plot.

Little translational motion occurs and only small flexural moment is present in the right-hand column during the first .05 of a second.

The computation was carried out only for times corresponding to the duration of the load; however, conditions at later times can be studied through the use of equation (33) reduced to the following form:

$$q_i^u = A_i \cos \omega_i t + B_i \sin \omega_i t$$

The constants A_i and B_i are determined making use of the conditions existing at the time the external load vanishes.

The static moment diagram corresponding to a distributed load of 266 pli is shown in Figure 7. The maximum dynamic moment occurs at the top of the left column and is approximately 1.5 times the maximum static moment which occurs at the top of the right column.

ACKNOWLEDGMENT

The writer wishes to acknowledge the aid and suggestions of Dr. F. DiMaggio and the computational assistance of A1/c R. Anderson.

BIBLIOGRAPHY

1. Vibration Frequencies of Continuous Beams, by E. Saibel, Journal of Aeronautical Sciences, Vol. 11, 1944, p. 88.
2. Free and Forced Oscillations of Continuous Beams, Treatment by the Admittance Method, by W. J. Duncan, Philosophical Magazine, Ser. 7, Vol. 34, 1943, p. 49.
3. Natural Frequencies of Continuous Beams of Uniform Span Length, by R. S. Ayre and L. S. Jacobsen, Journal of Applied Mechanics, Vol. 17, 1950, p. 391.
4. The Transverse Vibration of Uniform Beams, by D. M. Smith, Engineering, Vol. 120, 1925, p. 808.
5. The Transverse Vibrations of Beams and the Whirling of Shafts Supported at Intermediate Points, by F. R. Darnley, Philosophical Magazine, Vol. 41, 1921, p. 81.
6. On the Fundamental Frequencies of Vibration of Rigid Frames, by E. F. Masur; paper presented at the First Midwestern Conference on Solid Mechanics, University of Illinois, April 24, 1953.
7. Dynamik der Stabwerke, by K. Hohenemser and W. Prager, Julius Springer, Berlin, 1933.
8. Vibrations of a Single-Storyed Framed Structure, by K. Sezawa and K. Kanai, Bulletin Japan Earthquake Research Institute, Vol. 10, 1932.
9. Analysis of Rigid Frames Subjected to Time Dependent Loads. Thesis submitted in partial fulfillment of requirements for degree of Doctor of Philosophy, Illinois Institute of Technology.

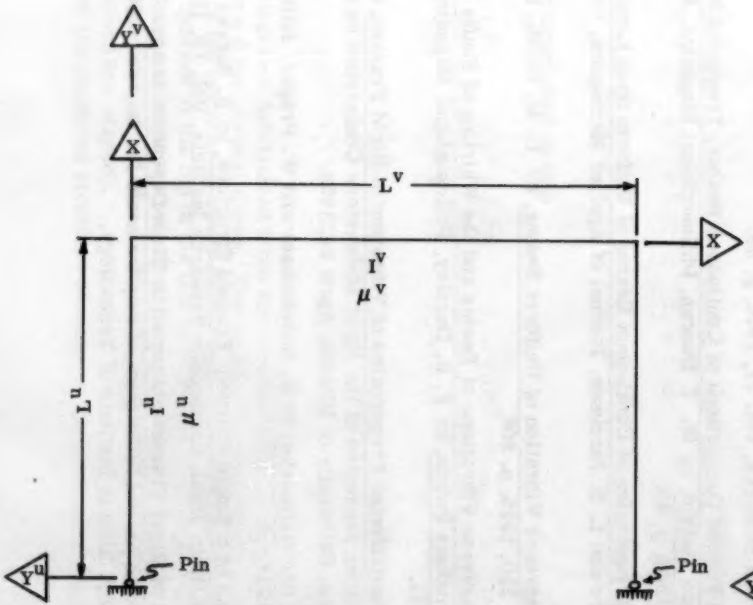

Figure 1. Rigid Frame Structure.

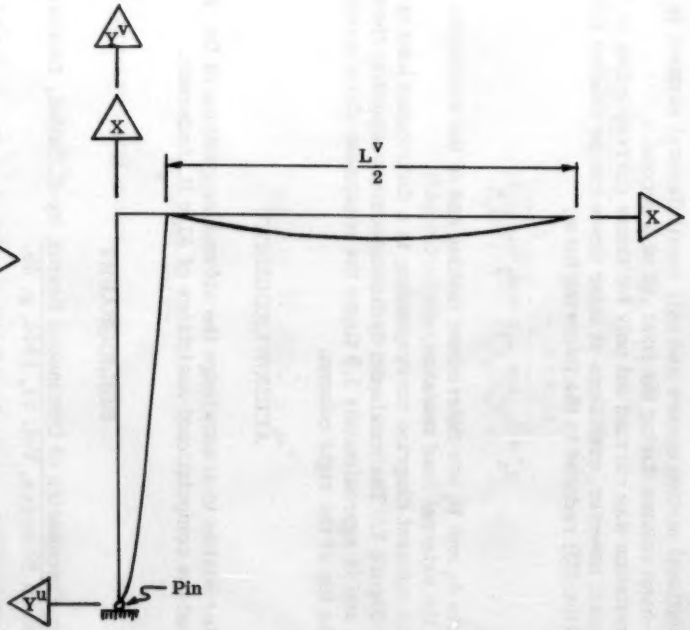

Figure 2. Rigid Frame Unsymmetrical Mode.

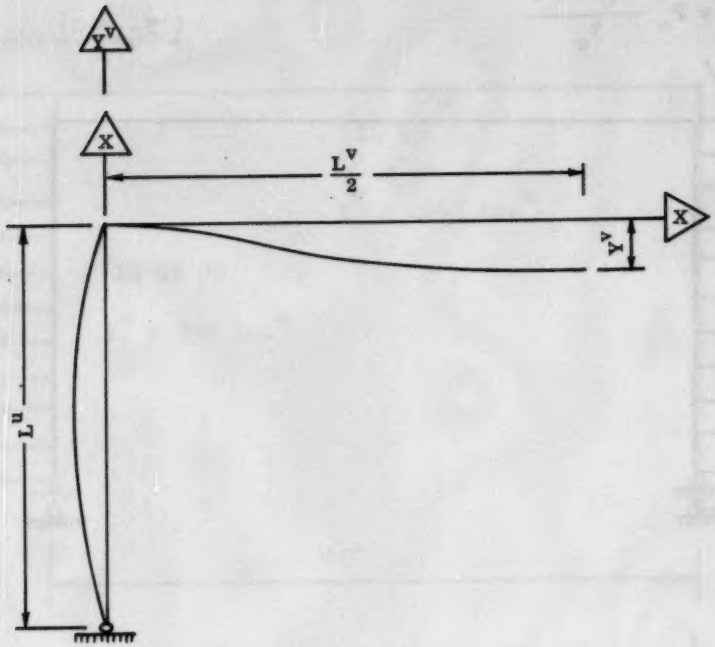

Figure 3. Rigid Frame Symmetrical Mode.

$$P(t) = P_e \frac{(t_e - \tau)}{t_e}$$

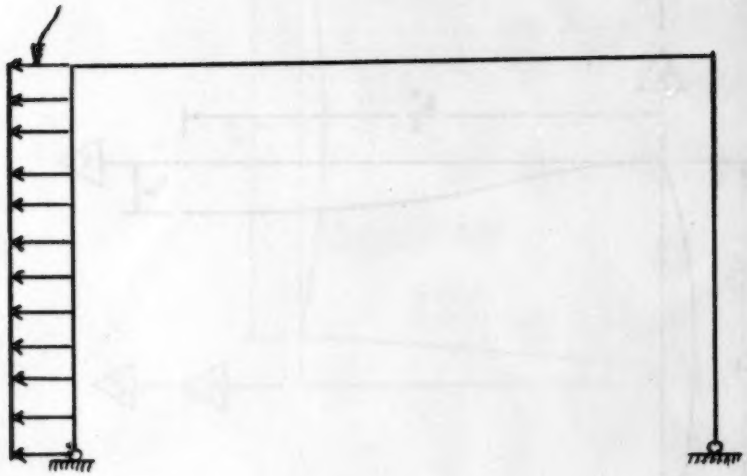

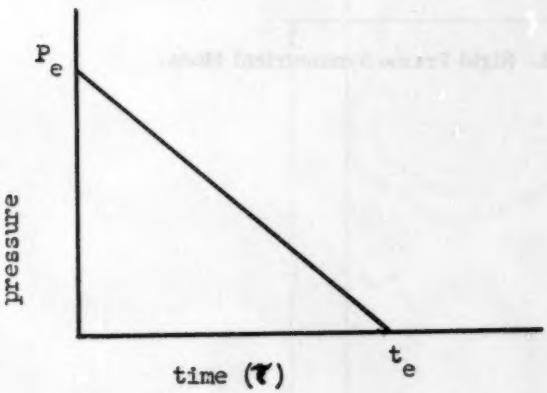

Figure 4. Pressure time relations for distributed force.

$$P(t) = 266\,\frac{(0.5 - \tau)}{0.5}$$

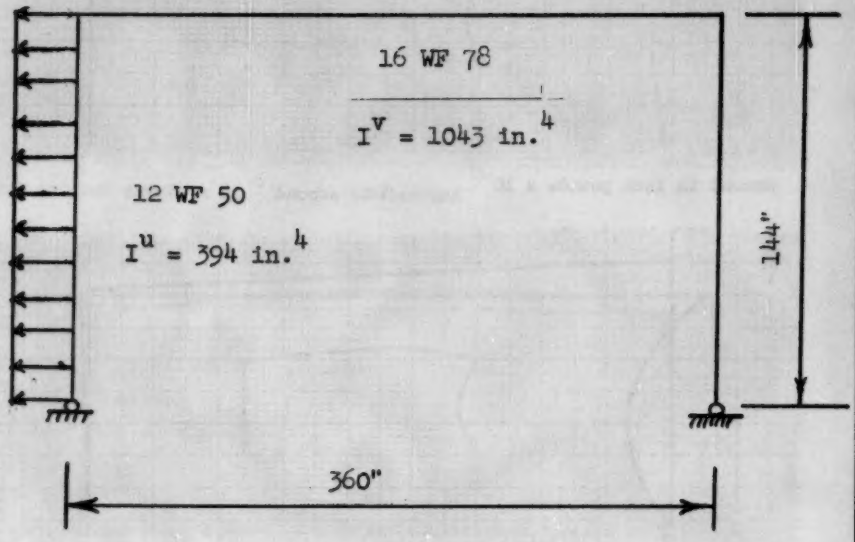

Figure 5. Frame subjected to distributed force.

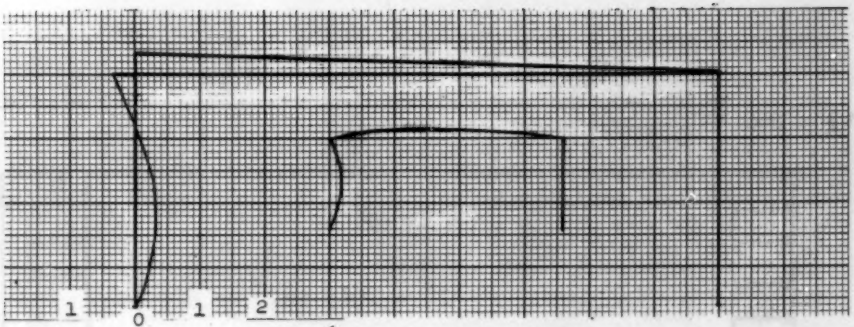

Moment in inch pounds x 10^{-6} 0.01 second

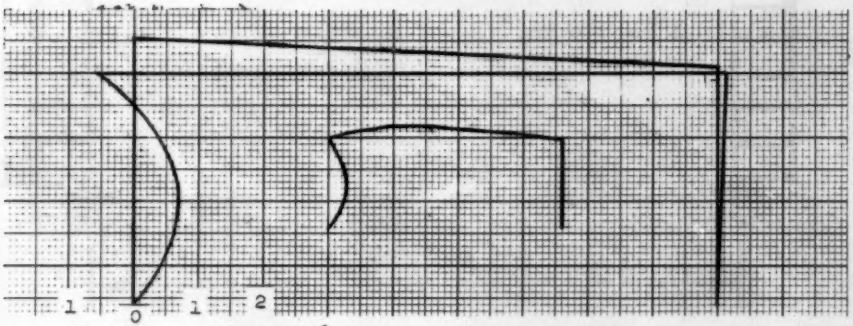

Moment in inch pounds x 10^{-6} 0.02 second

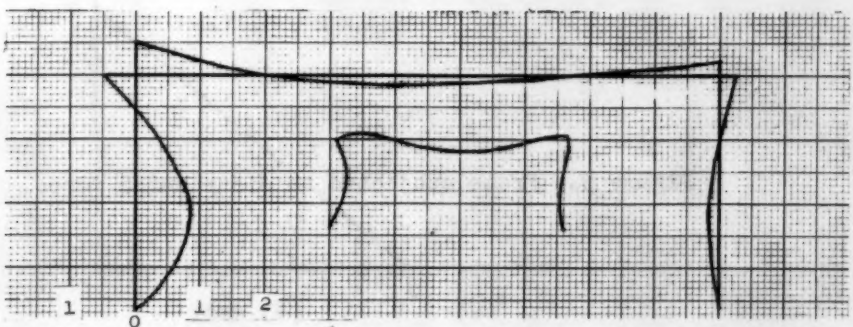

Moment in inch pounds x 10^{-6} 0.03 second

Figure 6. Moment-time and deflection-time relations.

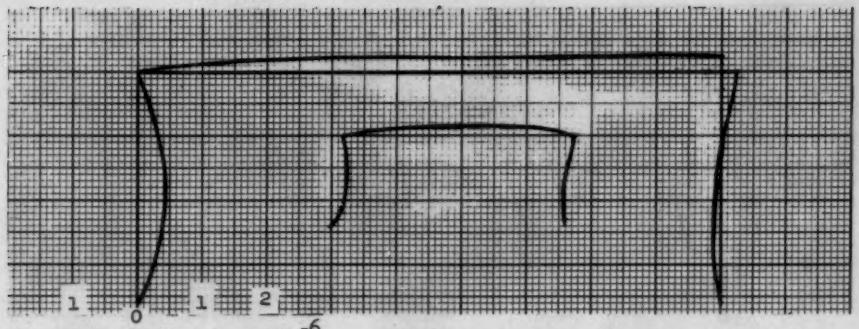

Moment in inch pounds x 10^{-6} 0.04 second

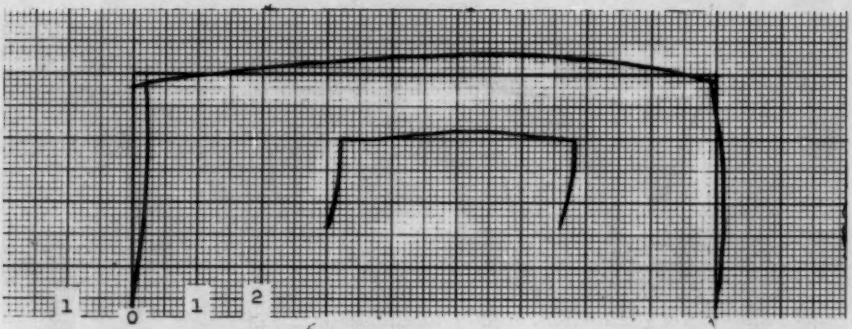

Moment in inch pounds x 10^{-6} 0.05 second

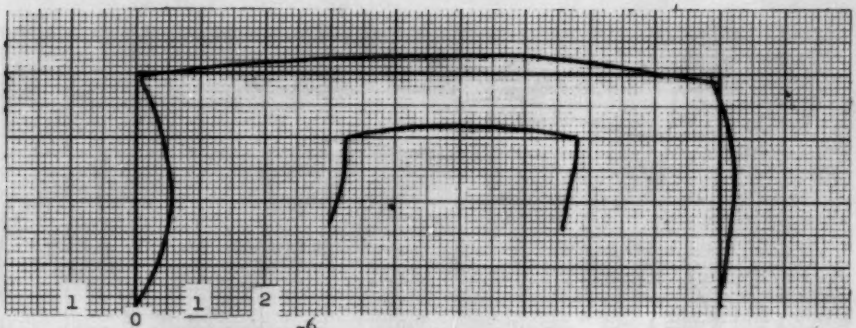

Moment in inch pounds x 10^{-6} 0.06 second

Figure 6 (Continued)

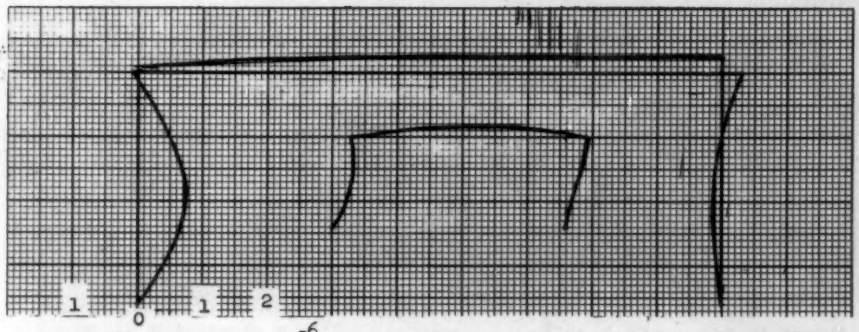

Moment in inch pounds x 10^{-6} 0.07 second

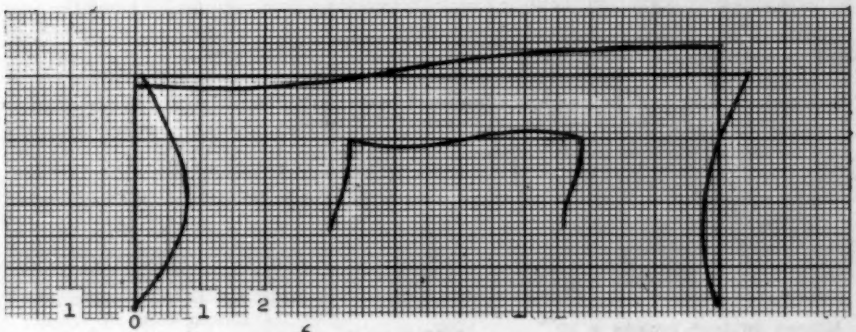

Moment in inch pounds x 10^{-6} 0.08 second

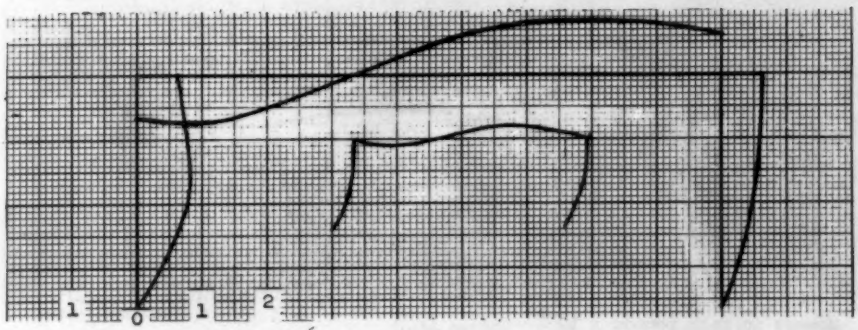

Moment in inch pounds x 10^{-6} 0.10 second

Figure 6 (Continued)

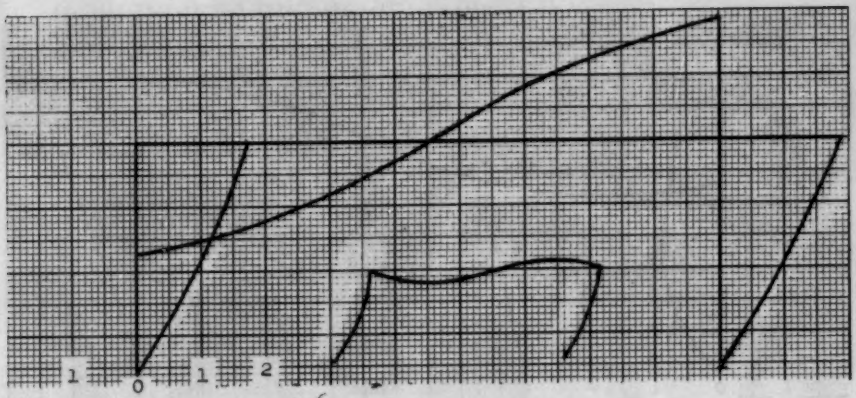

Moment in inch pounds x 10^{-6}

0.20 second

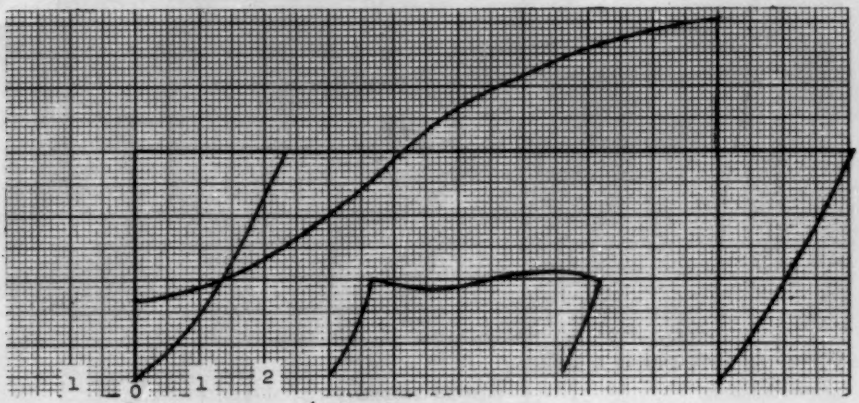

Moment in inch pounds x 10^{-6}

0.30 second

Figure 6 (Continued)

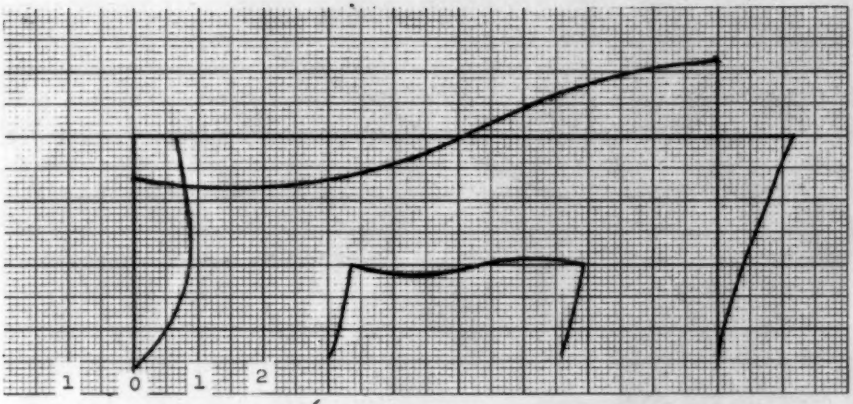

Moment in inch pounds x 10^{-6}

0.40 second

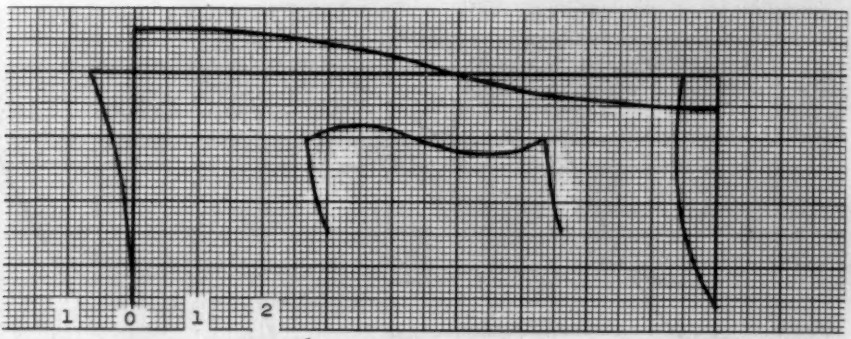

Moment in inch pounds x 10^{-6}

0.50 second

Figure 6 (Continued)

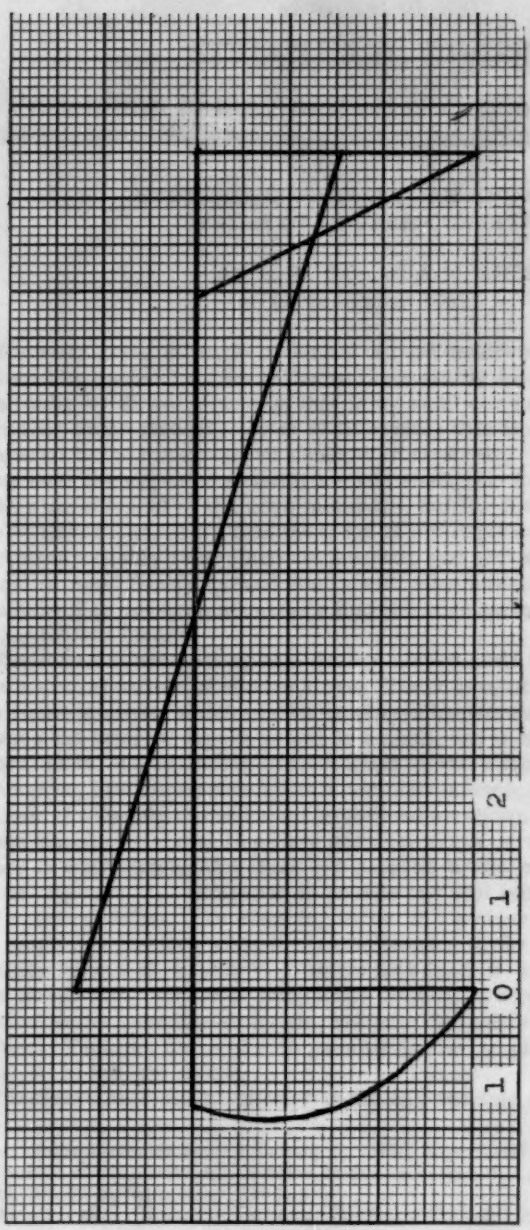

Figure 7. Static moment diagram.

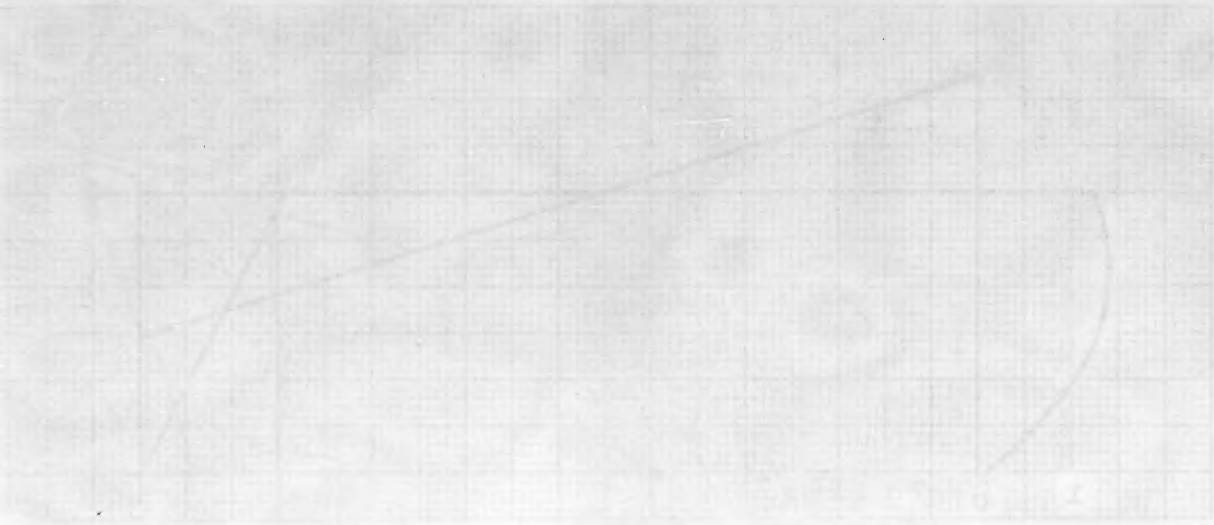

Paper 1057 ST 5

Journal of the
STRUCTURAL DIVISION
Proceedings of the American Society of Civil Engineers

HYPERBOLIC PARABOLOIDS AND OTHER SHELLS OF DOUBLE CURVATURE

Alfred L. Parme* A.M. ASCE
(Proc. Paper 1057)

The very great strength of doubly curved concrete shells with edges stiffened by arches or ribs is due to their ability to carry any continuous load principally by direct stresses, that is by axial compression or tension. Moreover these stresses for even extremely thin shells are relatively small compared to the compressive strength of concrete. Localized bending may occur near the edges of a doubly curved shell, due to the effect on the shell of the displacement of the edge members, but for the most part the shell is free of flexural forces. This behavior is not restricted solely to surfaces of revolution suitably restrained horizontally and vertically at the base but is typical of most doubly curved shells with edge beams. As will be shown subsequently it is not even necessary that the edge members be capable of resisting lateral forces.

The direct forces acting in a doubly curved shell are obtained directly from a consideration of statics alone. There are, of course, innumerable coordinate systems which can be employed to express the interrelationship between the internal forces acting in a shell, but it has been found that for the general case, the cartesian system leads to the simplest expressions.

Adopting this coordinate system for convenience, a representative small element of a doubly curved shell is formed as shown in Fig. 1 by two radial planes whose horizontal lines are parallel to the y axis and two other radial planes in which horizontal lines are parallel to the x axis. The direct forces T_x and T_y measured in pounds per unit length are positive when they create tension. The shearing force S, likewise measured in pounds per unit length, is positive when it creates tension in the diagonal direction of increasing values of x and y. The surface load w is considered positive when downward. Forces acting on the element are resolved into components parallel to the coordinate system, but with their direction tangential to the surface. Thus the force T_x is parallel to the zx plane but is inclined by the angle ϕ to the xy plane.

Considerable simplification** in the expressions for the equilibrium of

Note: Discussion open until February 1, 1957. Paper 1057 is part of the copyrighted Journal of the Structural Division of the American Society of Civil Engineers, Vol. 82, No. ST 5, September, 1956.

* Structural & Railways Bureau, Portland Cement Assn., Chicago, Ill.

** Johansen K. W. "Stress Conditions in Shells Neglecting Bending." Copenhagen, Dansk Selskab for Bygningsstetik. Bygningsstatiske Meddelesler 1938 p. 61-84.

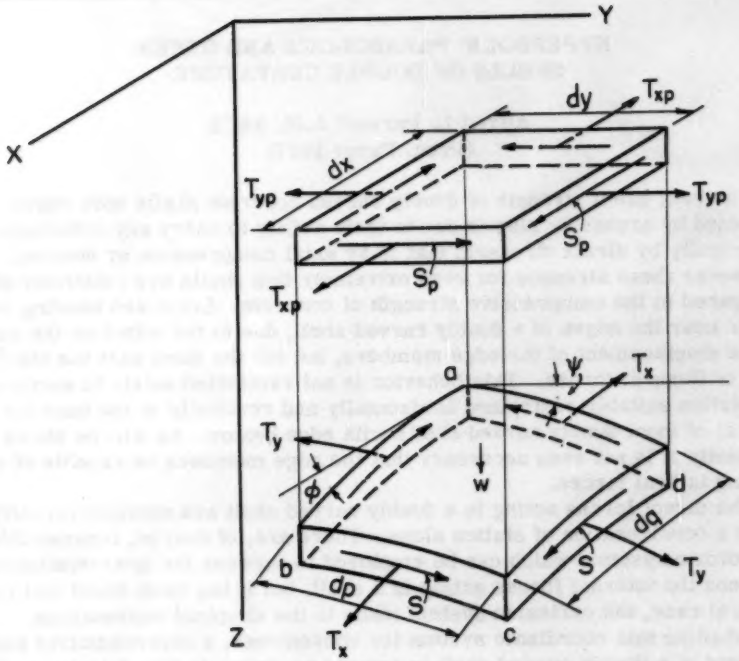

Fig. 1

forces parallel to the various axes results if the actual forces are transformed into fictitious forces acting on the projected area of the lower element in Fig. 1. From geometry it is evident that

$$dp \cos \psi = dy \tag{1a}$$

and

$$dq \cos \phi = dx \tag{1b}$$

The horizontal component of the normal force, T_x, acting on face ad is

$$T_x \cos \phi \, dp$$

which by equation (1a) becomes

$$T_x \frac{\cos \phi}{\cos \psi} dy$$

If the projected element is to have the same total force acting on it as the actual element, then

$$T_{xp} dy = T_x \frac{\cos \phi}{\cos \psi} dy \tag{2a}$$

or

$$T_{xp} = T_x \frac{\cos \phi}{\cos \psi} \tag{2b}$$

In a similar manner,

$$T_{yp} = T_y \frac{\cos \psi}{\cos \phi} \tag{3}$$

Equating the horizontal component of the shear acting on face ad to the shear on the projected element

$$S dp \cos \psi = S_p dy \tag{4a}$$

Substituting for dp its value in equation (1a), we have

$$S = S_p \tag{4b}$$

Assuming only a vertical load on the shell and recognizing that forces acting on the element vary from the near to the far face, equilibrium of forces in the x direction expressed in terms of T_{xp}, T_{yp} and S_p (horizontal components of the actual forces) yields:

$$\frac{\partial T_{xp}}{\partial x} + \frac{\partial S_p}{\partial y} = 0 \tag{5}$$

Equilibrium in the y direction gives:

$$\frac{\partial T_{yp}}{\partial y} + \frac{\partial S_p}{\partial x} = 0 \qquad (6)$$

To establish the equations of equilibrium of forces in the z direction, it is necessary first to obtain their vertical components. For the vertical component of the normal force T_x acting on face ad, we have

$$T_x \sin \phi \, dp$$

Substituting for T_x and dp their values as given by equations (2b) and (1a) gives:

$$T_{xp} \frac{\sin \phi}{\cos \phi} dy = T_{xp} \tan \phi \, dy$$

$$= T_{xp} \frac{\partial z}{\partial x} dy$$

The vertical component acting per unit of length along the y axis is therefore

$$T_{xp} \frac{\partial z}{\partial x}$$

In a similar manner, the vertical component of T_y per unit of length along the x axis is

$$T_{yp} \frac{\partial z}{\partial y}$$

The vertical component of the shear force on face ad is

$$S dp \sin \psi$$

$$= S_p \frac{\partial z}{\partial y} dy$$

which per unit of length along the y axis equals

$$S_p \frac{\partial z}{\partial y}$$

Similarly, the vertical component of shear acting on face ab is

$$S_p \frac{\partial z}{\partial x}$$

Taking into account the variation in the magnitude of forces from one face to the other, the summation of forces in the z direction yields

$$\frac{\partial}{\partial x}\left(T_{xp}\frac{\partial z}{\partial x}\right)+\frac{\partial}{\partial y}\left(T_{yp}\frac{\partial z}{\partial y}\right)+\frac{\partial}{\partial x}\left(S_p\frac{\partial z}{\partial y}\right)+\frac{\partial}{\partial y}\left(S_p\frac{\partial z}{\partial x}\right)+w_z=0 \qquad (7a)$$

in which w_z is the load per unit of projected area. Equation (7a) reduces to

$$T_{xp}\frac{\partial^2 z}{\partial x^2}+T_{yp}\frac{\partial^2 z}{\partial y^2}+2S_p\frac{\partial^2 z}{\partial x\partial y}$$
$$+\frac{\partial z}{\partial x}\left(\frac{\partial T_{xp}}{\partial x}+\frac{\partial S_p}{\partial y}\right)+\frac{\partial z}{\partial y}\left(\frac{\partial T_{yp}}{\partial y}+\frac{\partial S_p}{\partial x}\right)=-w_z \qquad (7b)$$

By equations (5) and (6), the terms in the parentheses equal zero; hence equation (7b) reduces to

$$T_{xp}\frac{\partial^2 z}{\partial x^2}+T_{yp}\frac{\partial^2 z}{\partial y^2}+2S_p\frac{\partial^2 z}{\partial x\partial y}=-w_z \qquad (7c)$$

The three simultaneous equations (5), (6), and (7a), can be reduced to one equation with one unknown by introducing the function F, so that

$$\frac{\partial^2 F}{\partial y^2}=T_{xp} \qquad (8a)$$

$$\frac{\partial^2 F}{\partial x^2}=T_{yp} \qquad (8b)$$

and

$$-\frac{\partial^2 F}{\partial x\partial y}=S_p \qquad (8c)$$

These values satisfy the requirements of equations (5) and (6) and reduce equation (7c) to

$$\frac{\partial^2 F}{\partial y^2}\frac{\partial^2 z}{\partial x^2}+\frac{\partial^2 F}{\partial x^2}\frac{\partial^2 z}{\partial y^2}-2\frac{\partial^2 F}{\partial x\partial y}\frac{\partial^2 z}{\partial x\partial y}=-w_z \qquad (9)$$

Except for a few special cases, the algebraic solution of differential equation (9) is difficult, and a numerical procedure such as finite differences must be resorted to. One of the simpler cases to solve is the hyperbolic paraboloid shell subject to a uniform load. The surface of a hyperbolic paraboloid shell (see Fig. 2) is formed by a series of straight lines parallel to the zx and zy planes and hence is defined by the expression

$$z=\frac{h}{ab}xy \qquad (10)$$

The second differential of equation (10) is zero. Therefore, for a hyperbolic paraboloid shell, equation (9) becomes

$$-2\frac{\partial^2 F}{\partial x\,\partial y}\,\frac{h}{ab} = w \tag{11}$$

which simplifies by means of equation (8c) to

$$S_p = \frac{ab}{2h}\,w \tag{12}$$

Because the differential of S_p with respect to y and x is zero it is seen from the relationships in equations (5) and (6) that:

$$T_{xp} = T_{yp} = 0 \tag{13}$$

Equation (13) indicates that there are no forces normal to the edges of a hyperbolic paraboloid shell subject to a uniform load. However, a uniform tangential shear exists along the edges and must be resisted by the edge member.

This state of pure shear, which actually resolves into principal stresses of equal and opposite magnitude acting on sections at 45 degrees to the shear plane, can be deduced from purely physical considerations without recourse to differential equations. As shown in Fig. 2, sections of a hyperbolic paraboloid surface taken at 45 degrees to the coordinate axes, form idential parabolic arches. In other words, the surface shown in Fig. 2 can be obtained by translating (moving) a parabolic curve along curve om. The parabolas parallel to om curve downward while those at right angles to these, curve in the opposite direction.

Assuming that the load is equally divided between the two sets of perpendicular parabolas, it is evident that at the edge parabolas parallel to om exert an outward thrust while those perpendicular to om exert an inward pull. Though opposite in character, the magnitude of these forces intersecting at any point on the boundary of the surface is equal because intersecting parabolas are identical. The net effect as shown in Fig. 3, is that the outward force acting on the edge is cancelled out, and only pure shear acts along the edge. This shear must be resisted by a rigid edge member. Because horizontal reactions are supplied to the ends of the parabolas by the interaction of one on the other the assumption made that the load is carried by a series of parabolas is valid.

For most hyperbolic paraboloid shells of moderate rise, it is deemed satisfactory to consider the load as uniform. However, when the rise is great, the dead load can no longer be considered as uniform on the projected area. For this condition, the dead load of the shell is

$$w_z = \frac{w}{\cos\phi\,\cos\psi} \tag{14a}$$

which, by trigonometry, can be shown to equal

$$w_z = w\sqrt{\left[1+\left(\frac{hx}{ab}\right)^2\right]\left[1+\left(\frac{hy}{ab}\right)^2\right]} \tag{14b}$$

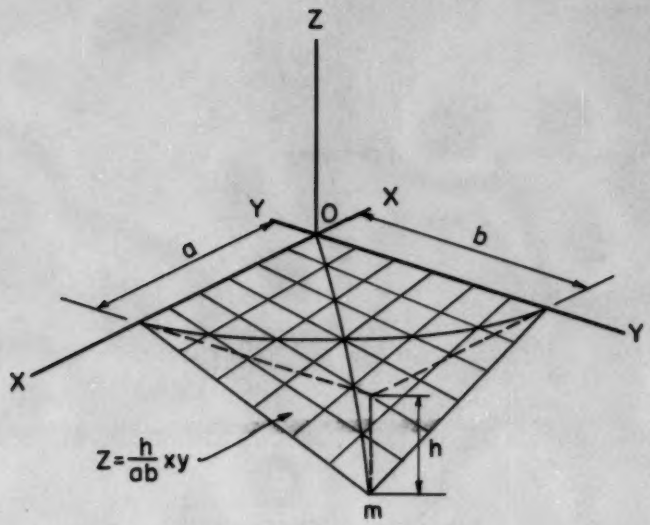

Fig. 2

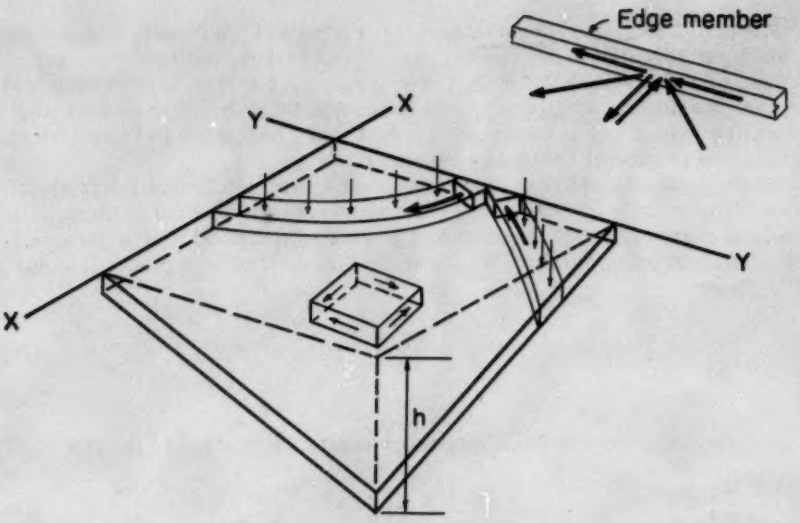

Fig. 3

Neglecting the term

$$\left(\frac{hx}{ab}\right)^2 \cdot \left(\frac{hy}{ab}\right)^2$$

because it is small, equation (14b) reduces to

$$w_z = w\sqrt{1+\left(\frac{hx}{ab}\right)^2+\left(\frac{hy}{ab}\right)^2} \tag{14c}$$

From equation (9) then

$$-\frac{\partial^2 F}{\partial x \partial y}\,\frac{2h}{ab} = S_p\frac{2h}{ab} = w\sqrt{1+\left(\frac{hx}{ab}\right)^2+\left(\frac{hy}{ab}\right)^2} \tag{15}$$

Differentiating equation (15) and then integrating according to equations (5) and (6), we find

$$T_{xp} = -w\frac{y}{2}\log\left[\frac{hx}{ab}+\sqrt{1+\left(\frac{hx}{ab}\right)^2+\left(\frac{hy}{ab}\right)^2}\right] + f(y) \tag{16}$$

$$T_{yp} = -w\frac{x}{2}\log\left[\frac{hy}{ab}+\sqrt{1+\left(\frac{hx}{ab}\right)^2+\left(\frac{hy}{ab}\right)^2}\right] + f(x) \tag{17}$$

in which f(y) and f(x) are constants of integration. With only one constant of integration available for each of the normal forces, and two edges for each force, i.e., at x=0 and x=a for T_{xp} or y=0 and y=b for T_{yp}, it is evident that for pure membrane or direct force action, normal reactions are required. If normal reactions are not provided at least along one of the two parallel edges, the surface is subject to bending moments.

Another surface which is amenable to albegraic solution although slightly more involved than the solution for the hyperbolic paraboloid surface, is the elliptical paraboloid. This surface is generated by translating a parabolic curve along another parabola as shown in Fig. 4. The equation of this surface is

$$z = \frac{h_y y^2}{b^2} + \frac{h_x x^2}{a^2} \tag{18}$$

The second differentials of this expression with respect to x and y are

$$\frac{\partial^2 z}{\partial x^2} = \frac{2h_x}{a^2} \tag{19a}$$

$$\frac{\partial^2 z}{\partial y^2} = \frac{2h_y}{b^2} \tag{19b}$$

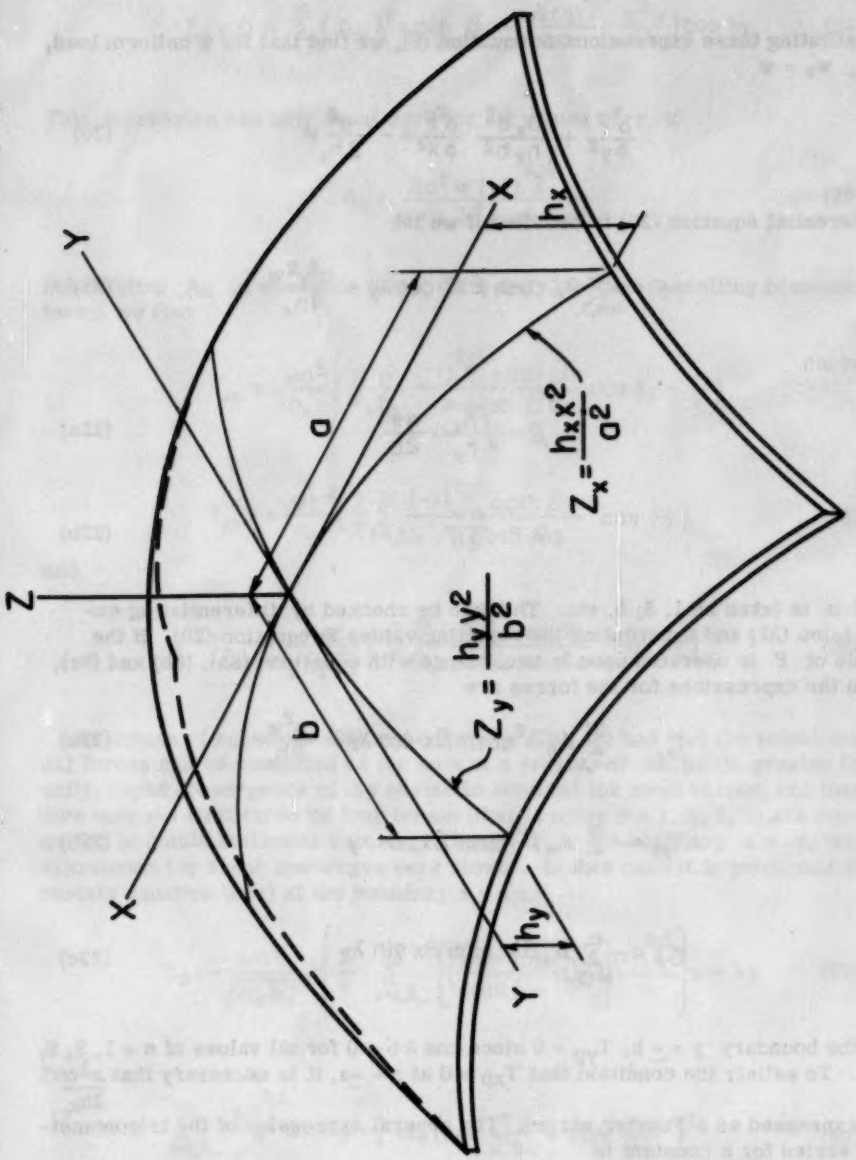

Fig. 4 -

$$\frac{\delta^2 z}{\delta x \delta y} = 0 \tag{19c}$$

Substituting these expressions in equation (9), we find that for a uniform load, i.e., $w_z = w$

$$\frac{\delta^2 F}{\delta y^2} + \frac{h_y a^2}{h_x b^2} \frac{\delta^2 F}{\delta x^2} = - \frac{a^2}{2h_x} w \tag{20}$$

Differential equation (20) is satisfied if we let

$$F = -\sum_{n=1,3..}^{\infty} A_n \cosh \beta x \cdot \cos \lambda y - \frac{a^2 y^2 w}{4h_x} \tag{21}$$

in which

$$\beta = \sqrt{\frac{h_x}{h_y}} \cdot \frac{n\pi}{2a} \tag{22a}$$

$$\lambda = \frac{n\pi}{2b} \tag{22b}$$

and n is taken as 1, 3, 5, etc. This can be checked by differentiating expression (21) and substituting the resulting values in equation (20). If the value of F is operated upon in accordance with equations (8a), (8b) and (8c), then the expressions for the forces are

$$T_{xp} = \sum_{n=1,3..}^{\infty} A_n \lambda^2 \cosh \beta x \cos \lambda y - \frac{a^2 w}{2h_x} \tag{23a}$$

$$T_{yp} = - \sum_{n=1,3..}^{\infty} A_n \beta^2 \cosh \beta x \cos \lambda y \tag{23b}$$

$$S_p = - \sum_{n=1,3..}^{\infty} A_n \beta\lambda \sinh \beta x \sin \lambda y \tag{23c}$$

At the boundary $y = \pm b$, $T_{yp} = 0$ since $\cos \lambda b = 0$ for all values of n = 1, 3, 5, etc. To satisfy the condition that $T_{xp} = 0$ at $x = \pm a$, it is necessary that $\frac{a^2 w}{2h_x}$ be expressed as a Fourier series. The general expression of the trigonometric series for a constant is

$$1 = \sum_{n=1,3..}^{\infty} \frac{4 (-1)^{\frac{n-1}{2}} \cos \lambda y}{n\pi}$$

Hence at $x = \pm a$, equation (23a) becomes

$$T_{xp} = 0 = \sum_{n=1,3...}^{\infty} \left(A_n \lambda^2 \cosh \beta a - \frac{4(-1)^{\frac{n-1}{2}}}{n\pi} \cdot \frac{a^2 w}{2h_x} \right) \cos \lambda y \qquad (24)$$

This expression can only equal zero for all values of y if

$$A_n = \frac{2a^2 w (-1)^{\frac{n-1}{2}}}{n\pi h_x \lambda^2 \cosh \beta a} \qquad (25)$$

Substituting A_n in equations (23a), (23b) and (23c) and cancelling common terms we find

$$T_{xp} = \frac{wa^2}{h_x} \left(\frac{2}{\pi} \sum_{n=1,3...}^{\infty} \frac{(-1)^{\frac{n-1}{2}} \cosh \beta x}{n \cosh \beta a} \cos \lambda y - \frac{1}{2} \right) \qquad (26a)$$

$$T_{yp} = -\frac{wb^2}{h_y} \left(\frac{2}{\pi} \sum_{n=1,3...}^{\infty} \frac{(-1)^{\frac{n-1}{2}} \cosh \beta x}{n \cosh \beta a} \cos \lambda y \right) \qquad (26b)$$

and

$$S_p = -\frac{wab}{\sqrt{h_x h_y}} \left(\frac{2}{\pi} \sum_{n=1,3...}^{\infty} \frac{(-1)^{\frac{n-1}{2}} \sinh \beta x}{n \cosh \beta a} \sin \lambda y \right) \qquad (26c)$$

By means of equations (26) and equations (2b), (3) and (4b) the actual internal forces can be computed as the sum of a series. If hx/hy is greater than unity, rapid convergence of the series is obtained for most values, and therefore only the first three or four terms (that is using n = 1, 3, 5, 7) are required to obtain sufficient accuracy. However, at the boundary $x = \pm a$, the expression for shear converges very slowly. In this case it is profitable to restate equation (26c) at the boundary x = a as

$$S_p = -\frac{wab}{\sqrt{h_x h_y}} \left\{ \frac{2}{\pi} \sum_{n=1,3...}^{\infty} \left[\left(\frac{\sinh \beta a}{\cosh \beta a} - 1 \right) + 1 \right] \frac{(-1)^{\frac{n-1}{2}}}{n} \right\} \sin \lambda y \qquad (27)$$

But

$$\sum_{n=1,3...}^{\infty} \frac{(-1)^{\frac{n-1}{2}}}{n} \sin \lambda y = \frac{1}{4} \log \left(\sec \frac{\pi y}{2b} + \tan \frac{\pi y}{2b} \right)^2 \qquad (28)$$

Therefore equation (27) reduces to

$$S_p = -\frac{wab}{\sqrt{h_x h_y}}\left[\frac{1}{2\pi}\log\left(\sec\frac{\pi y}{2b} + \tan\frac{\pi y}{2b}\right)^2 - \frac{2}{\pi}\sum_{n=1,3\ldots}^{\infty}\left(1-\tanh\beta a\right)\frac{(-1)^{\frac{n-1}{2}}}{n}\sin\lambda y\right] \qquad (29)$$

For values of h_x/h_y greater than 1, the $\tanh\beta a$ is for practical purposes equal to 1. Hence the second term in equation (29) can be ignored, or at most only the value of $n = 1$ is required. Thus the expression for shear converges rapidly.

At $y = \pm b$, since the sec $(\pi y/2b)$ and tan $(\pi y/2b)$ are infinite, the log of these values is infinite. Consequently equation (29) indicates that the shear at the corner is infinite. This would be true if the corner were completely free of normal forces and if the shell had no bending resistance. But because of the integral action of the supporting ribs and shell, normal forces exist at the corner. The presence of these normal forces alters the resistance to the extent that shear does not need to be infinite to satisfy statics. Moreover, at the corner some of the load can and is resisted by flexural resistance. From studies made of cylindrical shells, it has been found that this flexural action is confined to a distance of approximately $0.4\sqrt{rt}$ from the rib, in which r is the radius of the shell and t is the thickness. Therefore it is felt that equations (26c) and (29) do not apply within the distance $0.4\sqrt{rt}$ from the corner. Shear can be considered maximum at the point $y = b-0.4\sqrt{rt}$.

It should not be overlooked that the symbols T_x, T_y and S represent forces per unit of length. To obtain stresses, these values must be divided by the thickness of the shell.

The trigonometric functions involved in equations (2b), (3) and (4b) can be readily expressed as functions of x and y. Differentiating equation (18), with respect to x, we find

$$\frac{\partial z}{\partial x} = \frac{2h_x}{a}\cdot\frac{x}{a} = \tan\phi \qquad (30)$$

Utilizing the trigonometric identity that

$$\tan^2\phi = \frac{1}{\cos^2\phi} - 1$$

equation (2b) reduces to

$$\left(\frac{2h_x}{a}\cdot\frac{x}{a}\right)^2 + 1 = \frac{1}{\cos^2\phi} \qquad (31)$$

or

$$\cos\phi = \frac{1}{\sqrt{1+\left(\frac{2h_x}{a}\cdot\frac{x}{a}\right)^2}} \qquad (32a)$$

Similarly

$$\cos\psi = \frac{1}{\sqrt{1+\left(\frac{2h_y}{b}\cdot\frac{y}{b}\right)^2}} \tag{32b}$$

and therefore

$$\frac{\cos\phi}{\cos\psi} = \sqrt{\frac{1+\left(\frac{2h_y}{b}\cdot\frac{y}{b}\right)^2}{1+\left(\frac{2h_x}{a}\cdot\frac{x}{a}\right)^2}} \tag{32c}$$

In order to avoid mathematical complications, w_z was assumed constant in establishing equation (20). However, although the algebraic operations do become extensive and quite formidable, the procedure outlined for the uniform load can also be applied to cover the case of any symmetrical loading such as the dead weight of the shell by expressing the load in terms of the double Fourier series

$$w_z = \sum_{m=1,3\ldots}^{\infty}\sum_{n=1,3\ldots}^{\infty} \beta_{mn}\cos\gamma x\cos\lambda y \tag{33}$$

in which $\gamma = m\pi/2a$

The resulting expressions for T_{xp} and T_{yp} obtained by expressing w_z in this manner indicate that any symmetrical loading can be resisted by direct forces without the necessity for lateral or normal forces at the boundaries. The behavior of the elliptical paraboloid shell under dead load therefore differs from that of the hyperbolic paraboloid shell where it was found that the dead load induces some bending if no lateral restraint is provided.

To expedite the analysis of elliptical paraboloid shells, and to secure a better understanding of their load carrying characteristic, Table 1 has been compiled on the basis of equations (26). It should be noted that the expressions inside the parentheses in these equations contain only the parameter h_x/h_y. Therefore the behavior of this doubly curved shell can be expressed as a function of this single parameter.

Coefficients are given for calculating the three force components, T_x, T_y and S at the eighth points of a dome. In each case the forces are determined by multiplying the coefficients by the constants listed in the heading of Table 1. These constants depend only on the selected dimensions of the shell and on the load. In this connection, for the sake of completeness, the factor k has been included. In practice the additional accuracy secured by the inclusion of this term is unwarranted because the stresses due to T_x and T_y are never critical. As a matter of fact, except in the zone near the corners where the principal stress due to the combination of the three force components is tensile, the stresses are so low in compression for spans now being considered that an investigation of the stresses in a dome becomes only of academic interest. Therefore the real reason and need for computing stresses in a shell with a fair degree of accuracy is to obtain a reliable determination of the

Table 1 - Uniform Load on Elliptical Paraboloid Shell

$$T_y = -\frac{wb^2}{kh_y} \cdot \text{coef.}$$

$$T_x = -\frac{wa^2k}{h_x} \cdot \text{coef.}$$

$$S = -\frac{wab}{\sqrt{h_x h_y}} \cdot \text{coef.}$$

$$k = \sqrt{\frac{1+[(2h_x/a)(x/a)]^2}{1+[(2h_y/b)(y/b)]^2}}$$

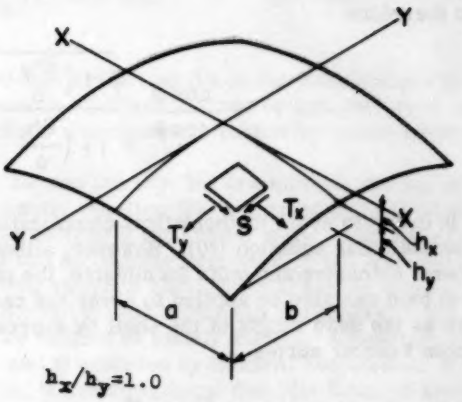

$h_x/h_y = 1.0$

			y/b				
			0	.25	.50	.75	1.0
x/a	0	T_y	0.250	0.233	0.182	0.101	0
		T_x	0.250	0.267	0.318	0.399	0.500
		S	0	0	0	0	0
	.25	T_y	0.267	0.250	0.199	0.111	0
		T_x	0.233	0.250	0.301	0.389	0.500
		S	0	0.029	0.068	0.096	0.108
	.50	T_y	0.318	0.301	0.250	0.150	0
		T_x	0.182	0.199	0.250	0.350	0.500
		S	0	0.068	0.140	0.210	0.244
	.75	T_y	0.399	0.389	0.350	0.250	0
		T_x	0.101	0.111	0.150	0.250	0.500
		S	0	0.096	0.210	0.356	0.465
	1.0	T_y	0.500	0.500	0.500	0.500	0
		T_x	0	0	0	0	0
		S	0	0.108	0.243	0.465	∞

Table 1 Cont.

$h_x/h_y=0.8$

			y/b				
			0	.25	.50	.75	1.0
x/a	0	T_y	0.289	0.270	0.213	0.119	0
		T_x	0.211	0.230	0.287	0.381	0.500
		S	0	0	0	0	0
	.25	T_y	0.304	0.285	0.228	0.130	0
		T_x	0.196	0.215	0.272	0.370	0.500
		S	0	0.034	0.069	0.100	0.114
	.50	T_y	0.347	0.331	0.277	0.169	0
		T_x	0.153	0.169	0.223	0.331	0.500
		S	0	0.065	0.139	0.215	0.255
	.75	T_y	0.416	0.406	0.369	0.270	0
		T_x	0.084	0.094	0.131	0.230	0.500
		S	0	0.091	0.201	0.353	0.480
	1.0	T_y	0.500	0.500	0.500	0.500	0
		T_x	0	0	0	0	0
		S	0	0.101	0.229	0.443	∞

$h_x/h_y=0.6$

			y/b				
			0	.25	.50	.75	1.0
x/a	0	T_y	0.336	0.316	0.252	0.143	0
		T_x	0.164	0.184	0.248	0.357	0.500
		S	0	0	0	0	0
	.25	T_y	0.348	0.329	0.267	0.155	0
		T_x	0.152	0.171	0.233	0.345	0.500
		S	0	0.031	0.067	0.103	0.120
	.50	T_y	0.383	0.367	0.312	0.197	0
		T_x	0.117	0.133	0.188	0.304	0.500
		S	0	0.060	0.132	0.216	0.265
	.75	T_y	0.436	0.426	0.392	0.296	0
		T_x	0.064	0.074	0.108	0.204	0.500
		S	0	0.081	0.185	0.342	0.494
	1.0	T_y	0.500	0.500	0.500	0.500	0
		T_x	0	0	0	0	0
		S	0	0.089	0.208	0.413	∞

Table 1 Cont.

$h_x/h_y=0.4$

			y/b=0.4				
			0	.25	.50	.75	1.0
x/a	0	T_y	0.395	0.374	0.307	0.180	0
		T_x	0.105	0.126	0.193	0.320	0.500
		S	0	0	0	0	0
	.25	T_y	0.403	0.383	0.319	0.192	0
		T_x	0.097	0.117	0.181	0.308	0.500
		S	0	0.026	0.060	0.101	0.125
	.50	T_y	0.425	0.410	0.357	0.235	0
		T_x	0.075	0.090	0.143	0.265	0.500
		S	0	0.049	0.115	0.208	0.274
	.75	T_y	0.459	0.451	0.419	0.331	0
		T_x	0.041	0.049	0.081	0.169	0.500
		S	0	0.065	0.156	0.316	0.506
	1.0	T_y	0.500	0.500	0.500	0.500	0
		T_x	0	0	0	0	0
		S	0	0.070	0.173	0.363	∞

$h_x/h_y=0.2$

			y/b				
			0	.25	.50	.75	1.0
x/a	0	T_y	0.462	0.446	0.388	0.248	0
		T_x	0.038	0.054	0.112	0.252	0.500
		S	0	0	0	0	0
	.25	T_y	0.465	0.451	0.396	0.261	0
		T_x	0.035	0.049	0.104	0.239	0.500
		S	0	0.014	0.040	0.088	0.128
	.50	T_y	0.473	0.462	0.414	0.303	0
		T_x	0.027	0.038	0.086	0.197	0.500
		S	0	0.027	0.074	0.174	0.280
	.75	T_y	0.485	0.480	0.456	0.383	0
		T_x	0.015	0.020	0.044	0.117	0.500
		S	0	0.034	0.098	0.246	0.510
	1.0	T_y	0.500	0.500	0.500	0.500	0
		T_x	0	0	0	0	0
		S	0	0.038	0.108	0.262	∞

Table 2 - Shear Along the Edges

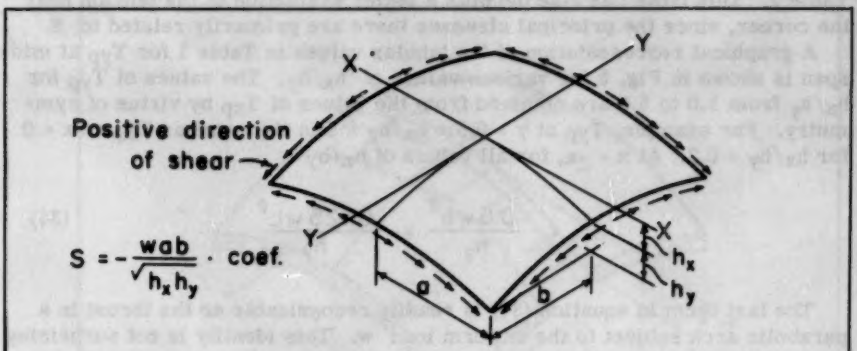

	h_x/h_y					
		1.0	0.8	0.6	0.4	0.2
	at $x=\pm a$					
y/b	0	0	0	0	0	0
	.1	0.0419	0.0389	0.0342	0.0307	0.0137
	.2	0.0854	0.0793	0.0701	0.0550	0.0286
	.3	0.1319	0.1231	0.1096	0.0872	0.0481
	.4	0.1836	0.1721	0.1546	0.1254	0.0731
	.5	0.2432	0.2294	0.2081	0.1728	0.1075
	.6	0.3204	0.3066	0.2859	0.2493	0.1818
	.7	0.4071	0.3897	0.3627	0.3173	0.2296
	.8	0.5363	0.5178	0.4887	0.4400	0.3443
	.85	0.6279	0.6090	0.5791	0.5292	0.4306
	.9	0.7570	0.7378	0.7074	0.6667	0.5659
	.95	0.9777	0.9582	0.9276	0.8763	0.7741
	1.0	∞	∞	∞	∞	∞
	at $y=\pm b$					
x/a	0	0	0	0	0	0
	.1	0.0419	0.0444	0.0468	0.0488	0.0500
	.2	0.0854	0.0903	0.0950	0.0990	0.1014
	.3	0.1319	0.1391	0.1460	0.1519	0.1553
	.4	0.1836	0.1930	0.2019	0.2095	0.2140
	.5	0.2432	0.2545	0.2652	0.2743	0.2798
	.6	0.3204	0.3317	0.3425	0.3516	0.3571
	.7	0.4071	0.4213	0.4348	0.4463	0.4532
	.8	0.5363	0.5515	0.5659	0.5782	0.5855
	.85	0.6279	0.6434	0.6582	0.6707	0.6782
	.9	0.7570	0.7728	0.7878	0.8005	0.8081
	.95	0.9777	0.9935	1.0087	1.0215	1.0290
	1.0	∞	∞	∞	∞	∞

tangential load which must be carried by the supporting arches.

For this purpose the tangential shear existing along the boundaries at the tenth and two twentieth intervals of half the chord have been tabulated in Table 2. This table likewise permits a better evaluation of the tension near the corner, since the principal stresses there are primarily related to S.

A graphical representation of the tabular values in Table 1 for T_{yp} at mid-span is shown in Fig. 5 for various values of h_x/h_y. The values of T_{yp} for h_x/h_y from 1.0 to 5.0 are obtained from the values of T_{xp} by virtue of symmetry. For example, Typ at y = 0 for $h_x/h_y = 5$ is the same as T_{xp} at x = 0 for $h_x/h_y = 0.2$. At $x = \pm a$, for all values of h_x/h_y

$$T_{yp} = -\frac{0.5\,w b^2}{h_y} = -\frac{0.125\,w L^2}{h_y} \qquad (34)$$

The last term in equation (34) is readily recognizable as the thrust in a parabolic arch subject to the uniform load w. This identity is not surprising since at the boundary, the force normal to the edge was made zero. Consequently the imposed condition of restraint compels the entire load in the immediate vicinity of the edge to be carried by arch action in the y direction. Furthermore, $0.5b^2/h_y$ equals the radius of the parabola at its crown and thus the value T_{yp} at x = a, and y = 0 represents merely the thrust induced in a ring with the appropriate radius due to a radial load w.

Near the crown, marked variations in the value of T_{yp} occur as h_x/h_y varies. When the rise in the x direction is small compared to that in the y direction, as for example when $h_x/h_y = 0.2$, it is seen that the curves in Fig. 5 are almost horizontal indicating that a large proportion of the load is being resisted in the y direction. This can be anticipated from the geometry of the shell. As the curvature in one direction is flattened, thereby approaching as a limit a horizontal plane, it is natural that the load be transmitted in the other direction.

With no normal forces present along the edges, it follows that the increase in the proportion of load carried in the y direction as h_x/h_y decreases must be accompanied by an increase in the tangential shears along the edges $x = \pm a$. This increase is confirmed by the coefficients in Table 2. Although these coefficients do diminish at $x = \pm a$ as h_x/h_y decreases, they do not diminish as rapidly as $\sqrt{h_x/h_y}$.

For large values of h_x/h_y, T_{yp} becomes appreciably smaller as the crown is approached, and therefore for such shells, only the exterior portion of the shell is resisting load in the y direction. At the crown, the curve for $h_x/h_y = 1.0$ shows that half the load is carried in one direction and half in the other direction, which is natural from the condition of equal rise in the two directions.

A question of paramount interest is whether or not the coefficients in Tables 1 and 2 can be applied to domes of other shapes with the same rise and span. As previously cited, the critical stresses are a function of the shear near the corners. But the summation of the vertical components of the shear along an edge must equal the load on the shell. If the same variation of shear along an edge is assumed for all shapes, it is apparent that to satisfy the above condition of equilibrium, the intensity of the tangential shear is dependent on the steepness of the slope near the corner. This is especially true since maximum shear occurs at the corner.

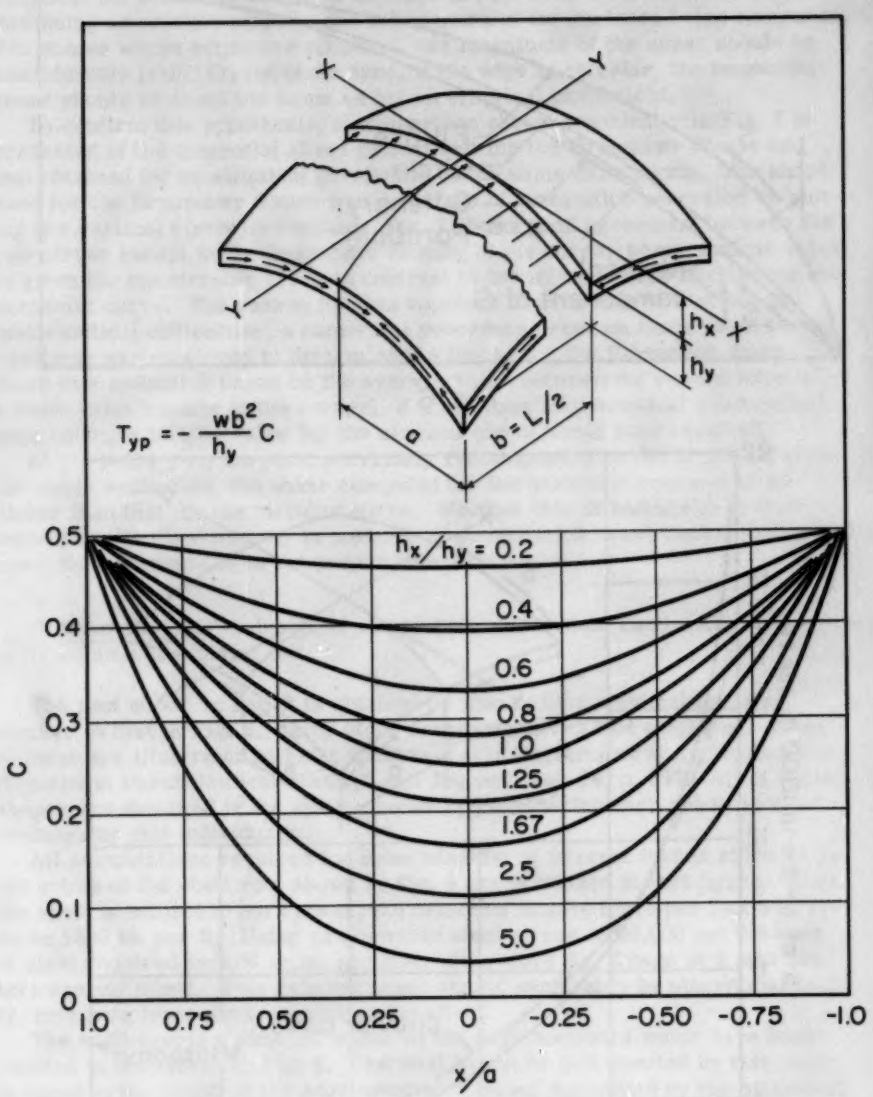
X
Y
Y
X
h_x
h_y
$T_{yp} = -\frac{wb^2}{h_y}C$
a
b = L/2
h_x/h_y = 0.2
0.4
0.6
0.8
1.0
1.25
1.67
2.5
5.0
C
0.5
0.4
0.3
0.2
0.1
0
1.0
0.75
0.50
0.25
0
-0.25
-0.50
-0.75
-1.0
x/a

Fig. 5

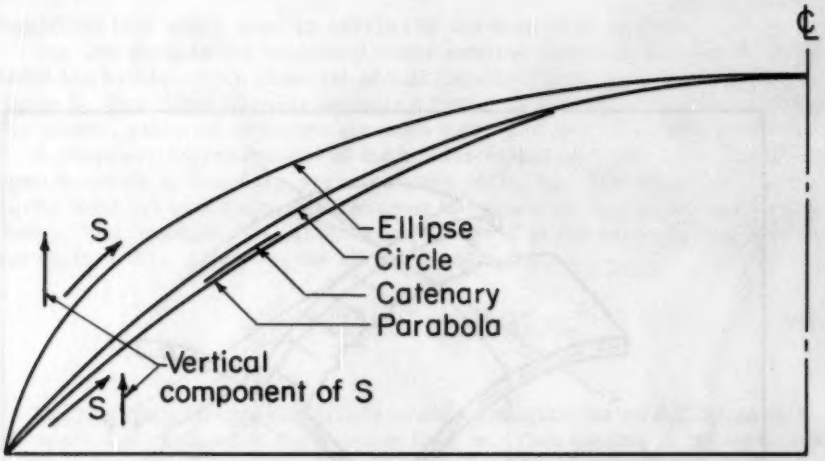
℄
S
Ellipse
Circle
Catenary
Parabola
Vertical
component of S
S

Fig. 6

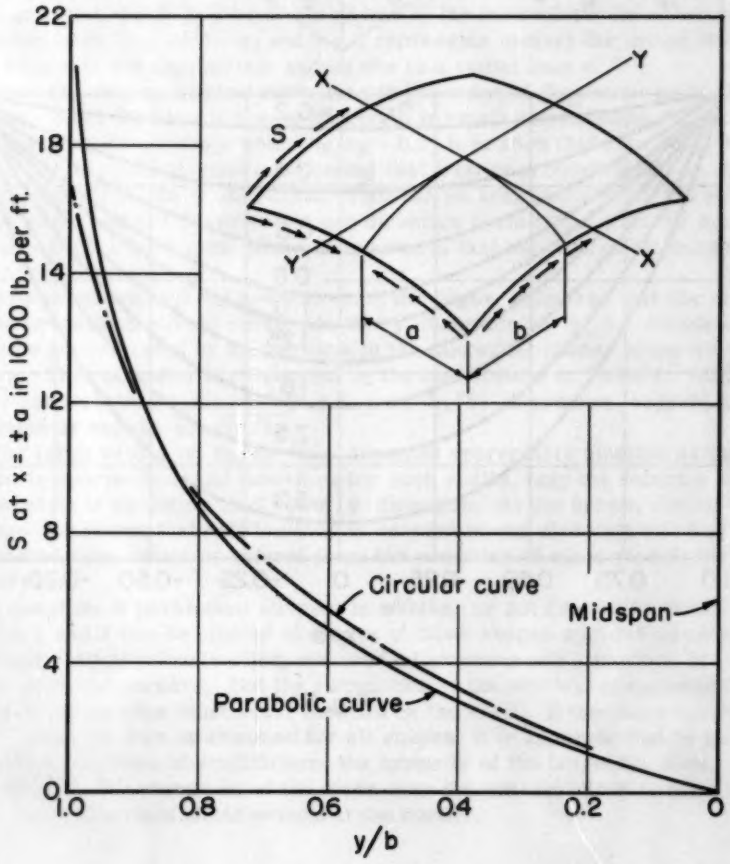
22
18
14
12
8
4
0
S at x = ± a in 1000 lb. per ft.
1.0
0.8
0.6
0.4
0.2
0
y/b
X
Y
S
Y
X
a
b
Circular curve
Midspan
Parabolic curve

Fig. 7

The slope near the corner of most commonly used shells of other curvature will, in general, be steeper than that of the elliptical paraboloid (see Fig. 6). Consequently, shear at the edge should be less for these than for an elliptical paraboloid of the same dimensions, the magnitude of the reduction depending on relative slopes near the corners of the surfaces being compared. For domes whose edges are elliptical, the magnitude of the shear should be considerably less. On the other hand, if the edge is circular, the tangential shear should be about the same as for an elliptical paraboloid.

To confirm this hypothesis, a comparison shown graphically in Fig. 7 is presented of the tangential shear calculated* for the Brynmawr domes and that obtained for an elliptical paraboloid of the same dimensions. The shape used for the Brynmawr domes was a surface of translation generated by moving one vertical circle on another. Fig. 7 shows good agreement between the two curves except in the immediate vicinity of the corner where a finite value is given for the circular curve in contrast to the infinite value implied for the parabolic curve. The reason for this apparent discrepancy is that due to mathematical difficulties, a numerical procedure based on finite differences equations was employed to determine the forces for the Brynmawr dome. Since this method is based on the average value between the chosen interval, a finite value results at the corner. If a rigorous mathematical solution had been used, an infinite value for the circular curve would have resulted.

At $y = b - 0.4\sqrt{rt}$, the point previously recommended as the break-off place for shear evaluation, the shear computed for the parabolic curve is about 7% higher than that for the circular curve. Whether this difference is real or merely due to dissimilarity in methods of computation is not known. However, the difference is in the proper direction.

Example 1 - The design of a hyperbolic paraboloid shell with column at center.

The roof shown in Fig. 8 is obtained by joining four identical sections similar to that in Fig. 2. Many other arrangements can be employed. A few of these are illustrated in Felix Candela's article "Structural Applications of Hyperbolic Paraboloidical Shells," ACI Journal, Vol. 26, p. 397. All of these shapes are designed in the same manner by considering each quadrant of a rectangular unit individually.

All computations required for determination of internal forces at the critical points of the shell roof shown in Fig. 8 are contained in that figure. Since the shell is subject to pure shear, the principal tensile force per foot will also be 1800 lb. per ft. Using an allowable steel stress of 20,000 psi the area of steel required is 0.09 sq.in. per foot. Therefore No. 2 bars at 6 inch centers are sufficient. This reinforcement should preferably be placed diagonally, extending from one free edge to the other.

The shell exerts a constant shear on the edge members which have been omitted in the sketch in Fig. 8. The total thrust or pull exerted by this shear is equal to the length of the edge member affected multiplied by the magnitude

* "The Design of a Reinforced Concrete Factory at Brynmawr, South Wales" by Ove Nyquist Arup and Ronald Jenkins. Proceedings of the Institution of Civil Engineers, part III, December 1953, p. 345 to 397.

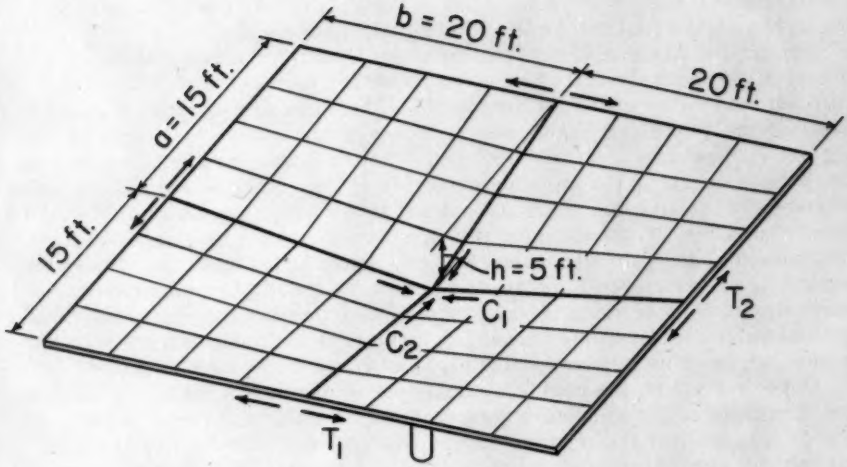

Calculations with w = 60 psf

$$S = \frac{wab}{2h} = \frac{60 \times 15 \times 20}{2 \times 5} = 1800 \text{ lb. ft.}$$

$$T_1 = -C_1 = 1800 \times 20 = 36{,}000 \text{ lb.}$$

$$T_2 = -C_2 = 1800 \times 15 = 27{,}000 \text{ lb.}$$

Fig. 8

Table 3 - Internal Forces in Elliptical Paraboloid

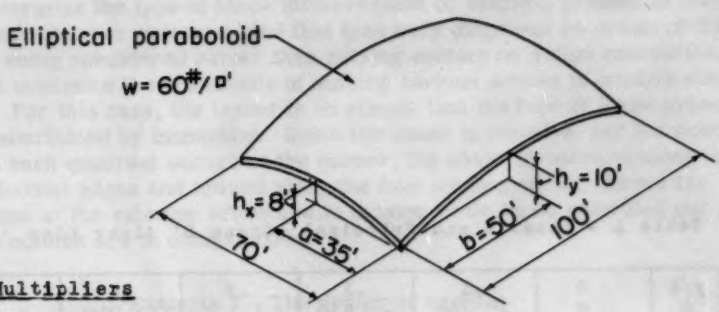

Multipliers

$\frac{wb^2}{h_y} = \frac{60 \times 50^2}{10}$ = 15,000 lb. per ft.

$\frac{wa^2}{h_x} = \frac{60 \times 35^2}{8}$ = 9,200 lb. per ft.

$\frac{wab}{\sqrt{h_x h_y}} = \frac{60 \times 50 \times 35}{\sqrt{8 \times 10}}$ = 11,700 lb. per ft.

			y/b				
			0	.25	.50	.75	1.0
x/a	0	T_y k	-4,300	-4,100	-3,200	-1,800	0
		T_x/k	-1,900	-2,100	-2,600	-3,500	-4,600
		S	0	0	0	0	0
	.25	T_y k	-4,600	-4,300	-3,400	-2,000	0
		T_x/k	-1,800	-2,000	-2,500	-3,400	-4,600
		S	0	- 400	- 800	-1,200	-1,300
	.50	T_y k	-5,200	-5,000	-4,200	-2,500	0
		T_x/k	-1,400	-1,600	-2,100	-3,000	-4,600
		S	0	- 800	-1,600	-2,500	-3,000
	.75	T_y k	-6,200	-6,100	-5,500	-4,100	0
		T_x/k	- 800	- 900	-1,200	-2,100	-4,600
		S	0	-1,100	-2,400	-4,100	-5,600
	1.0	T_y k	-7,500	-7,500	-7,500	-7,500	0
		T_x/k	0	0	0	0	0
		S	0	-1,200	-2,700	-5,200	∞

Table 4 - Shear S and Principal Stress S' Along Edge

σ_x	y/b	0	.1	.2	.3	.4	.5
	S	0	- 460	- 930	-1,440	-2,010	-2,680
	S'	0	+ 30	+ 110	+ 270	+ 500	+ 860
	y/b	.6	.7	.8	.85	.9	.95
	S	-3,590	-4,560	-6,060	-7,130	-8,630	-11,200
	S'	+1,440	+2,150	+3,380	+4,300	+4,880	+8,060
σ_y	x/a	0	.1	.2	.3	.4	.5
	S	0	- 520	-1,060	-1,630	-2,260	-2,980
	S'	0	+ 60	+ 230	+ 520	+ 920	+1,460
	x/a	.6	.7	.8	.85	.9	.95
	S	-3,880	-4,930	-6,450	-7,530	-9,040	-11,600
	S'	+2,210	+3,140	+4,550	+5,570	+7,030	+9,500

of the shear. In this example this equals 36,000 lb. Because there is no external reaction acting on the edge beams either at the corners or along the edge it is evident that the maximum tension or compression in the edge members occurs at midspan. Of course, the tension and compression in the edge member diminishes along the length to zero at the ends.

To determine the type of force (compression or tension) present in the edge members, it is recommended that free body diagrams be drawn of the member being considered rather than relying merely on a sign convention. This will minimize the possibility of making serious errors in complicated layouts. For this case, the layout is so simple that the type of force present can be ascertained by inspection. Since the shear is positive, and the coordinate of each quadrant occurs at the corner, the shear is outward along the four horizontal edges and inward along the four sloping edges. Hence the edge beams at the exterior edges are in tension while those extending out from the column are in compression.

Example 2 - The design of an elliptical paraboloid shell.

The internal forces divided by k or 1/k acting in an elliptical paraboloid subject to a uniform load of 60 psf and spanning 100 ft. in one direction and 70 ft. in the other with a total rise of 18 ft. are tabulated in Table 3. These values are obtained by multiplying the coefficients in section, $h_x/h_y = 8/10 = 0.8$ of Table 1 by the appropriate multiplier. Because the stresses are small, the effect of k is ignored. The maximum compression due to an assumed 60 psf load on the shell is 7500 lb. per foot. If the shell is assumed only 3 inches thick, the maximum compressive stress is only

$$f_c = \frac{7500}{3x12} = 208 \text{ psi}$$

which is considerably below the allowable stress of concrete.

To obtain some idea of the tensile forces existing in the shell, the minimum principal stresses have been evaluated along the edges in Table 4. The value of the shear S is computed by means of Table 2 with the multiplier in this case being 11,700 lb. per ft. taken from Table 3. S' the principal stress is computed as described in most standard text books on mechanics. The direct force at y = b is 4600 lb. per ft. and the direct force at x = a is 7500 lb. per ft. In most cases these principal values along the shell represent the maximum value in their zone.

At the corner the radius of curvature in the x direction can be computed from the formula

$$R_x = \frac{\left[1 + \left(\frac{\partial z}{\partial x}\right)^2\right]^{\frac{3}{2}}}{\frac{\partial^2 z}{\partial x^2}} \qquad (35)$$

With

$$z = \frac{8x^2}{35^2} + \frac{10y^2}{50^2}$$

$$\frac{\partial z}{\partial x} = \frac{16x}{35^2} \quad \text{and} \quad \frac{\partial^2 z}{\partial x^2} = \frac{16}{35^2}$$

Equation (35) yields at corner x = 35

$$R_x = \frac{35^2 \left[1 + (16/35)^2\right]^{3/2}}{16} = 102 \text{ ft.}$$

and similarly

$$R_y = 156 \text{ ft.}$$

The maximum shear can therefore be expected to be at

$$x/a = \frac{35 - 0.4\sqrt{101 \times 1/4}}{35} = 0.94$$

$$y/b = \frac{50 - 0.4\sqrt{156 \times 1/4}}{50} = 0.95$$

The largest minimum principal stress along the edges is therefore from Table 4, 9,500 lb. per ft. Several points in the interior should be also investigated to determine the extent of the tensile area. Using the internal forces shown in Table 3, we find the principal stress at y/b = x/a = 0.75 and y/b = x/a = 0.5 to be

$$S' = -\left(\frac{4100 + 2100}{2} - \sqrt{\frac{2000^2}{4} + 4100^2}\right) = +1100 \text{ lb.per ft.}$$

$$S' = -\left(\frac{4200 + 2100}{2} - \sqrt{\frac{2100^2}{4} - 1600^2}\right) = -1200 \text{ lb.per ft.}$$

Assuming a linear variation in principal stress between these points, zero tension would occur at x/a = y/b = 5/8.

From a theoretical point of view, the reinforcement should follow the lines of principal stress. However this is not practical and therefore it is customary to place the reinforcement in the corners along diagonal lines as shown in Fig. 9. For this particular example, and in all likelihood for all instances, the controlling tension for any group of bars occurs at the edge. The amount of reinforcement, with f_s = 20,000 psi, computed from the principal stresses tabulated in Table 4 is shown along the edge ribs of one corner.

For most shells of double curvature, even for a simple case as a translational shell formed by moving one circular curve on the other, an algebraic solution becomes extremely involved. In such cases, the conversion of the various differential equations into finite differences equations* is more

* "Solution of Difficult Structural Problems by Finite Differences" by Alfred Parme, Journal of ACI, vol. 22, November, 1950, p. 237-255.

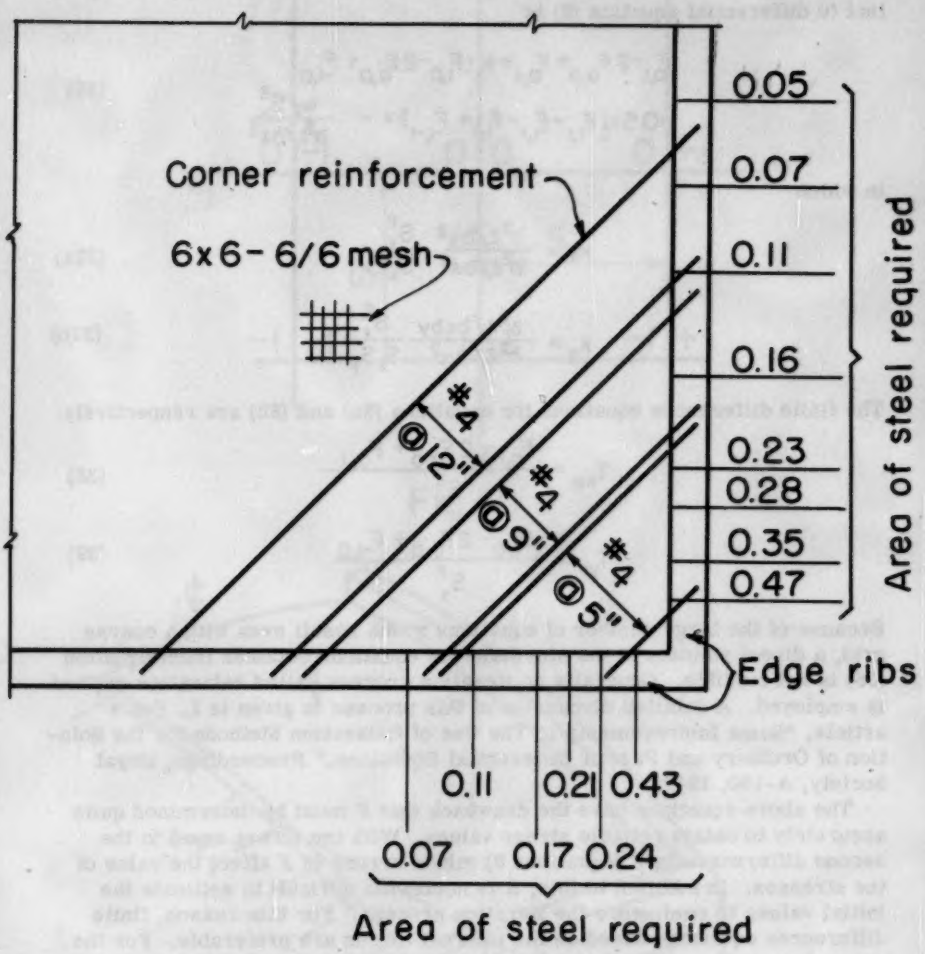
0.05
0.07
0.11
0.16
0.23
0.28
0.35
0.47
Area of steel required
Corner reinforcement
6x6 - 6/6 mesh
#4 @12"
#4 @9"
#4 @5"
Edge ribs
0.11
0.21
0.43
0.07
0.17
0.24
Area of steel required

Fig. 9

practical. This numerical procedure consists of substituting for the surface a grid of evenly spaced lines which simulate the behavior of the surface. For each intersection, a finite differences equation is established which expresses the relationship between the stresses or functions of the stresses at this and neighboring points and the load at the intersection.

Using the notation of Fig. 10 the general finite differences equation equivalent to differential equation (9) is

$$F_{0,1}-2F_{0,0}+F_{0,-1}+k_1(F_{1,0}-2F_{0,0}+F_{-1,0}) -0.5k_2(F_{1,1}-F_{1,-1}-F_{1,-1}+F_{-1,-1}) = -\frac{w_z S_y^2}{\partial^2 z/\partial x^2} \tag{36}$$

in which

$$k_1 = \frac{\partial^2 z/\partial y^2}{\partial^2 z/\partial x^2}\frac{S_y^2}{S_x^2} \tag{37a}$$

$$k_2 = \frac{\partial^2 z/\partial x \partial y}{\partial^2 z/\partial x^2}\frac{S_y^2}{S_x S_y} \tag{37b}$$

The finite differences equations for equations (8a) and (8b) are respectively

$$T_{xp} = \frac{F_{0,-1}-2F_{0,0}+F_{0,1}}{S_y^2} \tag{38}$$

$$T_{yp} = \frac{F_{1,0}-2F_{0,0}+F_{-1,0}}{S_x^2} \tag{39}$$

Because of the large number of equations which result even with a coarse grid, a direct solution of the simultaneous equations obtained from equation (36) is not feasible. Generally an iteration process called relaxation method is employed. A detailed discussion of this process is given in L. Fox's article, "Some Improvements In The Use of Relaxation Methods for the Solution of Ordinary and Partial Differential Equations," Proceedings, Royal Society, A-190, 1947.

The above equations have the drawback that F must be determined quite accurately to obtain reliable stress values. With the stress equal to the second differences in F (equations 8) minor errors in F affect the value of the stresses. In addition to this, it is somewhat difficult to estimate the initial values to commence the iteration process. For this reason, finite differences equations based on the internal forces are preferable. For the general case these equations become cumbersome. However, for the case of translational shells, the resulting equations are not more complicated than those represented by (36).

To express the relationship in terms of the internal forces, we first express T_{xp} in terms of T_{yp}, by differentiating equations (5) and (6) with respect to x and y respectively. This operation yields

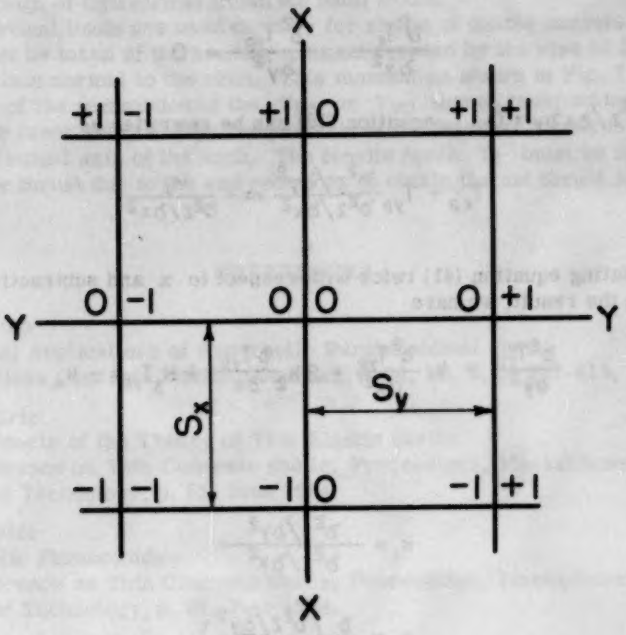
X
+1 -1 +1 0 +1 +1
0 -1 0 0 0 +1
Y
Y
S_x
S_y
-1 -1 -1 0 -1 +1
X

Fig. 10

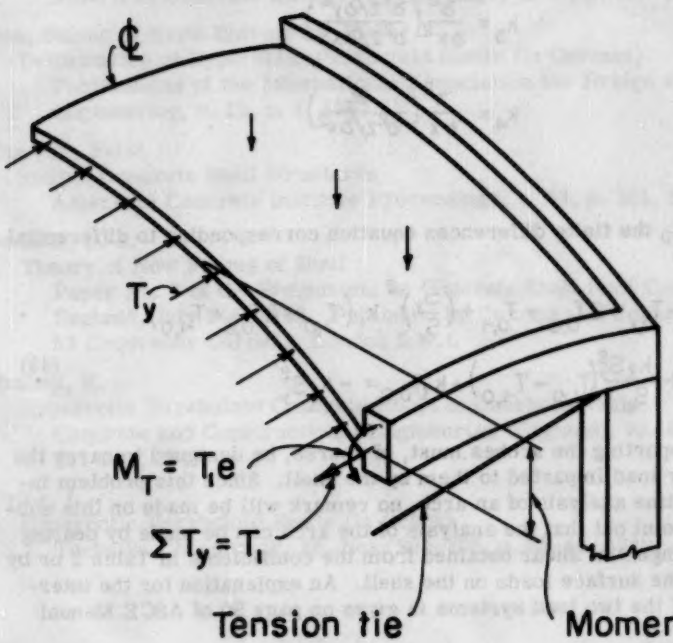
℄
T_y
$M_T = T_1 e$
$\Sigma T_y = T_1$
Tension tie
Moment arm = e

Fig. 11

$$\frac{\partial^2 T_x}{\partial x^2} - \frac{\partial^2 T_{yp}}{\partial y^2} = 0 \tag{40}$$

Since $\partial^2 z/\partial x \partial y = 0$, equation (7c) can be rewritten as

$$T_{xp} + T_{yp}\frac{\partial^2 z/\partial y^2}{\partial^2 z/\partial x^2} = -\frac{w_z}{\partial^2 z/\partial x^2} \tag{41}$$

Differentiating equation (41) twice with respect to x and subtracting equation (40) from the result, we have

$$\frac{\partial^2 T_{yp}}{\partial y^2} + k_1\frac{\partial^2 T_{yp}}{\partial x^2} + 2k_2\frac{\partial T_{yp}}{\partial x} + k_3 T_{yp} = -k_4 \tag{42}$$

in which

$$k_1 = \frac{\partial^2 z/\partial y^2}{\partial^2 z/\partial x^2}$$

$$k_2 = \frac{\partial}{\partial x}\left(\frac{\partial^2 z/\partial y^2}{\partial^2 z/\partial x^2}\right)$$

$$k_3 = \frac{\partial^2}{\partial x^2}\left(\frac{\partial^2 z/\partial y^2}{\partial^2 z/\partial x^2}\right)$$

$$k_4 = \frac{\partial^2}{\partial x}\left(\frac{w_z}{\partial^2 z/\partial x^2}\right)$$

Letting $T = T_{yp}$ the finite differences equation corresponding to differential equation (42) is

$$T_{0,1} - 2T_{0,0} + T_{0,-1} + \left(\frac{S_y}{S_x}\right)^2 k_1\left(T_{1,0} - 2T_{0,0} + T_{-1,0}\right) + \frac{k_2 S_y^2}{S_x}\left(T_{1,0} - T_{-1,0}\right) + k_3 T_{0,0} = -k_4 S_y^2 \tag{43}$$

The ribs supporting the arches must, of course, be designed to carry the tangential shear load imparted to them by the shell. Since this problem involves only routine analysis of an arch, no remark will be made on this subject except to point out that the analysis of the arch can be made by dealing only with the tangential shear obtained from the coefficients in Table 2 or by using directly the surface loads on the shell. An explanation for the interchangeability of the two load systems is given on page 90 of ASCE Manual

No. 31, "Design of Cylindrical Concrete Shell Roofs."

If the vertical loads are used directly for shells of double curvature, due account must be taken of the bending moment created by the rise of the shell in the direction normal to the arch. This moment as shown in Fig. 11, equals the product of the summation of the T_{xp} or T_{yp} forces from midspan to the edge and the lever arm between the centroid of the internal forces in the shell and the centroidal axis of the arch. The tensile force T_1 must be superimposed on the thrust due to the end reactions to obtain the net thrust in the arch.

REFERENCES

Candela, Felix
Structural Applications of Hyperbolic Paraboloidical Shells
American Concrete Institute Journal, v. 26, No. 5, p. 397-415, 1954.

Reissner, Eric
Some Aspects of the Theory of Thin Elastic Shells
Conference on Thin Concrete Shells, Proceedings, Massachusetts Institute of Technology, p. 81, June 1954.

Candela, Felix
Hyperbolic Paraboloids
Conference on Thin Concrete Shells, Proceedings, Massachusetts Institute of Technology, p. 91, June 1954.

Candela, Felix
Skew Shell Utilized in Unusual Roof
American Concrete Institute Proceedings, v. 49, p. 657-664, 1953.

Ban, Shisuo of Kioto University, Kioto
Deformation of Hyperbolic Paraboloid Shells (In German)
Publications of the International Association for Bridge and Structural Engineering, v. 13, p. 1, 1953.

Candela, Felix
Simple Concrete Shell Structures
American Concrete Institute Proceedings, v. 48, p. 321, 1952.

Jenkins, R. S.
Theory of New Forms of Shell
Paper No. 7 of the Symposium on Concrete Shell Roof Construction, England, July 2-4, 1952. Published by Cement and Concrete Association, 52 Grosvenor Gardens, London S.W.I.

Hruban, K.
Hyperbolic Paraboloid Concrete Roofs in Czechoslovakia
Concrete and Constructional Engineering (England), v. 44, No. 8, p. 247-252, 1949.

Fytos, I.
Hyperbolic Paraboloid Shells (In Greek)
Technika Chronika, v. 26, Nos. 295-296, p. 35-44, 1949.

Favini, A.
Analysis of Hyperbolic Tanks in Reinforced Concrete
Giornale del Genio Civile (Italy), v. 87, No. 10, p. 515-533, October 1949.
Extensive presentation of analysis based upon theory of thin shells with double curvature.

Borkowski, M. P.
Doubly Curved Thin Slab Structures
An English Translation from the Polish appears in Translation No. 31 of the Cement and Concrete Association, London, England, published in 1949, translated in 1951.

Pucher, A.
Calculations for Shells of Double Curvature Using Differential Equations (In German)
Bauingenieur, v. 18, p. 118, 1937.

Aimond, F.
Treatise on Statics of Parabolic Hyperboloidal Shells Not Stiff in Bending (In French with English Summary)
Publications of the International Association for Bridge and Structural Engineering, v. 4, p. 1, 1936.

Pilarski, L. Issenmann
Calculation of Thin Shells in Reinforced Concrete (In French)
Chapter VII is "General Theory of All Types of Surfaces" Published in 1935 by Dunod, 92 Rue Bonaparte, Paris, France.

Laffaille, B.
General Investigation Concerning Skew Surface Shells (In French)
Publications of the International Association for Bridge and Structural Engineering, v. 3, p. 295, 1935.

Laffaille, B.
Thin Shells in the Shape of Hyperbolic Paraboloids
Le Genie Civil (Paris), v. 104, No. 18, p. 409-410, 1934.

Paper 1058 ST 5

Journal of the
STRUCTURAL DIVISION
Proceedings of the American Society of Civil Engineers

MOMENT DISTRIBUTION CONSTANTS FROM MODELS

Otakar Ondra,* A.M. ASCE
(Proc. Paper 1058)

SYNOPSIS

This paper describes and illustrates an experimental method of determining the moment distribution constants for beams with variable moments of inertia.

The method does not rely upon the use of deformeter-type gages or other special instruments such as are used in the well known experimental methods developed by G. E. Beggs, W. J. Eney, and others. It is based on the concept of a three-dimensional M/EI solid whose properties are functions of the loads, slopes, and deflections of the statically indeterminate member which it represents. It is shown that each of the moment distribution constants is a function of a ratio J/Q which also defines the location of the center of gravity of the M/EI solid. This ratio is evaluated experimentally by weighing the solid and the use of statics. Mathematical integration or the approximate summation process are replaced by weighing, resulting in considerably simpler calculations and a greater reliability of results in comparison with standard methods of analysis. The method can be readily extended to the determination of the moment distribution constants of arches with constant or variable moments of inertia.

Once the moment distribution constants are known the Cross method of balancing moments is relatively simple to apply.

I - INTRODUCTION

In applying the moment distribution method of analysis to a given problem several factors or constants must be determined before the process of balancing moments can be carried out. In general, these constants include fixed end moments due to loads, carry-over, stiffness and distribution factors, shear stiffness, thrust stiffness, flexibility, etc. In the case of beams with a constant moment of inertia the determination of the required factors presents no difficulties inasmuch as they are simple functions of the span, moment of

Note: Discussion open until February 1, 1957. Paper 1058 is part of the copyrighted Journal of the Structural Division of the American Society of Civil Engineers, Vol. 82, No. ST 5, September, 1956.

* Associate Prof. of Civ. Eng., Manhattan College, New York, N. Y.

inertia, modulus of elasticity, etc., of the member considered.

For beams with variable moments of inertia and arches of either constant or variable moment of inertia the determination of the moment distribution constants is generally difficult. This is especially true of arches where complex functions involving integral calculus must be evaluated. In practice, the approximate summation process is frequently substituted for mathematical integration, or graphics are used. Although the work is greatly simplified, the necessary tabular computations are cumbersome and time-consuming. Moreover, the various methods of analysis are closely related to each other so that it is generally impossible to check results by an algebraically independent method.

The method of structural model analysis introduced by the late Professor G. E. Beggs of Princeton University and the more recent general methods of determining moment distribution constants developed by Professor W. J. Eney of Lehigh University[1] constitute a noteworthy simplification of the problem.

The Method

It will be shown elsewhere in this paper that the moment distribution constants for members with constant or variable moments of inertia exhibit a common parameter J/Q in which J and Q are the second and first moments, respectively, of the integral $A = \int ds/EI$ where ds is an infinitesimal element of length measured along the longitudinal axis of the member and EI is its flexural stiffness.

It will be recalled that in hydrostatics an analogous ratio J/Q defines the location of the so-called center of pressure upon a submerged plane surface exposed to hydrostatic pressure of the liquid above it. Since hydrostatic pressure increases linearly with the depth of submersion, the relationship between the resultant hydrostatic pressure and the size and configuration of the submerged surface area may be represented by a wedge-shaped "pressure solid" whose base is the area under consideration and whose altitudes vary linearly.

The pressure solid is analogous to a three-dimensional conjugate beam. The analogy, although not essential in developing the principle of the experimental method, is pointed out because it helps in visualizing and appraising the effect of a varying moment of inertia upon the moment distribution constants.

II - BEAMS

1. Carry-Over Factor

By definition, the carry-over factor of a flexural member is the ratio of the moment induced at the fixed end of the member to the moment causing rotation at the other simply supported end. In Fig. 1a, a beam simply supported at a and fixed at b is subjected to a moment M_a at a, causing a moment $C_{ab}M_a$ at b in which C_{ab} is the carry-over factor from a to b.

In Fig. 1b the beam is simply supported at a and b. An arbitrary moment M_a is applied at a causing end rotations θ_a and θ_b as shown. In Fig. 1c an additional moment load M_b is applied at b, inducing rotations ϕ_b and ϕ_a at

1. W. J. Eney, "Fixed Ended Moments by Cardboard Models," Engineering News-Record, December 12, 1935.

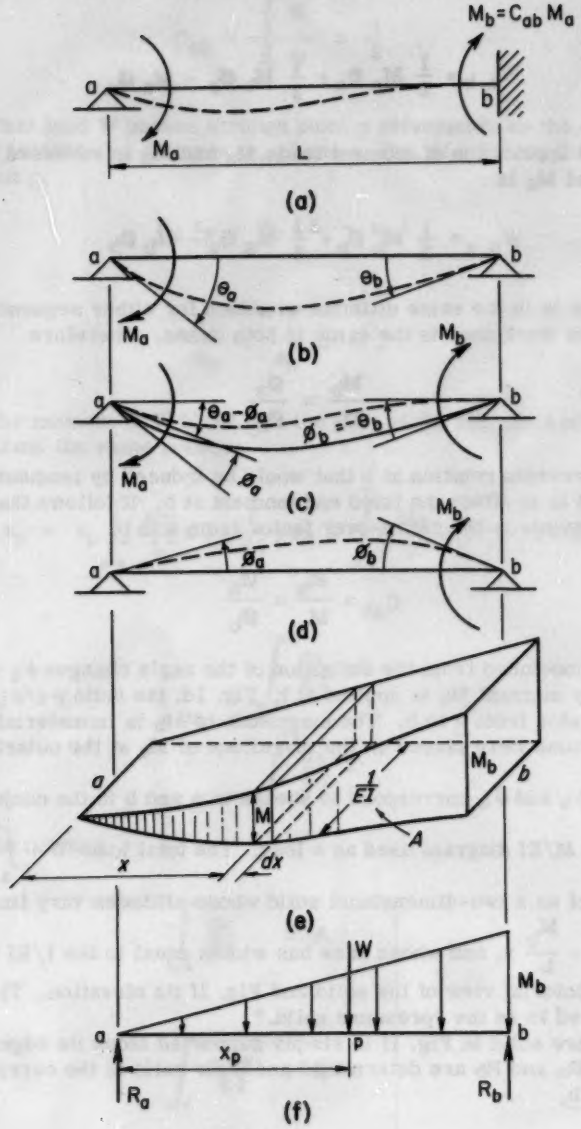

FIG. 1.

ends b and a. Let the magnitude of M_b be such that $\phi_b = -\theta_b$ so that the net rotation at b caused by M_a and M_b is zero.

The total work done by moments M_a and M_b applied in the order indicated is

$$W_{a,b} = \frac{1}{2} M_a \Theta_a + \frac{1}{2} M_b \phi_b - M_a \phi_a$$

If the order of application of moment loads M_a and M_b is reversed the work done by M_b and M_a is

$$W_{b,a} = \frac{1}{2} M_b \phi_b + \frac{1}{2} M_a \Theta_a - M_b \phi_b$$

Since the beam is in the same ultimate condition for either sequence of load application, the work done is the same in both cases. Therefore

$$\frac{M_b}{M_a} = \frac{\phi_a}{\phi_b}$$

Moment M_b prevents rotation at b that would be induced by moment M_a applied at a, and is in effect the fixed end moment at b. It follows that the ratio of the two moments is the carry-over factor from a to b,

$$C_{ab} = \frac{M_b}{M_a} = \frac{\phi_a}{\phi_b} \qquad \text{Eq. 1}$$

It may be concluded from the definition of the angle changes ϕ_b and ϕ_a that if an arbitrary moment M_b is applied at b, Fig. 1d, the ratio ϕ_a/ϕ_b is the carry-over factor from a to b. The magnitude of M_b is immaterial inasmuch as no restrictions were placed on the magnitude of M_a at the outset of the derivation.

Rotations ϕ_a and ϕ_b correspond to shears at a and b in the conjugate beam caused by the M/EI diagram used as a load. The total load $W = \int_a^b M \frac{1}{EI} dx$ is conceived of as a two-dimensional solid whose altitudes vary linearly with x, that is, $M = \frac{M_b}{L} x$, and whose base has widths equal to the 1/EI values. Fig. 1e is a pictorial view of the solid and Fig. 1f its elevation. This solid will be referred to as the "pressure solid."

The pressure solid in Fig. 1f is simply supported along its edges a and b. Its reactions R_a and R_b are determined and their ratio is the carry-over factor from a to b,

$$C_{ab} = \frac{\phi_a}{\phi_b} = \frac{R_a}{R_b} \qquad \text{Eq. 2}$$

If the moment of inertia is constant the carry-over factor is

$$C_{ab} = \frac{\frac{1}{3} W}{\frac{2}{3} W} = \frac{1}{2}$$

The resultant load W passes through point p referred to as the center of pressure and located at a distance x_p from a, Fig. 1f. Taking the sum of moments about p,

$$R_a x_p = R_b (L - x_p)$$

whence

$$\frac{R_a}{R_b} = \frac{1}{x_p} L - 1 \qquad \text{Eq. 3}$$

Equating the moment of W about a to the sum of the moments of elemental forces dW about the same point,

$$W x_p = x_p \int_a^b (\frac{M_b}{L} x) (\frac{1}{EI}) dx = \int_a^b (\frac{M_b}{L} x) (\frac{1}{EI}) x \, dx$$

from which

$$x_p = \frac{\int_a^b \frac{dx}{EI} x^2}{\int_a^b \frac{dx}{EI} x} \qquad \text{Eq. 4}$$

Introducing the notation

$$\left.\begin{aligned} \int_a^b \frac{dx}{EI} &= A \\ \int_a^b \frac{x \, dx}{EI} &= Q \\ \int_a^b \frac{x^2 \, dx}{EI} &= J \end{aligned}\right\} \qquad \text{Eqs. 5}$$

Eqs. 3 and 4 yield

$$C_{ab} = \frac{1}{x_p} L - 1 = \frac{Q}{J} L - 1 \qquad \text{Eq. 6}$$

Significantly, the parameter $1/x_p = Q/J$ appears in each of the moment distribution constants as it will be shown later.

2. Stiffness Factor

The stiffness factor at the simply supported end of a flexural member is defined as the moment required to rotate that end through a unit angle while the other end is held fixed. In Fig. 2a M_a is the stiffness factor S_a at a when θ_a is a unit angle in radian measure.

The bending moment diagram $M = M' - M''$ for the beam in Fig. 2a is shown in Fig. 2b. The load on the conjugate beam a' - b' is $\int_a^b M \frac{1}{EI} dx$.

Taking the sum of moments about b' in Fig. 2b,

$$-(1) L + \int_a^b \frac{M' dx}{EI} (L - x) - \int_a^b \frac{M'' dx}{EI} (L - x) = 0$$

substituting for M' and M'', simplifying and introducing the notation of Eqs. 5,

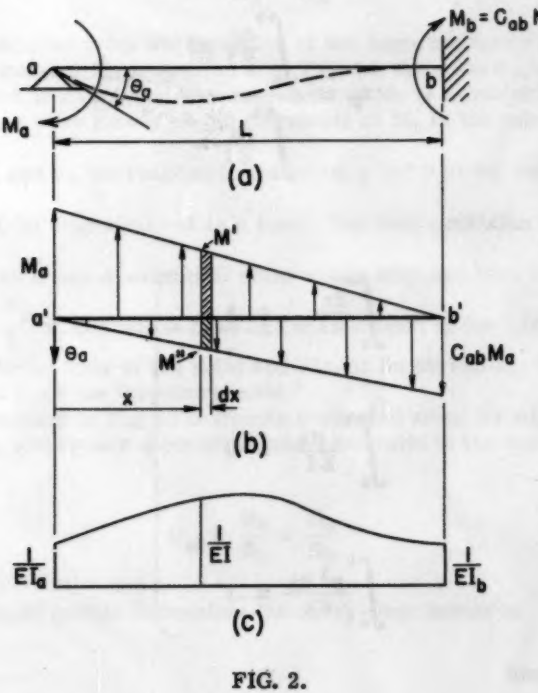

FIG. 2.

the last equation reduces to

$$S_a = \frac{1}{A - \frac{Q^2}{J}} \qquad \text{Eq. 7}$$

If the moment of inertia is constant Eq. 7 yields

$$S_a = \frac{1}{\frac{1}{EI} L - \frac{\left(\frac{1}{EI} L \frac{L}{2}\right)^2}{\frac{1}{3} \frac{1}{EI} L^3}} = \frac{4EI}{L}$$

3. Modified Stiffness Factor

The modified stiffness factor is the moment which must be applied at the end of a simply supported beam to rotate that end through a unit angle. In Fig. 1d, M_b is the modified stiffness factor S_b' at b when ϕ_b is a unit angle.

Taking the sum of moments about a in Fig. 1f,

$$x_p \int_a^b \left(\frac{S_b'}{L} x\right)\left(\frac{1}{EI}\right) dx - (1) L = 0$$

which reduces to

$$S_b' = \frac{L^2}{x_p Q} = \frac{L^2}{\frac{J}{Q} Q} = \frac{L^2}{J} \qquad \text{Eq. 8}$$

If the beam has a constant moment of inertia Eq. 8 yields

$$S_b' = \frac{L^2}{\frac{1}{3} \frac{1}{EI} L^3} = \frac{3EI}{L} = \frac{3}{4} S_b$$

4. Relationship between the Stiffness Factor and the Pressure Solid.

Fig. 3a represents a deepened beam for which it is desired to find the stiffness factors. Figs. 3b and 3c show the beam supported in a manner consistent with the definition of S_a and S_b, respectively.

Fig. 3d is an oblique view of a prismatic solid abb'a' whose base has a length equal to the span L of the beam and widths proportional to its 1/EI values. The solid is cut diagonally along the plane aa - b'b'. The lower half of the cut solid is shown in continuous outline while the upper half, volumetrically not equal to the lower, is dashed.

Let the lower half of the original solid be simply supported along edges aa and bb. The reactions are R_a and R_b and their sum is the weight W, Fig. 3e. Force W passes through the center of gravity of the half-solid and also

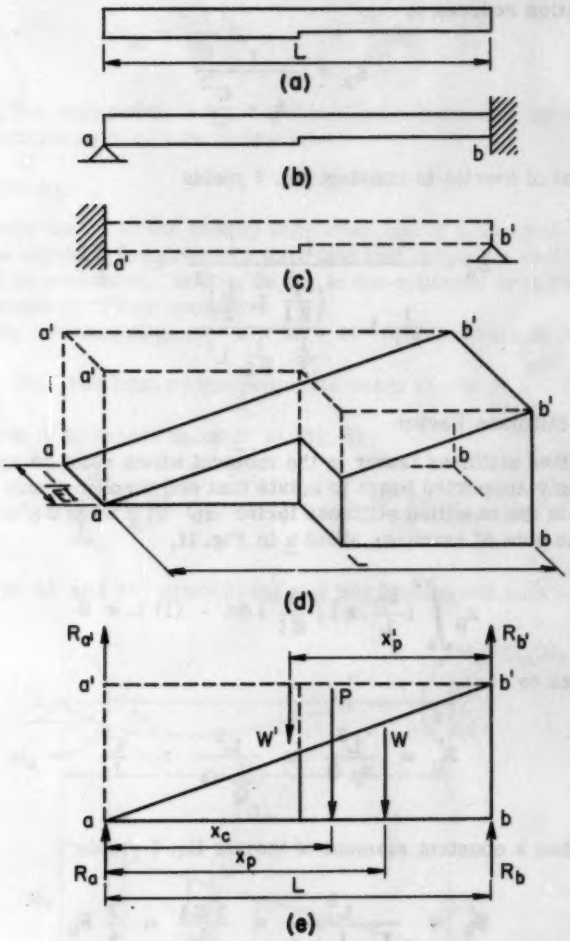

FIG. 3.

through the center of pressure in its base, located at a distance x_p to the right of a.

The stiffness factor S_a given by Eq. 7 may be expressed in the form

$$S_a = \frac{1}{A - \frac{Q^2}{J}} = \frac{1}{A - \frac{Q}{x_p}} = \frac{1}{A - \frac{A\,x_c}{x_p}} = \frac{x_p}{A\,(x_p - x_c)} \qquad \text{Eq. 9}$$

in which x_c is the distance of the centroid of the base a - b - b - a of the solid referred to a-a. It is found by the principle of moments, Fig. 3e:

$$(R_a + R_{a'})\,x_c = (R_b + R_{b'})(L - x_c)$$

so that

$$x_c = \frac{(R_b + R_{b'})\,L}{P}$$

Substituting for x_p from Eq. 3 and for x_c from above, Eq. 9 becomes

$$S_a = \frac{R_b\,P}{A\left[R_b\,P - (R_b + R_{b'})\,W\right]} = \frac{R_b\,P}{A\,(R_b\,W' - R_{b'}\,W)}$$

Similarly

$$S_b = \frac{R_{a'}\,P}{A\,(R_{a'}\,W - R_a\,W')}$$

Eqs. 10

The modified stiffness factor given by Eq. 8 is

$$S_b' = \frac{L^2}{J} = \frac{L^2}{\frac{J}{Q}\,Q} = \frac{L^2}{x_p\,A\,x_c}$$

Substituting for x_p and x_c the last expression becomes

$$S_b' = \frac{W\,P}{A\,R_b\,(R_b + R_{b'})}$$

Similarly

$$S_a' = \frac{W'\,P}{A\,R_{a'}\,(R_{a'} + R_a)}$$

Eqs. 11

Eqs. 10 and 11 express the stiffness factors in terms of the four pressure solid reactions R_a, R_b, $R_{a'}$, $R_{b'}$, and area A. Referring to Eq. 2 it will be recalled that the carry-over factors are also functions of the four reactions. The determination of carry-over and relative stiffness factors is illustrated in the following example.

Example 1 - Deepened Beam.

The following data were obtained by weighing the reactions of the two half-solids shown in Fig. 4b. The variation of 1/EI values is shown in Fig. 4c. All weights are expressed in grams.

$R_a = 95$	$R_{a'} = 221$	$P = 653$
$R_b = 240$	$R_{b'} = 97$	$A = \frac{3L}{2}$
$W = 335$	$W' = 318$	

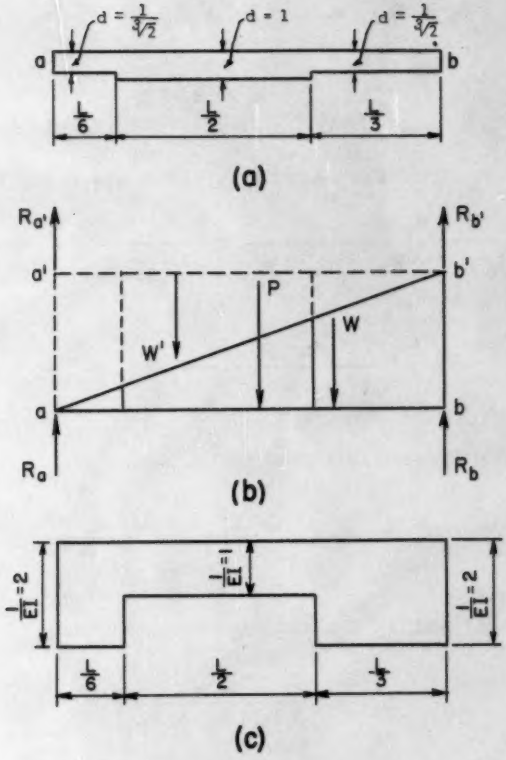

FIG. 4.

(a) Beam fixed at far end.

(Eq. 2)

$$C_{ab} = \frac{R_a}{R_b} = \frac{95}{240} = 0.396$$

$$C_{ba} = \frac{R_b'}{R_a'} = \frac{97}{221} = 0.438$$

(Eqs. 10)

$$S_a = \frac{R_b P}{A (R_b W' - R_b' W)} = \frac{(240)(653)}{\frac{3L}{2} [(240)(318) - (97)(335)]}$$

$$S_a = \frac{2.38}{L} \text{ (relative)}$$

$$S_b = \frac{R_a' P}{A (R_a' W - R_a W')} = \frac{(221)(653)}{\frac{3L}{2} [(221)(335) - (95)(318)]}$$

$$S_b = \frac{2.19}{L} \text{ (relative)}$$

(b) Beams simply supported at far end.

(Eqs. 11)

$$S_a' = \frac{W' P}{A R_a' (R_a' + R_a)} = \frac{(318)(653)}{\frac{3L}{2} (221) (221 + 95)}$$

$$S_a' = \frac{1.98}{L} \text{ (relative)}$$

$$S_b' = \frac{W P}{A R_b (R_b + R_b')} = \frac{(335)(653)}{\frac{3L}{2} (240) (240 + 97)}$$

$$S_b' = \frac{1.80}{L} \text{ (relative)}$$

The stiffness factors are relative inasmuch as relative 1/EI values were used in the calculations. For the purpose of distributing an unbalanced moment among the members framed into a joint relative stiffness factors may be used provided that the widths (1/EI values) of the respective solids are laid off to the same scale. If it is impractical to use the same scale or if absolute stiffness factors are required, an adjustment of scales is necessary.

In general, if the model represents the prototype to the lineal scale of 1 inch = m-inches of prototype, and the transverse 1/EI-scale is 1 inch = n-1/lb-in^2, the absolute stiffness factor for the prototype is

(Eq. 9)

$$S_a = \frac{x_p}{A\,(x_p - x_c)} \cdot \frac{m}{(m\,n)\,m} = \frac{x_p}{A\,(x_p - x_c)} \cdot \frac{1}{m\,n}$$

$$(S)_{prototype} = \frac{(S)_{model}}{m\,n} \qquad \text{Eq. 12}$$

If the model area A is evaluated in square inches, the units of m and n are as above, the prototype stiffness factor is expressed in lb-in.

5. Making and Weighing the Model.

It is a simple matter to make a model (that is, pressure solid, three-dimensional conjugate beam) capable of giving very good results. The model used in Example 1 was made of red oak although any kind of seasoned wood that is reasonably free of defects is equally suitable. The material should be uniformly dry to avoid a variation in its specific weight and to prevent warping when it is cut. Plaster of Paris, paraffin and other materials which can be molded or easily cut may also be used.

The composite specimen abb'a' was assembled by lightly gluing onto a prismatic block of red oak 12 in. long, 3.9 in. deep and 0.9 in. thick two pieces of the same thickness and depth, and L/6 = 2 in. and L/3 = 4 in. long, respectively. Next, the composite block was cut diagonally from a to b' as is shown in Fig. 5.

One reaction was weighed at a time while the other support was provided by a block of wood of suitable height. A carpenter's level was used to check the horizontal alignment of the scale platform and the supporting block at the other end. Fig. 6 shows the weighing of reaction R_b in Example 1. It is evident that the entire experiment required only a few minutes of time.

6. Verification of Experimental Data and Results.

Errors and inaccuracies in weighing the reactions are found by weighing the solids. If discrepancies appear between the weight of the solid and the sum of its reactions the weighing of reactions is repeated until a reasonably close agreement is obtained. The computed values of the four factors C_{ab}, C_{ba}, S_a and S_b may be checked in the following manner.

In Fig. 7a the moment required to cause a unit rotation at a while end b is held fixed is $M_a = S_a$. The fixed end moment at b is $C_{ab}\,S_a$. Similarly, in Fig. 7b moment $M_b = S_b$ causes a unit rotation at b and moment $C_{ba}\,S_b$ at a. Applying the Maxwell-Mohr reciprocal theorem[2] to the equilibrated moment load systems in Figs. 7 a and b and rotations in Figs. 7 b and a,

$$S_a\,(\phi_a) + C_{ab}\,S_a\,(\phi_b) = C_{ba}\,S_b\,(\theta_a) + S_b\,(\theta_b)$$

$$S_a\,(0) + C_{ab}\,S_a\,(1) = C_{ba}\,S_b\,(1) + S_b\,(0)$$

whence

2. L. C. Maugh, "Statically Indeterminate Structures," 1951 Edition, page 10.

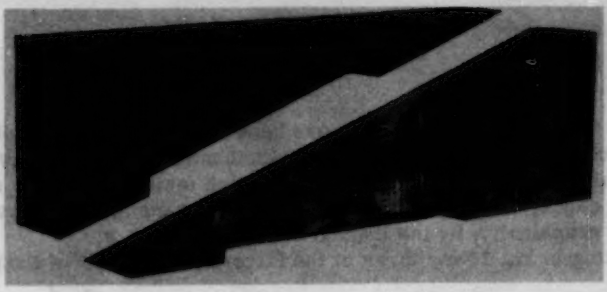

FIG. 5.

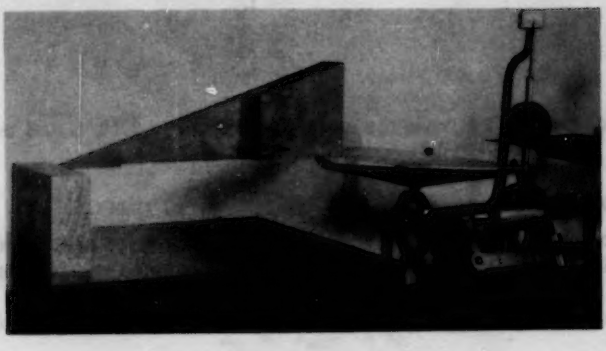

FIG. 6.

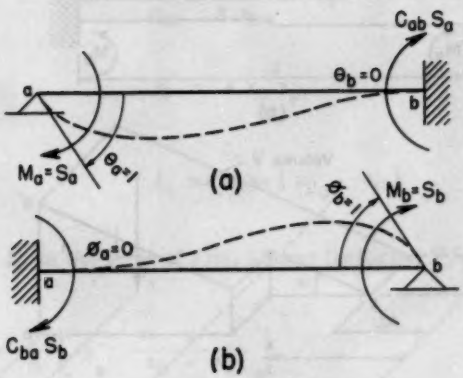

FIG. 7.

$$\frac{C_{ab}}{C_{ba}} = \frac{S_b}{S_a} \qquad \text{Eq. 13}$$

Thus if any three of the four factors are known the fourth may be obtained by means of Eq. 13. Since the experimental method and the necessary computations are quite simple it is best to evaluate each factor separately and to use Eq. 13 as a check. If a small discrepancy appears the individual values may be adjusted graphically, by the method of least squares, etc.

Substituting in Eq. 13 for three of the factors determined in Example 1,

$$\frac{0.396}{0.438} = \frac{S_b}{\frac{2.38}{L}}$$

$$S_b = \frac{2.145}{L}$$

This differs by about 2% from the experimental value 2.19/L and is quite acceptable.

7. Fixed End Moments in Beams.

Concentrated Load. - Fig. 8a represents a fixed-ended beam carrying a single unit load at point k. It is desired to find the fixed end moments M_a and M_b.

By the column analogy method of analysis[3] the fixed end moments are

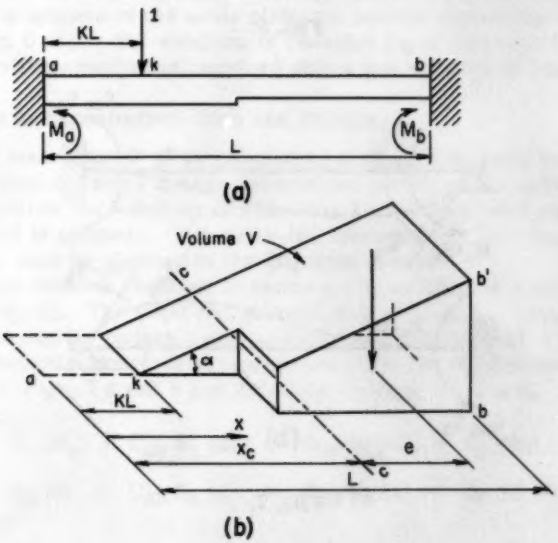

FIG. 8.

3. L. E. Grinter, "Theory of Modern Steel Structures," Vol. II, 1937 Edition, page 216.

$$M_a = \frac{V}{A} - \frac{V e x_c}{J_c}$$

$$M_b = -(1)(L - KL) + \frac{V}{A} + \frac{V e (L - x_c)}{J_c}$$

} Eqs. 14

in which

$$A = \int_0^L \frac{dx}{EI}$$ = area defined previously

$$V = \int_{KL}^L \frac{(1)(x - KL)}{EI}$$ dx = volume of the solid shown in Fig. 8

x_c = distance to the centroidal axis c - c of area A measured from a,

e = eccentricity of the centroid of volume V referred to axis c - c,

J_c = second moment of area A about axis c - c.

Applying the parallel-axis theorem of second moments,

$$J_c = J_a - A x_c^2$$

(Eq. 6)

$$\frac{J_a}{Q_a} = \frac{J_a}{A x_c} = x_p$$

or

$$J_a = A x_c x_p$$

Therefore

$$J_c = A x_c (x_p - x_c)$$

Substituting for J_c in the first of Eqs. 14 and factoring V/A, the fixed end moment at a is

$$M_a = \frac{V}{A}\left[1 - \frac{e}{x_p - x_c}\right]$$ Eq. 15

and

$$M_b = -(1)(L - KL) + \frac{V}{A}\left[1 + \frac{e(L - x_c)}{x_c(x_p - x_c)}\right]$$ Eq. 16

Distances x_c and x_p were already encountered in the expression for the

stiffness factor (Eq. 9). Quantities V and e may be determined experimentally by fashioning the solid shown in Fig. 8b. Its altitudes represent the moment of the unit load applied at k so that again the solid may be conceived of as a "pressure solid." To avoid confusion with the pressure solid utilized in the determination of the carry-over and stiffness factors, it will be referred to as the "load solid."

The volume V of the load solid is best determined by dividing its weight W_1 by the specific weight w of the material of which it is made.

The moment of the unit load applied at k at any distance x is M = (1)(x - KL). Since the altitudes of the load solid in Fig. 8b represent the moments of the load, the slope of its upper surface is dM/dx = 1. If a load P acts at point k, the slope should be (P)(1) = P.

It may be impractical to cut the solid at an angle corresponding to load P. If the slope is arbitrarily made equal to $\tan\alpha$, the volume determined by weighing must be multiplied by the ratio $P/\tan\alpha$ when substituted in Eqs. 15 and 16.

The distance e is determined by simply supporting the load solid along its edges k and b and weighing the reaction ρ_b at b, Fig. 9. Taking moments about k,

$$W_1 (x_c + e - KL) = \rho_b (L - KL)$$

$$e = \frac{\rho_b (L - KL) - W_1 (x_c - KL)}{W_1} \qquad \text{Eq. 17}$$

It is not advisable to support the load solid at c and b (part k - c overhanging). Although this arrangement permits a more direct evaluation of e, the necessity of a knife-edge support at c makes the weighing of the reaction at b more difficult on account of prolonged oscillations of the balance.

It will be noted that three solids are required for the experimental evaluation of Eqs. 15 and 16. The first solid, needed to find x_c has a span equal or proportional to the span of the fixed-ended beam, a base whose widths correspond to its 1/EI values, and a constant height.

The second solid, called the pressure solid, is required to find x_p by Eq. 3. It is obtained from the first by cutting it diagonally along the plane a - b'. The third solid, called the load solid, required for the evaluation of V and e, is obtained from the second by cutting it along the plane k - b' or other inclined plane passing through k. Area A may be readily found by

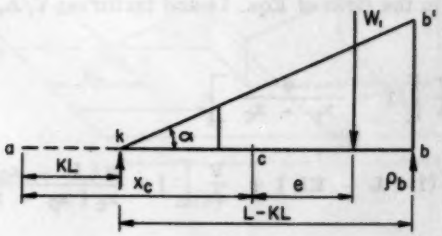

FIG. 9.

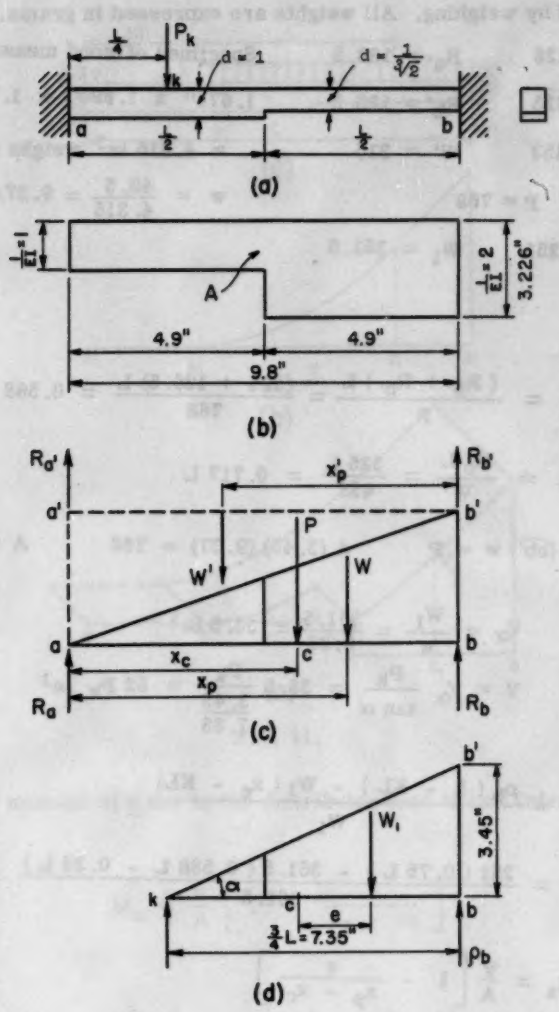

FIG. 10.

dividing the weight of the initial solid (prismatic solid of constant height) by its altitude $\overline{bb'}$ and the specific weight w of the material.

It follows that a single solid of constant height, when cut in the proper sequence, will suffice for an experimental evaluation of both carry-over and stiffness factors, and fixed end moments for a beam.

Example 2 - Deepened Beam.

Fig. 10a shows a deepened beam fixed at both ends. The fixed end moment at a will be determined for load P_k acting as shown. The data given below

were obtained by weighing. All weights are expressed in grams.

$R_a = 128$ $R_{a'} = 188.5$ Specimen of wood measuring

$R_b = 325$ $R_{b'} = 126.5$ 1.675" x 1.690" x 1.528"

$W = 453$ $W' = 315$ $= 4.315\ in^3$ weighs 40.5.

$P = 768$ $w = \frac{40.5}{4.315} = 9.37/in^3$

$\rho_b = 251$ $W_1 = 361.5$

(Fig. 10c)

$$x_c = \frac{(R_b + R_{b'})L}{P} = \frac{(325 + 126.5)L}{768} = 0.588\,L$$

$$x_p = \frac{R_b L}{W} = \frac{325\,L}{453} = 0.717\,L$$

$A(\overline{bb'})w = P$ $A(3.45)(9.37) = 768$ $A = 23.7\ in^2$

$$V_\alpha = \frac{W_1}{w} = \frac{361.5}{9.37} = 38.5\ in^3$$

$$V = V_\alpha \frac{P_k}{\tan\alpha} = 38.5\,\frac{P_k}{\frac{3.45}{7.35}} = 82\,P_k\ in^3$$

(Eq. 17)

$$e = \frac{\rho_b(L - KL) - W_1(x_c - KL)}{W_1}$$

$$e = \frac{251(0.75\,L) - 361.5(0.588\,L - 0.25\,L)}{361.5} = 0.1825\,L$$

(Eq. 15)

$$M_a = \frac{V}{A}\left[1 - \frac{e}{x_p - x_c}\right]$$

$$M_a = \frac{82\,P_k}{23.7}\left[1 - \frac{0.1825\,L}{0.717\,L - 0.588\,L}\right] = -1.435\,P_k$$

In terms of any span L the fixed end moment at a is

$$M_a = \frac{-1.435\,P_k}{9.8}\,L = -0.1464\,P_k\,L$$

8. Fixed End Moments.

Uniformly Distributed Load. - By the column analogy method, in Fig. 11

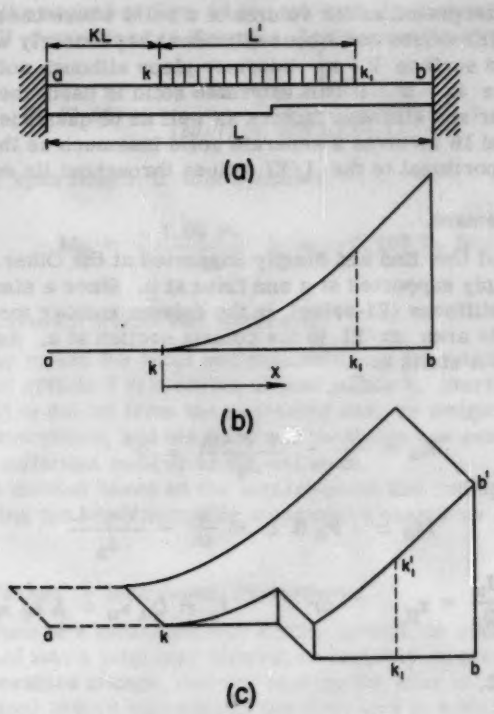

FIG. 11.

the fixed end moment at a due to the distributed load of unit intensity per unit of length is

(Eq. 15)

$$M_a = \frac{V}{A}\left[1 - \frac{e}{x_p - x_c}\right]$$

in which

$$V = \int_k^{k_1} \frac{\frac{x^2}{2}}{EI}\,dx + \int_{k_1}^{b} \frac{L'\left(x - \frac{L'}{2}\right)}{EI}\,dx$$

is the volume of the load solid shown in Fig. 11c. From k to k_1 the altitudes of the solid vary as the second power of x. From k_1 to b the variation is linear. Except for the parabolic variation of altitude between k and k_1 the principles of making and weighing the load solid remain valid.

The first of the two definite integrals may be written in the equivalent form

$$\int_k^{k_1} \frac{x}{2EI}\,x\,dx$$

which may be interpreted as the volume of a solid whose base has widths equal to the $x/2EI$ values and whose altitudes vary linearly with x. Accordingly, the curved surface $k - k_1'$ becomes plane although not continuous with the plane surface $k_1' - b'$. If this alternate solid is used, the determination of the carry-over and stiffness factors as well as of quantities A, x_c, x_p and J_c in Eqs. 15 and 16 involves a separate solid inasmuch as the latter must have widths proportional to the $1/EI$ values throughout its entire length.

9. Fixed End Moment.

Beam Fixed at One End and Simply Supported at the Other. - In Fig. 12a the beam is simply supported at a and fixed at b. Since a simple support or hinge has zero stiffness (EI-value), in the column analogy method of analysis it adds an infinite area dx/EI to the column section at a. As a result the centroid of area A shifts to a.

(Eqs. 14)

$$M_a = \frac{V}{\omega} - \frac{V\, e'(0)}{J_a} = 0$$

$$M_b = - P_k K' L + \frac{V}{\omega} + \frac{V\, e'\, L}{J_a}$$

But

$$\frac{J_a}{Q_a} = x_p \qquad \text{or} \qquad J_a = Q_a\, x_p = A\, x_c\, x_p$$

From Example 2,

$$e' = x_c + e = 0.588\, L + 0.1825\, L = 0.7705\, L$$

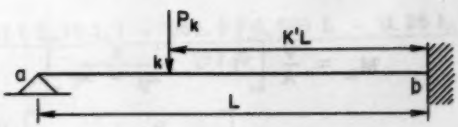

(a)

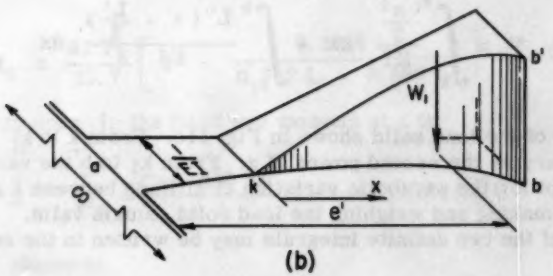

(b)

FIG. 12.

Substituting in the second of Eqs. 14 for e' and J_a and using the values of A, x_c, x_p and V determined in Example 2, the moment at b is

$$M_b = -P_k(7.35) + \frac{82\,P_k(0.7705\,L)\,L}{(23.7)(0.588\,L)(0.717\,L)} = -1.05\,P_k$$

In terms of any span length L this becomes

$$M_b = \frac{-1.05\,P_k}{9.8}\,L = -0.107\,P_k\,L$$

10. Influence Lines for Fixed End Moments.

Influence line values for fixed end moments may be obtained by applying the procedure of article 7 to a series of load points k. Starting from one end, a new load solid is cut off from the preceding one, its weight W_1 and reaction ρ_b are determined, and the fixed end moments are evaluated. This is repeated for a sufficient number of KL-values.

An alternate method based on the neutral-point and conjugate beam properties[4] and utilizing the experimentally determined quantities A, x_c and J_c may also be used.

11. Moments Caused by Impressed Distortions.

The foundations of a structure may settle, spread, or rotate. Furthermore, members framed into a joint may shorten or lengthen as a result of direct stress or temperature change, thereby causing the joint to move. These and similar distortions induce moments in the structure in addition to those caused by actual loads. The column analogy method is the most expedient method for analyzing the effects of such distortions.

(a) Transverse Displacement. Joint Rotation Prevented. - The effect of a

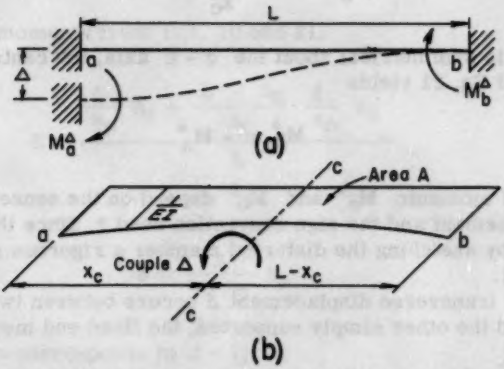

FIG. 13.

4. L. E. Grinter, "Theory of Modern Steel Structures," Vol. II, 1937 Edition, page 210.

relative transverse displacement Δ of ends a and b of the restrained member in Fig. 13a corresponds in the column analogy method to a couple equal to Δ, acting about the transverse centroidal axis c - c of the column across section, shown in Fig. 13b. The moments induced in the member correspond to the stresses in the column, that is,

$$M_a^{\Delta} = \frac{\Delta}{J_c} x_c \qquad \text{Eq. 18}$$

Using the relationships developed earlier in this paper, the expression for M_a may be written in the form

$$M_a^{\Delta} = \frac{\Delta}{J_a - A x_c^2} x_c = \frac{\Delta}{Q_a \left(\frac{J_a}{Q_a} - x_c \right)} x_c$$

or

$$M_a^{\Delta} = \frac{\Delta x_c}{Q_a (x_p - x_c)} = \frac{\Delta}{A (x_p - x_c)} \qquad \text{Eq. 19}$$

In terms of the stiffness factor given by Eq. 9 the last equation becomes

$$M_a^{\Delta} = \frac{\Delta}{x_p} S_a \qquad \text{Eq. 20}$$

Similarly, the moment induced at b is

$$M_b^{\Delta} = - \frac{\Delta}{J_c} (L - x_c) = - \frac{\Delta (L - x_c)}{A x_c (x_p - x_c)} = - \frac{\Delta (L - x_c)}{x_c x_p} S_a$$

or

$$M_b^{\Delta} = - \frac{L - x_c}{x_c} M_a^{\Delta} \qquad \text{Eq. 21}$$

If the member is symmetrical about the c - c axis, the centroidal distance x_c is L/2 and Eq. 21 yields

$$M_b^{\Delta} = - M_a^{\Delta}$$

The signs of moments M_a^{Δ} and M_b^{Δ} depend on the sense of the impressed displacement and the sign convention used.* Since they can be readily determined by sketching the distorted member a rigorous sign convention is not essential.

If a relative transverse displacement Δ occurs between two ends of which one is fixed and the other simply supported, the fixed end moment may be

* In this paper a downward displacement is considered negative and corresponds to a negative couple (beam sign convention) acting on the column section. A compressive stress caused by the couple is positive and is interpreted as a positive moment (beam sign convention) acting on the member.

obtained from the moments with both ends fixed by the method of moment distribution. Thus, when a is the simple support, the moment at b is

$$(M_b^{\Delta})' = M_b^{\Delta} + C_{ab} M_a^{\Delta} = -\frac{L - x_c}{x_c} M_a^{\Delta} + C_{ab} M_a^{\Delta}$$

Substituting from Eqs. 19 and 6 and reducing, the last equation becomes

$$(M_b^{\Delta})' = -\frac{\Delta}{A x_c x_p} L \qquad \text{Eq. 22}$$

(b) Joint Rotation. - By definition, if moment S_a is applied at joint or abutment a, the far end remaining fixed, the rotation at a is $\theta = 1$. The moment corresponding to any rotation θ_a is

$$M_a^{\theta_a} = \theta_a S_a \qquad \text{Eq. 23}$$

and

$$M_b^{\theta_a} = C_{ab} M_a = C_{ab} \theta_a S_a \qquad \text{Eq. 24}$$

12. Shear Stiffness and Flexibility.

The shear stiffness S_s of a restrained flexural member ab is defined as the shear at the ends of the member required to cause a unit relative transverse displacement of a and b. The flexibility F_s is the reciprocal of shear stiffness, i.e., the relative transverse displacement produced by a unit shearing force.

The shear at a in Fig. 13a is

$$S = \frac{M_a^{\Delta} + M_b^{\Delta}}{L}$$

Substituting for the moments from Eqs. 20 and 21,

$$S = \frac{\frac{\Delta}{x_p} S_a + \frac{L - x_c}{x_c} \cdot \frac{\Delta}{x_p} S_a}{L}$$

which reduces to

$$S = \frac{\Delta}{x_c x_p} S_a$$

Since shear stiffness corresponds to $\Delta = 1$,

$$S_s = \frac{S_a}{x_c x_p} \qquad \text{Eq. 25}$$

Combining Eqs. 18 and 20,

$$M_a^{\Delta} = \frac{1}{x_p} S_a = \frac{1}{J_c} x_c$$

and substituting for S_a/x_p in Eq. 25,

$$S_s = \frac{x_c}{x_c J_c} = \frac{1}{J_c} \qquad \text{Eq. 26}$$

and

$$F_s = \frac{1}{S_s} = J_c \qquad \text{Eq. 27}$$

13. Correlation between Model and Prototype

The stiffness factor S_a in Eqs. 20, 23, etc., is a function of area A (see Eq. 9). Since absolute values of fixed end moments caused by known or assumed distortions are generally required, the absolute value of the stiffness factor or area $A = \frac{ds}{EI}$ must be introduced in the respective expressions.

The absolute stiffness factor for the prototype is given by Eq. 12, article 4. Using the m- and n-scales defined in article 4 the prototype moments are

(Eq. 19)

$$M_a^{\Delta} = \frac{\Delta}{A(x_p - x_c)} \cdot \frac{1}{(m\,n)\,m} \qquad \text{Eq. 28}$$

When Δ, x_p and x_c are expressed in inches, A in square inches, M_a^{Δ} is expressed in lb-in.

(Eq. 23)

$$M_a^{\theta_a} = \theta_a (S_a)_{model} \cdot \frac{1}{m\,n} \qquad \text{Eq. 29}$$

When θ_a is expressed in radians and $(S_a)_{model}$ in $1/in^2$, M_a is expressed in lb-in.

Relative values of shear stiffness and flexibility given by Eqs. 25, 26 and 27 can be used for the purpose of distributing shears to the members of a structure analyzed by the moment distribution method. No scale adjustment is therefore necessary provided that the solids used to evaluate shear stiffness of the component members are laid out to the same scales. If this is not done an adjustment of scales is necessary, or absolute shear stiffness must be found.

The absolute shear stiffness is

(Eq. 25)

$$S_s = \frac{(S_a)_{model}}{x_c\,x_p} \cdot \frac{\frac{1}{m\,n}}{m^2} = \frac{(S_a)_{model}}{x_c\,x_p} \cdot \frac{1}{m^3\,n} \qquad \text{Eq. 30}$$

When $(S_a)_{model}$ is expressed in $1/in^2$, x_c and x_p are in inches, S_s is expressed in lb/in.

Example 3 - Deepened Beam

Assuming that the models in Example 2 represent the prototype to the lineal scale of 1 in. = 24.5 in., the cross section of the prototype is 6.35 in. deep and 6 in. wide at b, E is 2,000,000 psi., determine for the prototype:

a) carry-over factors
b) absolute stiffness factors
c) fixed end moments caused by a settlement Δ =0.5 in. at a
d) fixed end moments caused by a clockwise rotation of 0.2o at a
e) absolute shear stiffness

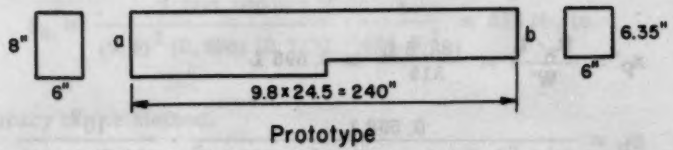

FIG. 14.

$$(E I_b)_{prot.} = 2,000,000 \times \frac{1}{12} 6 \times 6.35^3 = 2.56 \times 10^8 \text{ lb - in}^2$$

$$\frac{1}{(E I_b)_{mod.}} = 3.226 \text{ in}$$

$$\text{Scale } n = \frac{1}{3.226 \times 2.56 \times 10^8} = 1.21 \times 10^{-9}$$

$$\text{Scale } m = 24.5$$

$$x_p = 0.717 L = 0.717 \times 9.8$$

$$x_c = 0.588 L = 0.588 \times 9.8$$

$$A_{mod.} = 23.7 \text{ in}^2$$

(a)

(Eq. 2)

$$C_{ab} = \frac{R_a}{R_b} = \frac{128}{325} = 0.394$$

$$C_{ba} = \frac{R_{b'}}{R_{a'}} = \frac{126.5}{188.5} = 0.671$$

(b)

(Eq. 12)

$$S_a = \frac{x_p}{A\,(x_p - x_c)} \cdot \frac{1}{m\,n} = \frac{0.717\,L}{23.7\,[L\,(0.717 - 0.588)]} \cdot \frac{10^9}{(24.5)\,(1.21)}$$

$$S_a = 7,900,000 \text{ lb - in} = 658,000 \text{ lb - ft}$$

$$S_b = \frac{x_p'}{A\,[x_p' - (L - x_c)]}$$

$$x_p' = \frac{R_a'\,L}{W'} = \frac{188.5\,L}{315} = 0.598\,L$$

$$S_b = \frac{0.598\,L}{23.7\,[0.598\,L - (L - 0.588\,L)]} \cdot \frac{10^9}{(24.5)\,(1.21)}$$

$$S_b = 4,570,000 \text{ lb - in} = 381,000 \text{ lb - ft}$$

(Eq. 13)

$$\frac{C_{ab}}{C_{ba}} = \frac{S_b}{S_a}$$

$$\frac{0.394}{0.671} = \frac{S_b}{658,000}$$

$$S_b = 386,000 \text{ (check)}$$

(c)

(Eq. 28)

$$M_a^{\Delta} = \frac{\Delta}{A\,(x_p - x_c)} \cdot \frac{1}{m^2\,n} = \frac{0.5}{23.7\,[9.8\,(0.717 - 0.588)]} \cdot \frac{10^9}{(24.5)^2\,(1.21)}$$

$$M_a^{\Delta} = 22,900 \text{ lb - in} = 1,910 \text{ lb - ft}$$

(Eq. 21)

$$M_b^{\Delta} = -\frac{L - x_c}{x_c}\, M_a^{\Delta} = -\frac{L - 0.588\,L}{0.588\,L} \times 1,910 = 1,340 \text{ lb - ft}$$

(d)

(Eq. 23) $$M_a^{\theta_a} = \Theta_a S_a = (0.00349 \text{ rad})(658,000) = 2,300 \text{ lb - ft}$$

(Eq. 24) $$M_b^{\theta_a} = C_{ab}\,\Theta_a S_a = (0.394)(2,300) = 906 \text{ lb - ft}$$

(e)

(Eq. 30) $$S_s = \frac{(S_a)_{model}}{x_c\, x_p} \cdot \frac{1}{m^3\, n} = \frac{(S_a)_{prot.}}{x_c\, x_p} \cdot \frac{1}{m^2}$$

$$S_s = \frac{7,900,000}{(9.8)^2\,(0.588)\,(0.717)} \cdot \frac{1}{(24.5)^2} = 324 \text{ lb/in}$$

14. Accuracy of the Method.

The experimental results obtained in Examples 1, 2 and 3 are compared with those determined analytically.

CARRY-OVER FACTORS

Example	C_{ab}			C_{ba}		
	Exper.	Anal.	% Error	Exper.	Anal.	% Error
1	0.396	0.389	1.8	0.438	0.456	3.9
3	0.394	0.400	1.5	0.671	0.667	0.6

STIFFNESS FACTORS

	S_a			S_b		
1	2.380	2.505	5.0	2.190	2.130	2.8
3	658,000	647,000	1.7	381,000	388,000	1.8

FIXED END MOMENT

	Exper.	Anal.	% Error
2	0.1464	0.1495	2.1

IMPRESSED DISTORTIONS

		Exper.	Anal.	% Error
3	M_a^{Δ}	1,910	1,880	1.6
3	M_b^{Δ}	1,340	1,344	0.3
3	$M_a^{\theta a}$	2,300	2,260	1.8
3	$M_b^{\theta a}$	906	904	0.2
3	S_s	324	322	0.6

III - CONCLUSION

The experimental method of analysis described in this paper provides a numerically independent approach to the determination of moment distribution constants. Although the working equations of the method are essentially the same as those used in purely analytic solutions, tedious mathematical integration or the approximate summation process are replaced by weighing.

The concept of the three-dimensional M/EI solid, similar to the M/EI load-diagram evolved in the column analogy method of analysis, permits a visual interpretation of the effect of the physical characteristics of the member upon the various moment distribution constants. The respective solids may be readily sketched and their properties (reactions, location of centroids, etc.) estimated for the purposes of preliminary design. The two-dimensional moment-area and conjugate beam methods are not conducive to making such an estimate.

The notation consisting of the symbols J, Q, x_p, x_c, etc., permits a considerable simplification of the analytic expressions for the moment distribution constants. For example, the stiffness factor expressed by Eq. 7 is equivalent to a textbook formula involving five integrals.[5]

The method has been extended to the determination of moment distribution constants of symmetrical arches with constant or variable moments of inertia. The general procedure of making and weighing the solids remains the same. However, two "pressure solids" are required in order to determine the arch properties in the x- and y-directions. A separate paper dealing with arches will be submitted if the readers' interest in the method described herein warrants it.

BIBLIOGRAPHY

Costa, J. J., "Advanced Structural Analysis," Manhattan College Bookstore, 1953.

Cross, H. and Morgan, N. D., "Continuous Frames of Reinforced Concrete," John Wiley & Sons, Inc., 1932.

5. J. I. Parcel & R. B.B. Moorman, "Analysis of Statically Indeterminate Structures," 1955 Edition, page 275.

Grinter, L. E., "Theory of Modern Steel Structures," Vol. II, The Macmillian Company, 1937.

Maugh, L. C., "Statically Indeterminate Structures," John Wiley & Sons, Inc., 1951.

Ondra, O., "The Determination of Moment Distribution Constants of Members with a Variable Moment of Inertia," Dissertation, Lehigh University, 1955.

Parcel, J. I. and Moorman, R. B. B., "Analysis of Statically Indeterminate Structures," John Wiley and Sons, Inc., 1955.

Portland Cement Association, "Handbook of Frame Constants," 1947.

Journal of the
STRUCTURAL DIVISION
Proceedings of the American Society of Civil Engineers

CONTENTS

DISCUSSION
(Proc. Paper 1067)

Note: Paper 1067 is part of the copyrighted Journal of the Structural Division of the American Society of Civil Engineers, Vol. 82, No. ST 5, September, 1956.

Journal of the

STRUCTURAL DIVISION

Proceedings of the American Society of Civil Engineers

CONTENTS

DISCUSSION
(Proc. Paper 1067)

Note: Paper 1067 is part of the copyrighted Journal of the Structural Division of the American Society of Civil Engineers, Vol. 82, No. ST 5, September, 1956.

Discussion of "NATURAL FREQUENCIES OF CONTINUOUS FLEXURAL MEMBERS"

by A. S. Veletsos and N. M. Newmark
(Proc. Paper 735)

A. S. VELETSOS,* J. M. ASCE, and N. M. NEWMARK,** M. ASCE.—The procedure presented by the writers for the calculation of the natural frequencies of continuous flexural members is indeed only one of a number of possible procedures for applying the general method described in the paper. Mr. Karol discusses an alternate procedure based on the so called "effective stiffness criterion." This procedure consists of (a) computing, for a number of frequencies, the effective stiffness of some joint of the structure, and (b) determining the frequencies for which this stiffness becomes identically equal to zero. The information presented by Mr. Karol is of considerable value and his discussion is greatly appreciated.

It may be of interest to note that, in the course of the investigation which resulted in the present paper, the writers studied several alternate procedures together with a brief discussion of their relative merits are contained in pp. 31-37 of Ref. (15). It turns out that for particular problems, some of these alternate procedures, especially the procedure described by Mr. Karol, may be somewhat simpler to apply than the procedure presented. However, for the fairly broad class of problems considered by the writers, the procedure described in the paper is found to be generally superior to all the other procedures investigated.

It is proposed to discuss here three of the reasons which, in the opinion of the writers, make the procedure described in the paper generally superior to the procedure involving the computation of the effective stiffness.

1) In so far as the computation of only the fundamental frequencies of continuous beams is concerned, there does not seem to exist any advantage in the use of one procedure over the other. However, for the determination of the higher frequencies, the procedure described in the paper requires fewer trials than the procedure involving the computation of the effective stiffness.

As an illustration consider the curves in Fig. C1. These curves pertain to the beam analyzed in Example 1. The curve in solid line is the same as that given in Fig. 4. The curve in dashed line, reproduced from Fig. 20 of Ref. (15), shows the variation of the effective stiffness at support 5, K'_5, as a function of the frequency parameter λ_1. For both curves the λ_1-intercepts correspond to the unknown natural frequencies. One observes that, for the range of frequencies corresponding to the fundamental frequency of the beam, the variations in shape of the two curves with variations in the frequency parameter λ_1 are of the same type and order of magnitude. Accordingly, either curve can be defined with the same number of points. Since the computation of each individual point involves essentially the same amount of work by

* Research Asst. Prof. of Civ. Eng., Univ. of Illinois, Urbana, Ill.
** Research Prof. of Structural Eng., Univ. of Illinois, Urbana, Ill.

either procedure, it really makes little difference which of the two procedures is used in this case. However, for the range of frequencies corresponding to the higher natural frequencies, the situation is quite different. In this range of frequencies, the curve represented by the dashed line is discontinuous (the discontinuities correspond to the natural frequencies of the beam when fixed at the right end), and in certain regions it varies from positive values to infinite negative values and then returns to positive values over a very small range of frequency. One can easily miss one of the natural frequencies by investigating the problem with too coarse a variation in forcing frequency. The curve in dotted line can be said to be "sensitive" to minor variations of the frequency. On the other hand, the curve represented by the solid line is both continuous and much less sensitive to variations in frequency. It becomes apparent that the number of points necessary to approximate the curve in dashed line is considerably larger than that required to establish the curve in solid line. In other words, the higher natural frequencies can be determined with fewer trials by the procedure described in the paper than by the procedure involving the computation of the effective stiffness.

2) The procedure presented in the paper has a wider field of application than the procedure involving the computation of effective stiffnesses. Whereas, the first procedure has been generalized to apply to continuous frames involving any number of closed loops, the second procedure does not appear to be capable of extension to frames involving more than a single closed loop.

Mr. Karol's procedure for determining the effective stiffness of the frame analyzed in Example 3 is both interesting and efficient. However, as appropriately pointed out, this frame is basically a single quadrangular loop with rotational restraints at the joints. Extension of the same procedure to multiple-loop frames does not appear to be possible.

In some cases the effective stiffness of a multiple-loop frame may be determined by moment distribution or slope distribution. It should be noted, however, that these procedures do not always converge to an answer. Convergence of the moment distribution procedure can be insured only for frequencies of vibration which are smaller than the lowest natural frequency of the system considered (12). A similar condition appears to exist for the slope distribution procedure. In general, these procedures can be used to determine only the fundamental frequency of a structure. But even for the range of frequencies corresponding to the fundamental frequency, the procedures of moment distribution and slope distribution may converge so slowly that they become of questionable practical value.

3) An important feature of the procedure described in the paper is that it provides also information on the distortions of the structure during vibration. Since the rotations of the joints are evaluated in this procedure, the natural modes can be sketched readily. From the shape of a natural mode, it may be possible to determine also the order of the corresponding natural frequency.

With reference to the solution of Example 1 by the effective stiffness criterion, Mr. Karol states: "If the end support had been fixed, the computation of the effective stiffnesses would be carried only to the penultimate support, and the natural frequency would be that for which the effective stiffness at that support was zero." For the computation of the fundamental frequency, which is actually the problem considered by Mr. Karol, this procedure is quite satisfactory. However, it is worth noting that the same procedure, when applied to the computation of the higher natural frequencies, will in general fail to detect those natural frequencies for which the joint at the penultimate

support remains stationary. To avoid this difficulty, one should compute the effective stiffness at the fixed support. The natural frequencies are then those frequencies for which the effective stiffness at that support becomes infinite. (If these frequencies were to be evaluated graphically, it would be more convenient to plot the reciprocal of the effective stiffness, which is proportional to the rotation of the joint, and then determine the frequencies for which the reciprocal of the stiffness becomes equal to zero.)

A word of explanation appears necessary regarding the use of determinants in the procedure described in the paper. The reason for using determinants was to make it possible to compute also the natural frequencies corresponding to modes of partial vibration.

Mr. Karol refers to the possibility of determining the natural frequencies of a multi-story building by considering only the two top stories instead of the complete structure. In commenting on the limitations of such a simplification it is necessary to distinguish between fundamental frequencies and higher natural frequencies.

In so far as the computation of the fundamental frequencies is concerned, it is believed that the proposed simplification will be sufficiently accurate for most practical purposes. Obviously, if the stiffnesses of the restraints at the base of the simplified structure could be determined accurately, then the natural frequencies of both structures would be the same. The fact that these restraints cannot be evaluated in advance is not very serious. The natural frequencies of a system, such as a two-story frame which involves several members, are not very sensitive to the conditions of restraint at the ends. Therefore, any reasonable approximation for the dynamic stiffness of these restraints should lead to an accurate prediction of the desired natural frequency. The fact should not be overlooked, however, that these stiffnesses may actually be negative rather than positive. As a possible aid in estimating the magnitude of the dynamic restraints at the base of the equivalent two-story frame, the reader is referred to Eq. 6 of an earlier paper.*

With reference to the computation of the higher natural frequencies, an analysis which considers only a portion of the structure rather than the complete structure does not appear to be very promising. For multi-story frames the spectra of natural frequencies are functions of the number of stories. It appears therefore unlikely that all significant higher natural frequencies of a multi-story frame can be determined by considering only the two top stories. Additional studies are necessary before the degree of accuracy and the range of applicability of this simplification can be established adequately.

In the solution of the illustrative examples of the paper, the use of shortcuts which may confuse the casual reader was purposely avoided. As may readily be inferred from Mr. Karol's discussion, the solution of Example 3 could be simplified by replacing the columns (1) and (2) by rotational springs and by expressing the distortions of the structure in terms of θ_3 and θ_4 rather than in terms of θ_1 and θ_2. An additional simplification could be achieved by using available tabular data (15) for the dynamic stiffness of bars simply supported at the far ends.

The writers wish to thank Mr. Karol for his pertinent comments. His discussion of the effective stiffness procedure and of some of the practical aspects of the problem are very valuable indeed.

---

* "A Simple Approximation for the Fundamental Frequencies of Two-Span and Three-Span Continuous Beams" by A. S. Veletsos and N. M. Newmark, Proceedings of Second U. S. National Congress of Applied Mechanics, ASME, 1954, pp. 143-146.

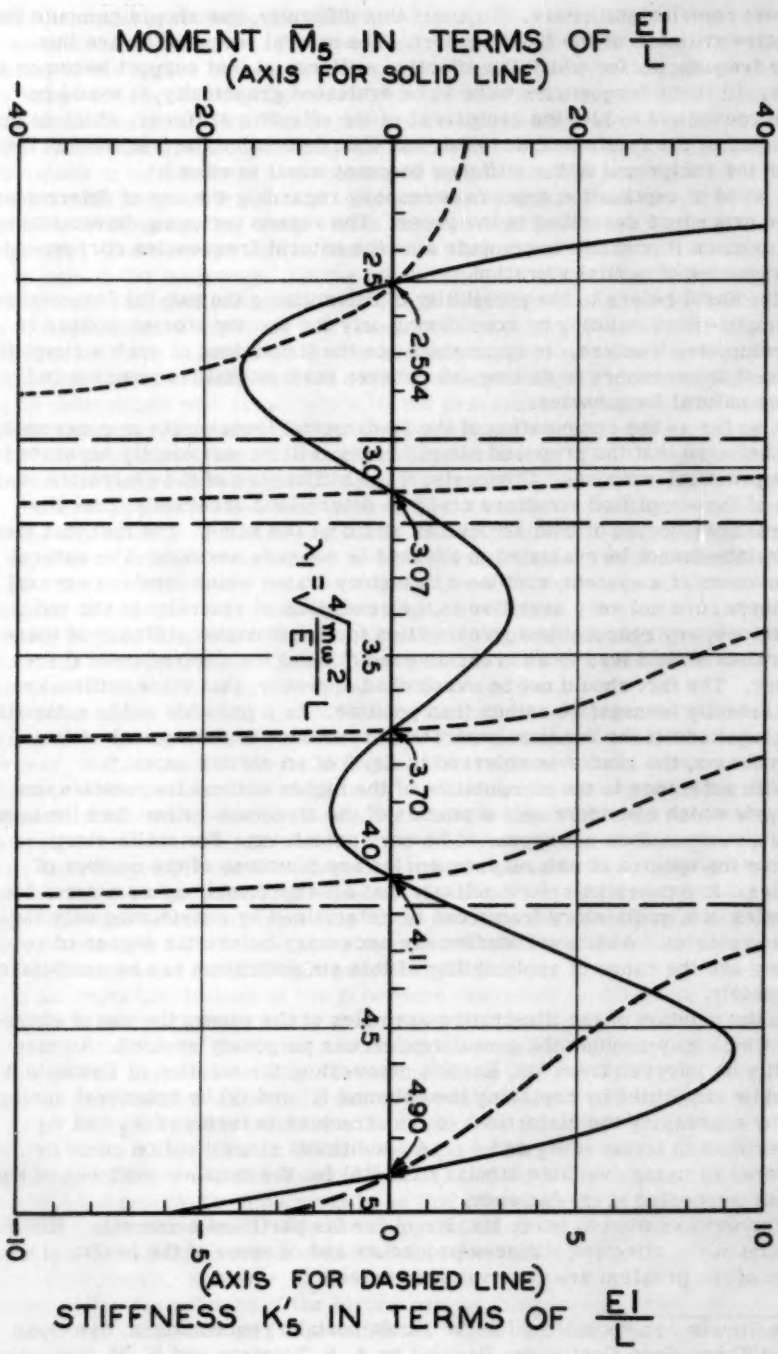

FIG. C1 COMPARISON OF ALTERNATE SOLUTIONS FOR EXAMPLE 1.

Discussion of "SEQUENCE SUMMATION FACTORS"

by Adrian Pauw
(Proc. Paper 763)

ADRIAN PAUW,* A.M. ASCE.—The writer wishes to thank Messrs. Polivka, Weleff, and Giangreco for contributing their time and thought to the discussion of his paper. Their comments have been constructive as well as informative.

Mr. Polivka re-emphasized one of the important points the writer had hoped to make in his paper; namely, the time saving possible when a structure must be analyzed for various types of loadings. This saving is due to the fact that the parameters introduced in this paper are functions only of the geometry of the structure; they may, therefore, be calculated once and for all and can be used for any loading whatsoever.

The writer was interested to learn of the several variations of the sequence-summation concept which have been developed abroad. To the best of his knowledge, these methods have not been published previously in the English language.

In addition to the references cited by Messrs. Weleff and Giangreco the writer has also been informed of a similar variation developed by Professor T. Yoshimura.[1,2] These several variations have one factor in common—they extend the sequence-summation procedure to provide formulas for the direct calculation of support moments or rotations. For exact results these formulas are quite complex. As pointed out, both by Mr. Weleff and by Mr. Giangreco, the use of simplifying assumptions results in excellent approximations. The moments obtained at a central point with these approximations are essentially equivalent to those obtained by distributing unbalanced moments at adjacent joints, followed by over-relaxing the central joint, and subsequently relaxing the moments induced at the adjacent joints.

Although the use of the more complex formulas suggested by the discussors may yield support moments somewhat more rapidly than the writer's procedure (especially where only the moments at certain critical points are to be calculated), the use of such formulas tends to obscure the physical behavior of the structure under load before it reaches equilibrium. It is precisely this concept of the adjustment of the structure under load which is not only the basis but one of the greatest assets of the relaxation method. This asjustment furnishes the analyst a visualization of the manner whereby the

* Prof. of Civ. Eng., Univ. of Missouri, Columbia, Mo.

1. Torazo Yoshimura, "Analysis of Rigid Frames by Balancing Member-Series," Memoirs of the Faculty of Engineering, Kumamoto University, Vol. II, No. 1, Kumamoto, Japan, 1955.
2. Torazo Yoshimura and T. Murakami, "Balancing Member-Series by Parts," Memoirs of the Faculty of Engineering, Kumamoto University, Vol. III, No. 1, Kumamoto, Japan, 1955.

structure supports the applied loads. On the other hand, when explicit formulas are used, the designer is reduced to merely a human calculating machine.

Consideration of these factors caused the writer to abandon the possibility of developing formulas for the direct computation of moments in favor of the central-joint summation-factor procedure described in his paper. With this procedure only one simple basic equation is required and most of the basic features of the "Moment Distribution" method are retained. In most instances convergence is so rapid that for practical purposes only one cycle is required to obtain the joint-rotation moments. In the final analysis the method used to compute the joint-rotation moments is of secondary importance; the only condition which must be fulfilled is that the final support moments must satisfy moment and shear equilibrium. The designer, therefore, is provided with an automatic check of the joint-rotation moment computations. In addition the procedure is expedient in that the original joint-rotation moments can be used to advantage when design modifications are required. Where sections require adjustment the original joint-rotation moments can usually be corrected by a single relaxation cycle.

The joint sequence-summation factor defined by Mr. Weleff as

$$K_n = \frac{1}{1 - \alpha_n}$$

may be seen to be identical with the "over-relaxation factor" defined by the writer as

$$(1 + \beta_A^B) = 1 + \frac{\alpha_{AB}}{1 - \alpha_{AB}} = \frac{1}{1 - \alpha_{AB}}$$

The writer prefers the use of the sequence, summation factor as defined; i.e.,

$$\beta_A^B = \frac{\alpha_{AB}}{1 - \alpha_{AB}}$$

Since α usually has a value much smaller than unity, the use of the parameter, β, results in better accuracy when a slide rule is to be used in computing the sequence-summation factors.

The "modified" parameter

$$\gamma_{AB} = \frac{\alpha_{AB}}{1 - \alpha_{BC}}$$

as introduced by the writer is correct for the example shown in Fig. 5 and is equal to $\alpha_{AB} \overline{K}_B$ (using Mr. Weleff's notation for the modified over-relaxation factor for joint B). The assumption that $\overline{K}_B$ is equal to unity is equivalent to assuming that joint C is fixed; i.e., $\alpha_{BC} = 0$. It is quite

evident, therefore, that for this case the assumption of $\bar{K}_B = 1$ is equivalent to a single cycle of over-relaxation of the moment at joint A using the central-joint sequence-summation factor for joint A.

CORRECTIONS—On page 763-3, Equation (5) should read

$$\theta_B = \frac{-C_{AB} D_{AB} (1 + \beta_A^B) M}{\Sigma K_B}$$

On page 763-24, the value of the story shear in the top story, Fig. 8k, should be -5.00k.

Discussion of "INFLUENCE LINES FOR REACTIONS OF CONTINUOUS TRUSSES"

by Andrew John Pyka
(Proc. Paper 914)

A. C. SCORDELIS,[1] J.M. ASCE.—The problem of finding displacements at a number of points in a trussed structure can be a very tedious one involving considerable computational effort. The author has outlined a procedure which undoubtedly will be very valuable in reducing the computational time involved in a problem of this type.

It would have been desirable, the writer feels, for the author to have verified the validity of the procedure by a derivation using the principle of virtual work. Only by understanding why, when, where, and how a computational procedure is possible can one avoid the inherent possibilities that the procedure may be used improperly or that some factors may be neglected resulting in a solution which is incorrent.

The purpose of this discussion is to present a derivation verifying the procedure outlined by the author and to indicate some of the factors that must be considered in applying the procedure to cases other than the one used by the author.

In computing truss deflections the author uses the method of virtual work which consists of equating the external virtual work done by the external forces acting on a structure to the internal virtual work performed by the members of the truss. It should be noted that the external virtual work must include work done by all external forces including reactions.

Generally speaking the method is used by applying the deformations and displacements of a real structure, Fig. 1a, to a virtual structure, Fig. 1b, having the same configuration of members and support conditions as the real structure. Displacements in the real structure are obtained by placing a one lb. load on the virtual structure at the point and in the direction of the desired displacement and thence an equating of external to internal virtual work yields the displacement.

$$1\# \times \Delta_{VC} = \Sigma u_1(\delta L) = \Sigma\, u_1 \frac{PL}{AE} \qquad (1)$$

The virtual structure selected in Fig. 1b is only one of the many possible. The virtual structure may have any shape or form, the only requirement being that the force system acting on it must be in static equilibrium. For example the virtual structure shown in Fig. 1c could have been selected and the following equation would have resulted:

$$1\# \Delta_{VA} + 1\# \Delta_{VC} + K_{H2} \Delta_{HK} + C_{H2} \Delta_{HC} = \Sigma\, u_2 \frac{PL}{AE} \qquad (2)$$

Since the vertical displacement of point A in the real structure is zero the first term of equation (2) equals zero.

---

1. Asst. Prof. of Civ. Eng., Univ. of California, Berkeley, Calif.

Similarly a virtual structure as shown in Fig. 1d could have been selected and the following equation would have resulted:

$$1\# \Delta_{VG} + 1\# \Delta_{VC} - K_{H3} \Delta_{HK} - C_{H3} \Delta_{HC} = \Sigma u_3 \frac{PL}{AE} \qquad (3)$$

and here again the first term of equation (3) equals zero since the vertical displacement of point G in the real structure is zero.

If all panel lengths of the truss are the same and equal L:

$$K_{H2} = C_{H2} = \frac{1\# NL}{h} \text{ from Fig. 1c.}$$

$$K_{H3} = C_{H3} = \frac{1\#(T-N)L}{h} \text{ from Fig. 1d}$$

$$\frac{K_{H2}}{K_{H3}} = \frac{C_{H2}}{C_{H3}} = \left(\frac{N}{T-N}\right)$$

Where T = total number of panels in the truss and N = the number of panels from the left end to the point at which the vertical displacement is desired.

Now multiplying equation (3) by $\left(\frac{N}{T-N}\right)$:

$$\left(\frac{N}{T-N}\right) 1\# \Delta_{VC} - \left(\frac{N}{T-N}\right) K_{H3} \Delta_{HK} - \left(\frac{N}{T-N}\right) C_{H3} \Delta_{HC} = \left(\frac{N}{T-N}\right) \Sigma u_3 \frac{PL}{AE}$$

$$\text{or } \left(\frac{N}{T-N}\right) 1\# \Delta_{VC} - K_{H2} \Delta_{HK} - C_{H2} \Delta_{Hc} = \left(\frac{N}{T-N}\right) \Sigma u_3 \frac{PL}{AE} \qquad (4)$$

adding equation (2) and (4) yields the following result:

$$\left[1+\left(\frac{N}{T-N}\right)\right] \Delta_{VC} = \left[\Sigma u_2 \frac{PL}{AE} + \left(\frac{N}{T-N}\right) \Sigma u_3 \frac{PL}{AE}\right]$$

$$\Delta_{VC} = \left[\frac{T-N}{T}\right] \left[\Sigma u_2 \frac{PL}{AE} + \left(\frac{N}{T-N}\right) \Sigma u_3 \frac{PL}{AE}\right] \qquad (5)$$

The procedure outlined by the author is an application of equation (5). He obtains the virtual stresses u_2 and u_3 by considering an "analogous cantilevered truss" first cantilivered from the right Fig. 2a, and then from the left Fig. 2b. Note that the member stresses produced in Fig. 2a and 2b are the same as those produced in the same members of Fig. 1c and 1d.

On page 914-7 the author states: "A correction for the relative influence ordinates of column 14, Table 1 at panel points 9 and 31 only as indicated be-

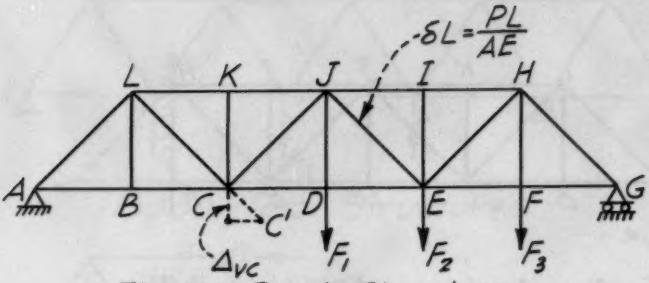

Fig. 1a -- Real Structure

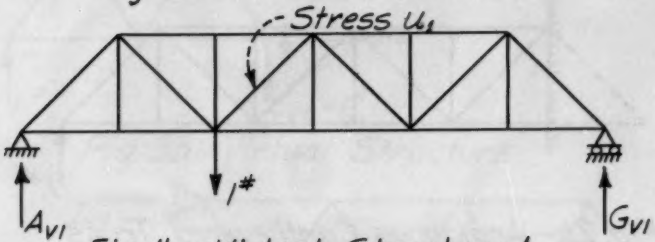

Fig. 1b -- Virtual Structure 1

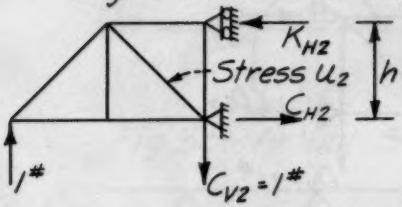

Fig. 1c -- Virtual Structure 2

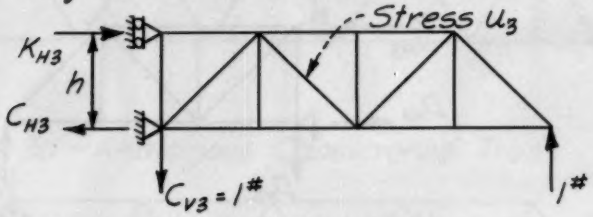

Fig. 1d -- Virtual Structure 3

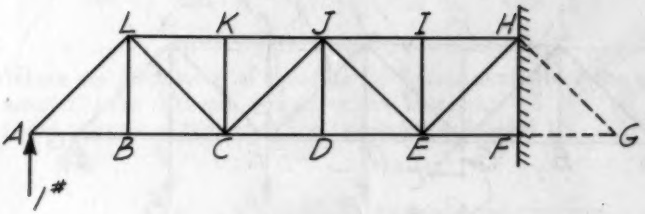

Fig. 2a--Analagous Cantilevered Truss

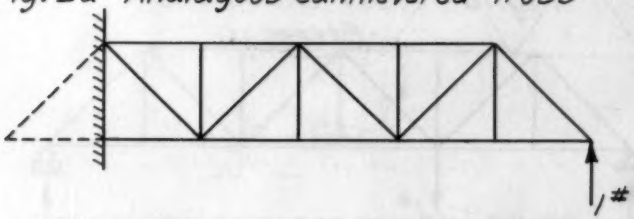

Fig. 2b--Analagous Cantilevered Truss

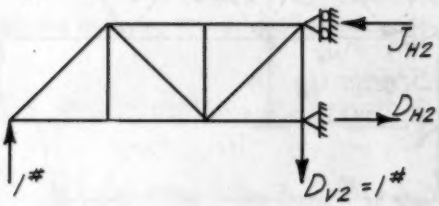

Fig. 2c--Virtual Structure

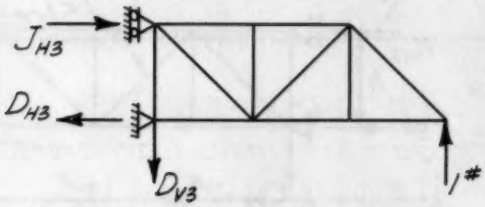

Fig. 2d--Virtual Structure

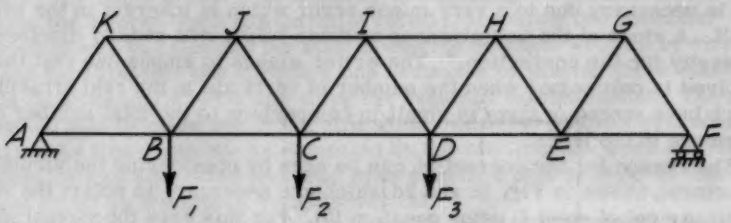

Fig.3a--Real Structure

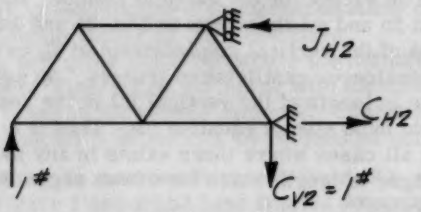

Fig.3b--Virtual Structure

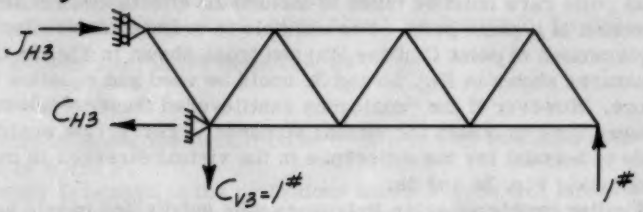

Fig.3c--Virtual Structure

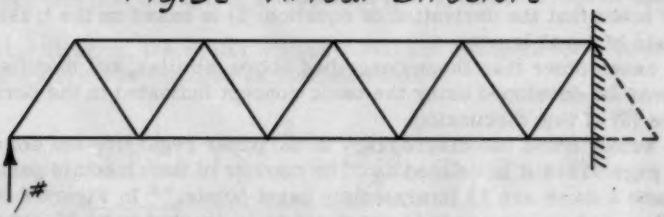

Fig.3d--Analagous Cantilevered Truss

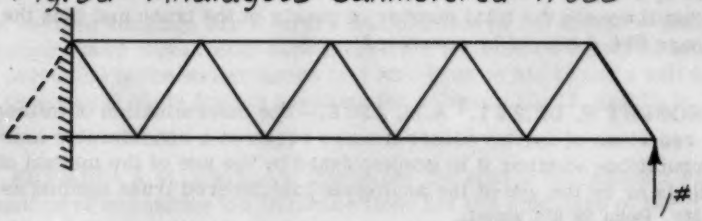

Fig.3e--Analagous Cantilevered Truss

low is necessary due to a very minor error which is inherent in the system itself. A study of the unit stresses at these points will readily disclose the necessity for the correction." The writer wishes to emphasize that the error involved is only minor when the number of verticals in the real structure which have stress in them is small in comparison to the total number of members in the truss.

The reason for the correction can be seen by considering the virtual structures shown in Fig. 2c and 2d which are necessary to obtain the vertical displacement of point D using equation (5). For this case the virtual stresses obtained using the "analogous cantilever trusses" of Fig. 2a and 2b are the same as those for Fig. 2c and 2d except for the vertical member DJ which has zero stress in Fig. 2a and 2b and a 1 lb. stress in Fig. 2c and 2d. In order to obtain the correct value of the vertical displacement at D, using the author's procedure with the "analogous cantilevered trusses," an addition of 1 lb. multiplied by the change in length of the vertical DJ in the real structure, must be made to the right hand side of equation (5). Thus it is seen that a correction must be made in all cases where there exists in any member virtual stresses and real changes in length which have been neglected using the "analogous cantilevered truss."

In applying the author's procedure to a truss without verticals at each panel point care must be taken to include all effects contributing to the dispacement of a panel point. For example in order to determine the vertical displacement of point C of the Warren truss shown in Fig. 3a the virtual structures shown in Fig. 3b and 3c could be used and equation (5) applied as before. However if the "analogous cantilevered trusses" shown in Fig. 3d and 3e were used to obtain the virtual stresses, a correction would have to be made to account for the difference in the virtual stresses in member JC as found using Fig. 3c and 3e.

Similar problems arise in trusses with subdivided panels and the necessary corrections in these cases become somewhat more complex. It should also be noted that the derivation of equation (5) is based on the truss having all panels of equal length.

For cases other than those described above, similar, but modified procedures may be developed using the basic concept indicated in the derivation of equation (5) of this discussion.

The writer noted one discrepancy in the paper regarding the definition of T. On page 914-4 it is defined as "The number of intermediate panel points (in Figure 1 there are 13 intermediate panel points." In Figure 8 on page 914-6 the number intermediate panel points is counted to be 39 and yet in table 1, T is taken as 40. The writer believes that the definition of T should be that it equals the total number of panels in the truss and thus the statement on page 914-4 should be corrected.

ROBERT R. DICKEY,[1] A.M. ASCE.—The determination of influence lines for reactions of indeterminate trusses requires a considerable amount of computations whether it is accomplished by the use of the method of elastic weights or by the use of the analogous cantilevered truss method as presented by Mr. Pyka in his paper.

1. Design Engr., Richardson, Gordon & Associates, Consulting Engrs., Pittsburgh, Pa.

The writer came to this conclusion by determining the influence lines for reactions for a three-span non-parallel chord truss using two methods. The first method was to calculate the elastic weights or angle weights by virtual work and then compute the influence line ordinates by placing these elastic weights on a conjugate beam and doing the required manipulations. The second method was to make use of the analogous cantilevered truss procedure. The influence line ordinates as computed by the two methods were essentially the same. It was also noted that Mr. Pyka's method took at least as much time and effort as the elastic weights method.

Another conclusion was that the writer is not entirely in accord with the author's contention that computational errors are more easily detected and corrected in the analogous cantilevered truss method as compared with other procedures for obtaining influence lines.

There are some instances where the definitions for the various items as listed under Figure 4 do not agree with the computational use of the corresponding items in the typical example. Therefore, the writer suggests that the following author's definitions be devised as indicated below:

P = Stress in member when reactions R2 and R3 are removed in Figure 1 and a unit load applied downward at R2. These stresses are equal to $[(-L_1)/L]\,U$ for members to left of R2, and equal to $(L_1/L)U'$ for members to right of R2 (Fig. 1).

T = number of intermediate panel points plus 1 (in Figure 1, T = 14)

Or another evident alternative definition for T is:

T = number of panels

Also, for completeness, the definition of U' might well be listed between the definitions of U and P.

Since the letter L is used in the definitions under Figure 4 to indicate the length of members in inches and also the length of span in Figure 1, the writer suggests that the author introduce a new symbol for one of the definitions.

For clarification, the writer suggests that the headings for columns 12, 13, and 14 in Figure 4 be changed as indicated below:

11	12	13	14
$\frac{\Sigma PU'L}{A}$	$\frac{N}{T} \times (11)$	$\frac{T-N}{T} \times (8)$	(12) + (13)

These revised headings are a direct manipulation of the author's headings. The author could conceivably have included a little more theory in his paper, but particularly the writer hopes that Mr. Pyka is his closure will indicate the theoretical basis for his headings for columns 12, 13, and 14 in Figure 4.

A. A. EREMIN,[1] A.M. ASCE.—In this paper the author has shown a simplified method of computing the influence lines for the reactions of the

1. Associate Bridge Engr., Bridge Dept., California Div. of State Highways, Sacramento, Calif.

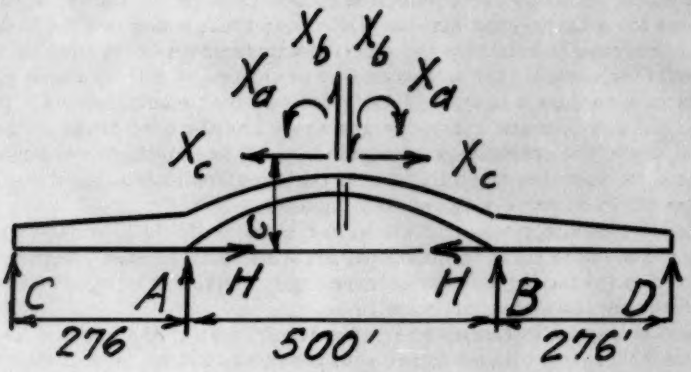

Fig. 1

statically indeterminate trusses. The method is convenient for tabulating and tracing the computations during checking as correctly stated by the author.

Often, however, it is desirable that the checking be performed by independent computations or by the computation method in which the computations are performed in the separate steps. Therefore, the writer wishes to compare the "Analogous Cantilever Method" introduced by the author with a simplified method developed by Professor Krivoshein.[2] In Fig. 1 is shown the diagram of a bridge truss identical with that shown by the author in his Fig. 8. Prof. Krivoshein used this truss in design of a bridge over the Angara river in Russia, in 1914.[3] The bridge spans in feet are, 276, 500, and 276. By introducing the redundant forces X_a X_b and X_c Prof. Krivoshein converted the three-times statically indeterminate bridge truss to a statically determinate one. Distance c to the redundant force X_c is computed in the same manner as the elastic center in the arch rib. Each redundant force is determined from the single equation. Therefore, solution of the simultaneous equations proposed by the author is avoided and computation of the influence lines is reduced to the method generally used in the statically determinate trusses.

JACOB KAROL,[4] M. ASCE.—A supposedly new method for the determination of the influence lines for reactions of continuous trusses is presented in this paper in which an analogous cantilevered truss is used as the basic statically determinate structure. Deflections at every panel point are determined for the basic structure. Then, for unit loads applied at the interior panel points, use is made of the fact that the simple beam moment diagram for the load at a particular point consists of two segments to the right and left of the point which are cantilever moment diagrams proportional to the initial

1. Associate Bridge Engr., Bridge Dept., California Div. of State Highways, Sacramento, Calif.
2. "Simplified Calculations of Statically Indeterminate Bridges" by G. G. Krivoshein, 1930.
3. P. III, See Ref. (2).
4. Prin. Design Engr., Howard, Needles, Tammen & Bergendoff, Kansas City, Mo.

cantilever moment diagram for the unit load applied at the end of the structure. The deflections for the load at the interior panel points can therefore be determined by proportion from the cantilever deflection curve for the unit load applied at the end. The influence line for the intermediate reaction of a three span continuous truss can then be found by proper combination of the simple beam deflection curve and its reversed image, as shown in Figure 5.

The structure chosen by the author to illustrate his method is the Mississippi River Bridge at Dubuque, Iowa. Since the writer calculated the influence lines for this bridge, the author's comments regarding the great amount of labor involved using the method of virtual work and the possibilities for error are of particular interest.

The change in section of a single chord or diagonal member subsequent to the original analysis will change the deflection of every panel point determined either by the author's procedure or by virtual work. In evaluating the summations for the deflections due to the unit loads at the interior panel points, the writer also made use of the fact that they were proportional to the value calculated for the unit load applied at the end of the structure, hence the work was not as time-consuming as the author infers. The detailed calculations cover two pages of the final design. Regarding the possibilities for error, investigation of the influence lines computed by the author in Tables 3 and 4 shows that the ordinates at panel points 13 and 13' do not lie on a smooth curve passing through the ordinates at the adjacent panel points. It would be interesting to know whether this indicates a local error at these points or whether the ordinates at all intervening points are in error.

The author's method, in common with other exact methods of analysis of indeterminate structures, requires knowledge of the areas of all the members in the structure. It is therefore applicable only for final design. The designer of an indeterminate structure must first make an approximate design based on preliminary influence lines for the reactions in order to have a structure to analyze. These preliminary influence lines may be obtained by comparison with previously designed structures of similar proportions or by other means. It is obvious that if these influence lines closely approximate those to be determined from the final design, little or no re-design will be necessary. A simple, rapid and accurate method for calculating preliminary influence lines will now be presented.

A study of numerous continuous truss bridges indicates that the outline of the truss is of greater importance in determining the shape of the influence line than is the variation in areas of the members. Furthermore, since relative rather than absolute deflections are involved, the effect of the web members on the deflection may be neglected. The problem is therefore reduced to the simple case of determining the influence line for an equivalent beam of the same outline as the truss. The moment of inertia at each panel point is proportional to the square of the depth of the truss at that point. For parallel chord trusses this is equivalent to the assumption of uniform moment of inertia.

Detailed computations for the influence line for R_2 for the Dubuque bridge with the tie omitted are given in Table D-1. Ordinates were computed at the odd-numbered panel points only to save time and space. A comparison of the influence lines computed by four methods is shown in Table D-4. It is evident that the assumption of an equivalent beam with moment of inertia proportional to the square of the depth gives results accurate enough for preliminary design.

To compute the influence line for R_2 for the structure including the tie, it is first necessary to determine the deflections of the center span with the tie. These are given in Table D-2. The chords have been assumed equal in area in locating the centerline of the rib in column 2. Assuming the amount of inertia $I = h^2$, the chord area = 2 and the rib area = 2 x 2 = 4. The tie area is assumed to be 120% of the chord area = 2.4. The vertical deflections due to a unit pull in the tie are shown in column 7 and the horizontal deflection in column 9. The effect of rib shortening and tie stretch is added to the bending deflection to obtain the total horizontal deflection. It is computed from the formula

$$\Delta_H = \left(\frac{1}{A_R} + \frac{1}{A_T}\right) \times n \times \left(\frac{\ell_I}{\ell_S}\right)^2 \times k \qquad (1)$$

in which A_R = rib area; A_T = tie area; n = number of segments in arch span = 11; ℓ_I = base length for moment of inertia computations = 40 ft; ℓ_S = base length of segment = 76.83 ft; and k = proportion of total deflection due to chords only = 0.90 (estimated).

The influence ordinates for H for the center span only acting as a simple span are shown in column 8. The ordinates determined by the author are shown in column 10. The excellent agreement indicates the validity of the writer's procedure.

The other deflections required for the analysis are given in notes (a), (b) and (c) below Table D-2.

The computation of the influence lines for R_2 and H for the Dubuque bridge with the tie in place is presented in Table D-3. The deflections shown in column 7 are for the entire span simply supported at the ends for a tie pull H = 6.681 and a vertical load at L_9. The influence ordinates for R_2 are given in column 9 and those for H in column 12. A comparison with the design values and the author's values is presented in Table D-4.

Since all the computations in Tables D-1 to D-3 were made by slide rule using only the geometric outline of the structure, it is evident that preliminary influence lines can be computed for continuous trusses with or without a tied center span in a small fraction of the time used by the author.

In his conclusion, the author suggests the use of the analogous cantilevered truss for determining the influence lines for the reactions of continuous trusses with more than three spans. For a symmetrical five span structure this would require the computation of deflections due to unit vertical loads at R_1, R_2 and R_3 extending over the entire length of the structure. Evaluation of the influence lines would involve small differences of large quantities. The writer believes that a more accurate and expeditious analysis of the structure could be made using the moments at the interior supports as redundants, as is done in the analysis of continuous beams.

The salient points in this discussion will now be summarized:

1) The author's procedure differs from the usual methods of indeterminate analysis primarily in the evaluation of deflections at the interior panel points.
2) Since any method of analysis can be shortened by the use of symmetry and proportional relationships, the time required for a solution is probably dependent on the designer's familiarity with the particular method.

3) Since the theory involved is the same regardless of the method of analysis, errors are due only to the computer.
4) Preliminary influence lines can be determined by the writer's method in a Small fraction of the time used by the author.
5) For structures of more than three spans, an analysis using the moments at the interior supports as redundants will be more accurate and expeditious.

TABLE D-1 DEFLECTION ORDINATES WITHOUT TIE

(1) Panel Point	(2) Truss Height in Feet = h	(3) Rel. Truss Height = h/40	(4) Rel. I = $(\frac{h}{40})^2$	(5) Mom. Vert. Load at L_9 = u	(6) Angle Change $\frac{u}{I}$	(7) Trial Slope = $\Sigma \frac{u}{I}$	(8) Trial Defl. = Σ (7)	(9) Linear Corr.	(10) Final Defl. (8)+(9)	(11) $-\frac{313.6}{369.5}$ × (10) Reversed	(12) Rel. Infl. Ord. (10)+(11)	(13) Actual Infl. Ord. for R_2
0							0	0	0	0	0	0
						95.0						
1	40.00	1.000	1.000	1.72	1.3		47.5	-1.8	45.7	-30.8	14.9	0.194
						93.7						
3	40.00	1.000	1.000	5.16	5.2		141.2	-5.2	136.0	-91.9	44.1	0.426
						88.5						
5	43.33	1.083	1.173	8.61	7.3		229.7	-8.8	220.9	-151.7	69.2	0.669
						81.2						
7	53.33	1.333	1.778	12.05	6.8		310.9	-12.2	298.7	-209.6	89.1	0.861
						74.4						
9	70.00	1.750	3.063	15.5	5.1		385.3	-15.8	369.5	-266.0	103.5	1.000
						69.3						
11	57.53	1.438	2.067	14.5	7.0		454.6	-19.2	435.4	-321.0	114.4	1.105
						62.3						
13	46.22	1.156	1.335	13.5	10.1		516.9	-22.8	494.1	-374.0	120.1	1.160
						52.2						
15	37.18	0.930	0.865	12.5	14.4		569.1	-26.2	542.9	-422.5	120.4	1.163
						37.8						
17	30.37	0.759	0.576	11.5	20.0		606.9	-29.8	577.1	-464.0	113.1	1.093
						17.8						
19	25.76	0.644	0.415	10.5	25.3		624.7	-33.2	591.5	-492.5	99.0	0.956
						-7.5						
19'	25.76	0.644	0.415	9.5	22.9		617.2	-36.8	580.4	-501.5	78.9	0.762
						-30.4						
17'	30.37	0.759	0.576	8.5	14.7		586.8	-40.2	546.6	-489.0	57.6	0.556
						-45.1						
15'	37.18	0.930	0.865	7.5	8.7		541.7	-43.8	497.9	-460.9	37.0	0.357
						-53.8						
13'	46.22	1.156	1.335	6.5	4.9		487.9	-47.2	440.7	-419.0	21.7	0.210
						-58.7						
11'	57.53	1.438	2.067	5.5	2.7		429.2	-50.8	378.4	-369.2	9.2	0.089
						-61.4						
9'	70.00	1.750	3.063	4.5	1.5		367.8	-54.2	313.6	-313.6	0	0
						-62.9						
7'	53.33	1.333	1.778	3.5	2.0		304.9	-57.8	247.1	-253.6	-6.5	-0.063
						-64.9						
5'	43.33	1.083	1.173	2.5	2.1		240.0	-61.2	178.8	-187.5	-8.7	-0.084
						-67.0						
3'	40.00	1.000	1.000	1.5	1.5		173.0	-64.8	108.2	-115.4	-7.2	-0.070
						-68.5						
1'	40.00	1.000	1.000	0.5	0.4		104.5	-68.2	36.3	-38.8	-2.5	-0.024
						-68.9						
0'							70.0	-70.0	0	0	0	0

TABLE D-2 DEFLECTIONS OF ARCH SPAN

1 Panel Point	2 Vert. Arm to ℄ Rib in Feet = y	3 Rel. Arm = y/76.83 = v	4 Rel. I Col. 4 Table D-1	5 Angle Change v/I = 3/4	6 Slope = Σ 5	7 Defl. = Σ 6	8 Ordinates for H = 7/27.09	9 v²/I (3 × 5)	10 Ordinates for H (Ayka)
					9.05				
9	35.00	0.456	3.063	0.07		0	0	0.03	0
					8.98				
11	62.84	0.818	2.067	0.40		8.98	0.331	0.33	0.329
					8.58				
13	85.29	1.110	1.335	0.83		17.56	0.648	0.92	0.655
					7.75				
15	101.81	1.326	0.865	1.53		25.31	0.934	2.03	0.943
					6.22				
17	112.42	1.465	0.576	2.55		31.53	1.164	3.74	1.173
					3.67				
19	117.12	1.525	0.415	3.67		35.20	1.299	5.60	1.309
							Total =	12.65	
								× 2	
								25.30	

Rib Shortening and Tie Stretch $= \left(\frac{1}{4} + \frac{1}{2.4}\right) \times 11 \times \left(\frac{40}{76.83}\right)^2 \times 0.9 = \frac{1.79}{27.09}$

Notes

(a) Deflection at Lo for unit pull in tie = 4.5 × 9.05 = 40.73

(b) $\Sigma \frac{uv\,ds}{I}$ = (15.5 + 4.5) × 9.05 = 181.0

Hence H_u = 181.0 ÷ 27.09 = 6.681

(c) Truss deflection (supported at Lo and Lo') due to H_u is shown below:

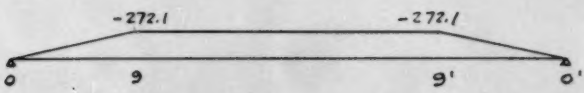

TABLE D-3 DEFLECTION ORDINATES WITH TIE

(1) Panel Point	(2) Arch Defl -6.681 = Col. (1) Table D-2	(3) Truss Defl. Note (c) Table D-2	(4) Total Defl. with Tie (2) + (3)	(5) Defl. due to U Col. (10) Table D-1	(6) Net Defl. with Tie (5) + (4)	(7) -41.5/97.4 = (6) Reversed	(8) Rel. Infl. Ord. (6) + (7)	(9) Actual Infl. Ord. for R_2	(10) Col. (9)/181.0	(11) -1.503 = (R_2 to R_3)	(12) Infl. Ord. for H (10) + (11)
0		0	0	0	0	0	0	0	0	0	0
1		-30.2	-30.2	45.7	15.5	-2.6	12.9	0.162	0.167	-0.235	-0.068
3		-90.7	-90.7	136.0	45.3	-7.5	37.8	0.475	0.501	-0.679	-0.178
5		-151.2	-151.2	220.9	69.7	-11.8	57.9	0.727	0.835	-1.052	-0.217
7		-211.6	-211.6	298.7	88.1	-15.1	73.0	0.916	1.169	-1.339	-0.170
9	0	-272.1	-272.1	369.5	97.4	-17.7	79.7	1.000	1.503	-1.503	0
11	-59.9	-272.1	-332.0	435.4	103.4	-19.8	83.6	1.049	1.834	-1.620	0.214
13	-117.2	-272.1	-389.3	494.1	104.8	-21.9	82.9	1.040	2.151	-1.691	0.460
15	-169.0	-272.1	-441.1	542.9	101.8	-24.2	77.6	0.974	2.437	-1.716	0.721
17	-210.4	-272.1	-482.5	577.1	94.6	-27.3	67.3	0.845	2.667	-1.719	0.948
19	-235.0	-272.1	-507.1	591.5	84.4	-31.2	53.2	0.668	2.802	-1.709	1.093
19'	-235.0	-272.1	-507.1	580.4	73.3	-35.9	37.4	0.469			
17'	-210.4	-272.1	-482.5	546.6	64.1	-40.3	23.8	0.299			
15'	-169.0	-272.1	-441.1	497.9	56.8	-43.4	13.4	0.168			
13'	-117.2	-272.1	-389.3	440.7	51.4	-44.6	6.8	0.085			
11'	-59.9	-272.1	-332.0	378.4	46.4	-44.1	2.3	0.029			
9'	0	-272.1	-272.1	313.6	41.5	-41.5	0	0			
7'		-211.6	-211.6	247.1	35.5	-37.5	-2.0	-0.025			
5'		-151.2	-151.2	178.8	27.6	-29.7	-2.1	-0.026			
3'		-90.7	-90.7	108.2	17.5	-19.3	-1.8	-0.023			
1'		-30.2	-30.2	36.3	6.1	-6.6	-0.5	-0.006			
0'		0	0	0	0	0	0	0			

Note Influence ordinates for H are symmetrical abt. ℄

TABLE D-4 COMPARISON OF INFLUENCE LINES

Panel Point	R_2 (WITHOUT TIE)				R_2 (WITH TIE)			H (WITH TIE)		
	Unif. I	I varies as h^2	Design HNTB	Pyka	I varies as h^2	Design HNTB	Pyka	I varies as h^2	Design HNTB	Pyka
0	0	0	0	0	0	0	0	0	0	0
1	0.139	0.144	0.149	0.149	0.162	0.168	0.167	-0.068	-0.070	-0.067
3	0.413	0.426	0.439	0.440	0.475	0.492	0.491	-0.178	-0.195	-0.195
5	0.657	0.669	0.684	0.685	0.727	0.747	0.747	-0.217	-0.237	-0.232
7	0.858	0.861	0.867	0.868	0.916	0.912	0.911	-0.170	-0.165	-0.161
9	1.000	1.000	1.000	1.000	1.000	1.000	1.000	0	0	0
11	1.070	1.105	1.106	1.105	1.049	1.045	1.044	0.214	0.228	0.224
13	1.077	1.160	1.170	1.150	1.040	1.039	1.010	0.460	0.488	0.518
15	1.028	1.163	1.179	1.161	0.974	0.973	0.951	0.721	0.765	0.781
17	0.936	1.093	1.113	1.107	0.845	0.847	0.827	0.948	0.992	1.039
19	0.812	0.956	0.968	0.963	0.668	0.660	0.641	1.093	1.156	1.189
19'	0.663	0.762	0.757	0.759	0.469	0.448	0.441			
17'	0.509	0.556	0.544	0.545	0.299	0.280	0.265			
15'	0.363	0.357	0.356	0.371	0.168	0.152	0.160			
13'	0.207	0.210	0.205	0.224	0.085	0.073	0.084			
11'	0.086	0.089	0.088	0.089	0.029	0.027	0.028			
9'	0	0	0	0	0	0	0			
7'	-0.048	-0.063	-0.066	-0.066	-0.025	-0.023	-0.023			
5'	-0.060	-0.084	-0.095	-0.095	-0.026	-0.031	-0.033			
3'	-0.049	-0.070	-0.078	-0.078	-0.023	-0.027	-0.024			
1'	-0.016	-0.024	-0.027	-0.028	-0.006	-0.009	-0.010			
0'	0	0	0	0	0	0	0			

Note Influence lines for H are symmetrical abt. ℄

Discussion of "ARCHING ACTION THEORY OF MASONRY WALLS"

by E. L. McDowell, K. E. McKee, and E. Sevin
(Proc. Paper 915)

A. A. EREMIN,[1] A.M. ASCE.—In this paper the authors presented an interesting study of the arch theory of stress distribution in masonry walls. The derived method of stress distribution the authors have successfully proved by the experimental tests performed with the full-scale masonry beams. The arch theory of stress distribution in the beams requires beam-ends restraints or special reaction forces applied at the ends. It would be interesting to have more details in regard to the ends restraint used by the authors in their test beams. In the practice often the beam-end restraints require special complicated details. The simplest detail is providing the

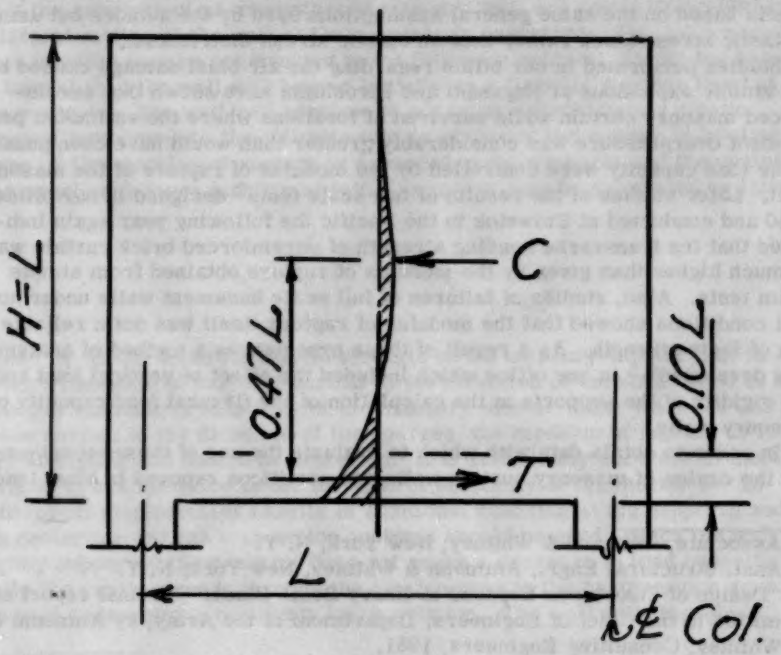

Fig. 1.

1. Associate Bridge Engr., Bridge Dept., California Div. of State Highways, Sacramento, Calif.
2. P. 338. Beton-Kalender, 1951.

tensile members in the areas of concentrations of the tensile stresses or inserting the reinforcing steel bars.

The tensile stresses in the simply supported masonry wall beam is shown in Fig. (1), (2), which is

$$T = 0.15\ qL$$

where, q is loading uniformly distributed along the span length. The shaded area in Fig. 1 indicates the stress diagram at the section at the mid-span.

However, in practice there are cases when neither tensile member, nor tensile reinforcing bars can be placed. Therefore, the arch theory of stress distribution developed by the authors may find useful practical application and the authors deserve acknowledgment for their valuable contribution.

EDWARD COHEN,[1] and EDWARD LAING,[2] J.M., ASCE.—The authors have done a careful and most interesting piece of work in giving a method for computing the load carrying capacity of unreinforced masonry panels. With the recent impetus in blast and earthquake resistant design, research of this type is most welcome. It is the purpose of this discussion to describe a simplified method of obtaining the resistance function for unreinforced masonry panels based on the same general assumptions used by the authors but using a plastic stress block rather than an elastic stress distribution.

Studies performed in our office regarding the air blast damage caused by the atomic explosions at Nagasaki and Hiroshima have shown that unreinforced masonry curtain walls survived at locations where the estimated peak incident overpressure was considerably greater than would have been possible if the load capacity were controlled by the modulus of rupture of the masonry wall. Later studies of the results of full scale tests[3] designed in our office in 1950 and conducted at Eniwetok in the Pacific the following year again indicated that the transverse bending strength of unreinforced brick curtain walls is much higher than given by the modulus of rupture obtained from simple beam tests. Also, studies of failures of full scale basement walls under normal conditions showed that the modulus of rupture itself was not a reliable index of their strength. As a result of these experiences a method of analysis was developed[4,5] in our office which included the effect of vertical load and the rigidity of the supports in the calculation of the flexural load capacity of masonry walls.

In order to obtain data with which to evaluate the use of these techniques for the design of masonry curtain walls and partitions exposed to blast loads

1. Associate, Ammann & Whitney, New York, N. Y.
2. Asst. Structural Engr., Ammann & Whitney, New York, N. Y.
3. "Design of Structures Exposed to Heavy Bomb Blast." A final report submitted to the Chief of Engineers, Department of the Army, by Ammann & Whitney, Consulting Engineers, 1951.
4. "Design of Structures to Resist Heavy Blast." A report submitted to the Chief of Engineers, Department of the Army, by Ammann & Whitney, Consulting Engineers, 1954.
5. "Design of Blast Resistant Construction for Atomic Explosions," ACI Journal, March 1955, Proc. V. 51, pp. 589-683.

and to proof test typical wall constructions, a full scale test program[6,7] was organized by the Federal Civil Defense Administration and designed by Ammann & Whitney in 1952 and tested at Yucca Flats, Nevada the following year.

The additional work involved in dealing with the "elastic" portion of the stress distribution as proposed by the authors, is unjustified and gives only an apparent, but not real, increase in the accuracy. It should be noted that it is implicit in the arch action analysis that the modulus of rupture has been exceeded prior to the calculation. In this case, when the modulus of rupture is greater than the tensile strength obtained from a tensile test, the wall may be assumed to have already passed beyond the elastic range, the proportional limit being passed prior to reaching the modulus of rupture.

The method used for computing the resistance functions as described in this discussion were verified to a good degree for restrained unreinforced masonry panels (solid and hollow) by the results of the above field tests and by the results of the MIT laboratory tests cited by the authors.

Rigid Supports

If the supports of an unreinforced masonry wall are completely rigid and if lateral motion of the wall at the supports is prevented, (Fig. 1a) a resistance function may be constructed in the following manner. Under the action of lateral load the wall will behave initially as a flexural member fixed at the supports. The wall will continue to act as an approximately elastic flexural member until the ultimate tensile stress of the mortar in bending as given by the modulus of rupture is exceeded at the supports and the center. The panel resistance function at initial cracking may be expressed as follows:

$$R_t = \frac{2t^2 f_t}{h} \quad ; \quad x_t = \frac{R_t h^3}{32\, E t^3}$$

where f_t is the apparent tensile strength of the masonry-mortar unit in flexure (modulus of rupture) normal to the direction of the span and E is the effective modulus of elasticity of the masonry mortar unit. When the unit spans normal to the direction of the courses, the modulus of rupture is small and unreliable and should be neglected. It is sufficiently accurate in most instances to use the value of the modulus of elasticity of the mortar for E. Subsequent displacement results in additional cracking at the supports and at the centerline and the arch action analysis should be used. Since the wall is rigidly supported the cracking does not cause a decrease in load capacity while the crack spreads through the tension zone to the compression zone, the wall undergoing a relatively large rotation. The wall will, therefore,

6. "Proposed Program for Test of Structures Exposed to Bomb Blast." A final report prepared for the Federal Civil Defense Administration by Ammann & Whitney, Consulting Engineers, 1952.
7. "Blast Effects of Atomic Weapons Upon Curtain Walls and Partitions of Masonry and Other Materials—Chapters 2 & 3." A report submitted to the Federal Civil Defense Administration by Ammann & Whitney, Consulting Engineers, 1956.

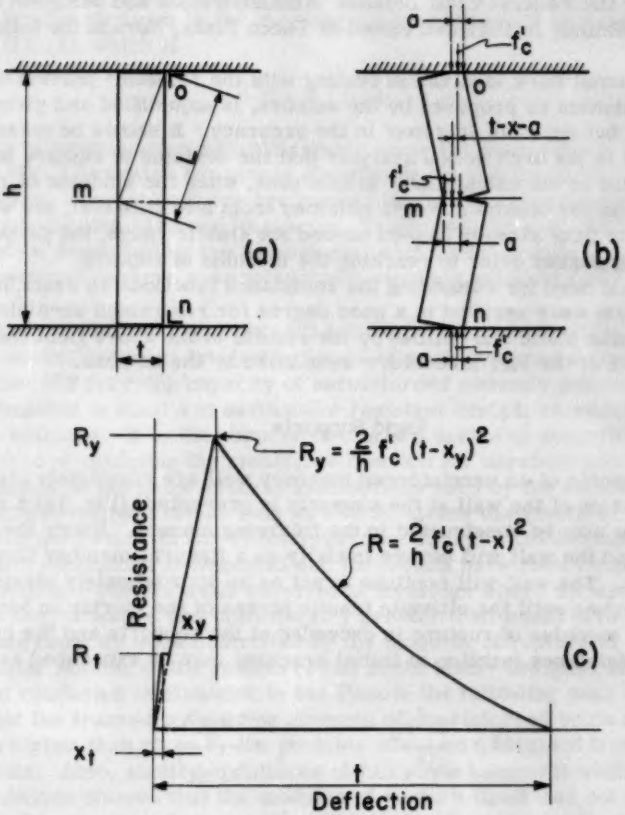

$$x_y = \frac{t\, f'_c}{E_m \epsilon_m} \quad ; \quad \epsilon_m = \frac{L - 0.5h}{L}$$

E_m = effective modulus of elasticity of masonry mortar unit

f'_c = ultimate compressive stress of masonry mortar

Fig. 1 Resistance Function for Unreinforced Solid Masonry Panel with Rigid Supports.

continue to resist a load approximately equal to that at initial cracking until the crack reaches the compression zone and will increase thereafter in accordance with the arch action analysis.

For additional displacement, it is assumed that each half of the wall rotates as an independent elastic body as shown in Figure 1b. The displacement of point m due to the assumed rigid body rotation shown in Figure 1 produces compressive stresses along the contact surfaces at points m, n, and o. These compressive forces form a couple that produces a resistance R = 8M/h to lateral loads.

The compressive stress distribution at points m, n, and o at maximum resistance is assumed to be represented by an equivalent uniform stress block of a magnitude f_c' and a width equal to the contact area "a" as shown in Figure 1b.

When point m has been deflected to the position at which the centerline of the compression block at the supports of the wall coincides with the centerline of the compression block at the center of the wall the moment arm of the resisting couple will have been reduced to zero and the wall will become unstable with no further resistance to deflection. In this position the diagonals, om and mn, will have been shortened by an amount L-h'/2, and the maximum unit strain in the wall caused by this shortening will be $\epsilon_m = (L-h'/2)/L$. The elastic compressive stress corresponding to the strain ϵ_m is given by $f_m = E\epsilon_m$. Based on the above conditions, f_m in most instances will be greater than the ultimate compressive stress of the mortar f_c' and is therefore a fictional stress. Since for walls of normal span and thickness, each half of the wall undergoes a small rotation to obtain the ultimate load position, the shortening of the diagonals om and mn, can be considered a linear function of the displacement of point m. The deflection, x_y, at which a compressive stress of f_c' exists at points m, n and o, can therefore be found from the following relation.

$$\frac{x_y}{t} = \frac{f_c'}{f_m} = \frac{f_c'}{E\epsilon_m}$$

$$x_y = \frac{tf_c'}{E\epsilon_m}$$

The resisting moment that is caused by a deflection of x_y is found by assuming rectangular compressive stress blocks to exist at the supports and at the center as shown in Fig. 1b.

The bearing width, a, is chosen so that the moment, M_y, is a maximum by differentiating M_y with respect to a, and setting the derivative equal to zero, which results in $a = (1/2)(t - x_y)$.

$$M_y = \frac{f_c'}{4}(t-x_y)^2$$

$$R_y = \frac{2f_c'}{h}(t-x_y)^2$$

When the midspan deflection is greater than x_y the expression for resistance becomes:

$$R = \frac{2f'_c (t-x)^2}{h}$$

As the deflection increases the resistance is reduced until at x = t the resistance is zero.

A typical resistance function for a masonry wall of this type is shown in Fig. 1c. As the span to thickness ratio of the wall decreases, the flexural action up to cracking becomes less pronounced and may usually be neglected for span to thickness ratios less than approximately 12. However, for span to thickness ratios greater than 12, the flexural action is quite important. This trend is well illustrated in the comparisons shown in Figures 5 and 6.

Rigid Supports - Clearance at a Support

For walls with an incompletely filled end joint the preceding equations may be used with the following modifications. The width of the crack is assumed as h'-h as shown in Figure 2a. Under the action of lateral load the wall will behave initially as a flexural member restrained at one support and pinned at the other. The resistance function at cracking is expressed as follows:

$$R_t = \frac{1.33\, t^2 f_t}{h} \qquad x_t = \frac{R_t h^3}{15.3Et^3}$$

Subsequent displacement results in additional cracking at the restrained support and at the centerline. The rotation up to cracking will normally not be sufficient to close the open joint and therefore the resistance of the wall will drop abruptly from R_t to zero. For the majority of walls of this type, the flexural action may be neglected (except for members with large span to thickness ratios.) For additional displacement each half of the wall is assumed as a rigid body until the wall takes the position shown in Figure 2b. During this rotation, point m has undergone a lateral motion $x_c - x_t$, no resistance to motion has been developed in the wall, and the corner of the wall at point o will be just touching the support. The magnitude of x_c can be found from the geometry of the wall in its deflected position.

$$(t - x_c)^2 = L^2 - \left[\frac{h}{2} + \frac{h'-h}{2}\right]^2 = L^2 - \left[\frac{h'}{2}\right]^2$$

$$x_c = t - \sqrt{L^2 - \left[\frac{h'}{2}\right]^2}$$

where $L = \sqrt{\left[\frac{h}{2}\right]^2 + t^2}$ and all other symbols are as shown in Fig. 2.

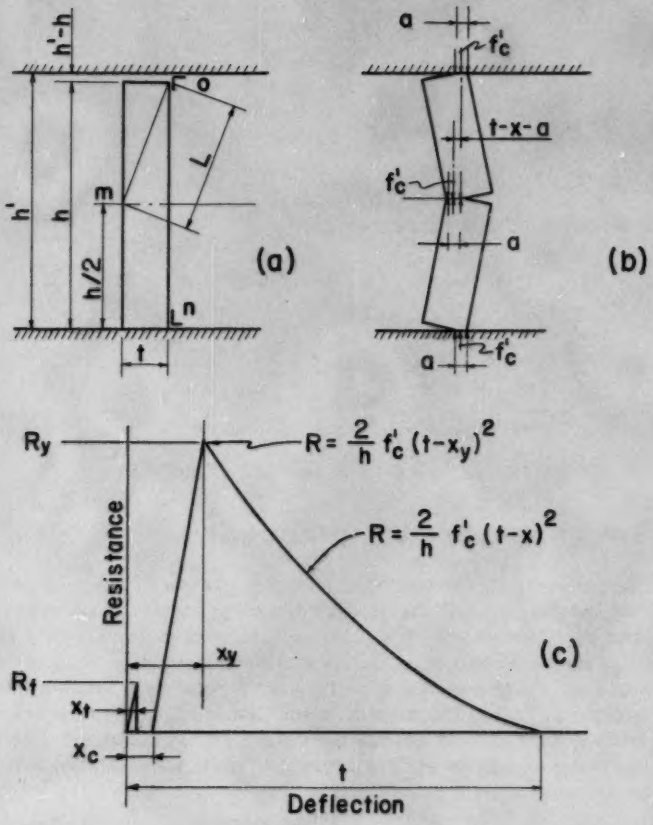

$$x_c = t - \sqrt{L^2 - 0.25(h')^2} \quad ; \quad x_y = \frac{(t - x_c) f'_c + x_c}{E\ \epsilon_m} \quad ; \quad \epsilon_m = \frac{L - 0.5\,h'}{L}$$

E = effective modulus of elasticity of masonry mortar
f'_c = ultimate compressive stress of masonry mortar

Fig.2 Resistance Function for Unreinforced Solid Masonry Panel with Clearance at a Rigid Support.

The deflection, x_y, at which a compressive stress of f'_c exists at points m, n, and o can be found from the following relation

$$\frac{x_y - x_c}{t - x_c} = \frac{f'_c}{f_m} = \frac{f'_c}{E\epsilon_m}$$

$$x_y = \frac{(t-x_c)f'_c}{E\epsilon_m} + x_c$$

The resistance function may be expressed as:

$$R_y = \frac{2f'_c}{h}(t-x_y)^2 \qquad \text{for } x = x_y$$

$$R = \frac{2f'_c}{h}(t-x)^2 \qquad \text{for } x > x_y$$

A typical resistance function of this type is shown in Figure 2c.

Walls With Large Span to Thickness Ratios

The preceding procedures for computing the resistance function is reasonably close for the majority of unreinforced masonry walls. However, for unusual walls and partitions where the span to thickness ratio may be about 24 or greater it is necessary to build up the resistance function in a somewhat different manner. Walls of this type require a relatively large amount of rotation in order to develop the maximum unit stress f'_c and therefore the maximum resistance will develop before the value of f'_c is reached. For this condition the following equations should be used to build the resistance function up to its maximum value.

$f = f_t$: $R_t = \frac{Kt^2 f_t}{h}$; where K = 2.0 for end joints completely filled (x_c = o); K = 1.33 for one end joint not completely filled

$x_t = \frac{R_t h^3}{32Et^3}$; for end joints completely filled

$x_t = \frac{R_t h^3}{15.3Et^3}$; for one end joint not completely filled

$f > f_t$: $R = \frac{8f_c a}{h}(t-a-x)$

where $x = 0.5\ h \sin\theta + x_c$; $f_c = \frac{(x-x_c)E\epsilon_m}{t-x_c}$

$$a = \frac{\epsilon L \cos(\phi-\theta) - h' + h}{2 \sin\theta \cos\theta} \quad ; \epsilon = 1 - \frac{h'}{L\cos(\phi-\theta)}$$

θ = angular rotation of wall

ϕ = arc tan $\frac{2t}{h}$

f_t = tensile strength of mortar in flexure

Other terms as previously defined

After maximum resistance, the resistance function may be approximated by substituting the value of compressive stress at maximum resistance for f'_c in the equations shown in Figures 1 and 2.

Hollow Block Walls

The compression area, a, of unreinforced hollow masonry walls is limited by the thickness of the hollow block flanges. The resistance function for walls of this type may be computed by a procedure similar to that used for solid walls. The resistance function at initial cracking is computed as follows:

Wall with end joints completely filled

$$R_t = \frac{24If_t}{ht} \quad ; \quad x_t = \frac{R_t h^3}{384EI}$$

Wall with end joint not completely filled

$$R_t = \frac{16If_t}{ht} \quad ; \quad x_t = \frac{R_t h^3}{185EI}$$

where I is the moment of inertia masonry mortar unit and other terms are as previously defined.

The expressions to be used after initial cracking are shown in Figure 3 and 4. Modifications to hollow panels having large span to thickness ratios would also be similar to those described for solid panels.

Non-Rigid Supports

For the case where the wall is supported by elastic supports, the resistance curve must be constructed in a different manner. The compressive force built up in walls of this type is a function of the stiffness of the supports, i.e., $F = kaf'_c$ where k is an effective spring constant. Once F is determined, equations similar to those derived for the case of the rigid supports may be used.

If the supports offer no resistance to vertical motion, the compression in the wall will be limited by the weight of the wall above plus the floor and roof loads carried by the wall. If the wall carries no vertical loads, then the wall must be analyzed as a simply supported beam, the maximum resisting moment being determined by the modulus of rupture. For normal basement walls spanning vertically, (in the weak direction) the modulus of rupture is controlled by the mortar and is unreliable. The strength therefore depends

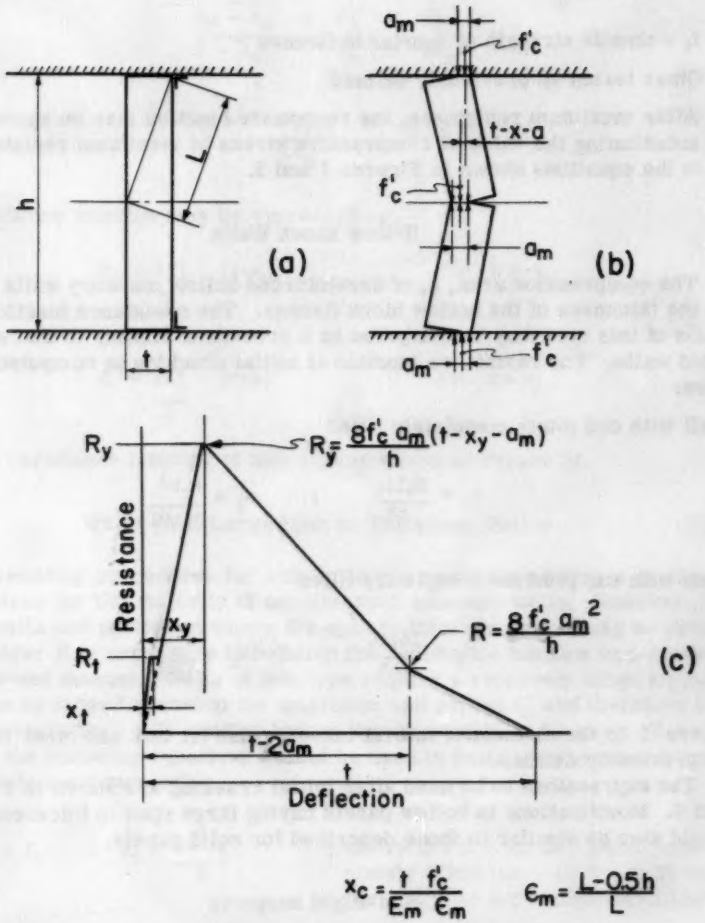

$$x_c = \frac{t\ f'_c}{E_m\ \epsilon_m} \qquad \epsilon_m = \frac{L - 0.5h}{L}$$

E = effective modulus of elasticity of masonry mortar unit
f'_c = ultimate compressive stress of masonry mortar
a_m = hollow block flange thickness

Fig. 3 Resistance Function for Unreinforced Hollow Masonry Panel with Rigid Supports.

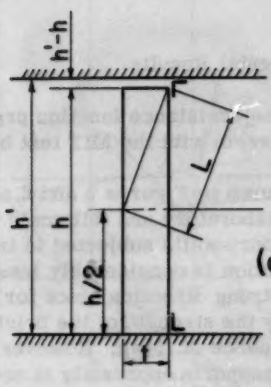

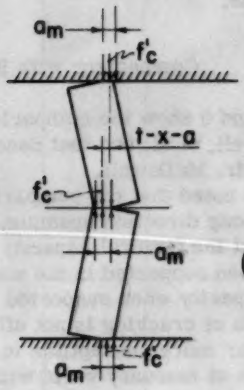

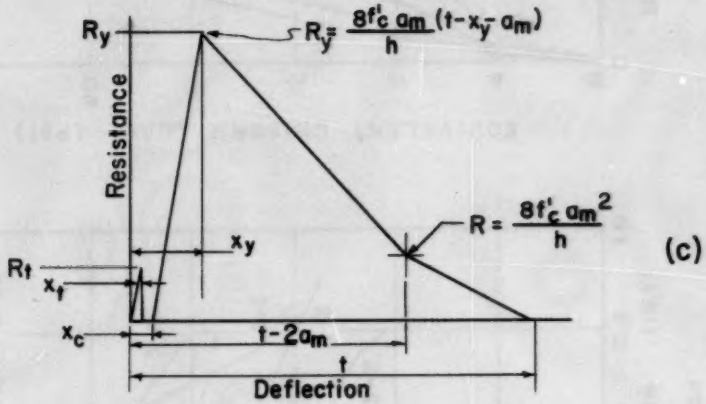

$$x_c = t - \sqrt{L^2 - 0.25(h')^2} \quad ; \quad x_y = \frac{(t - x_c)f'_c}{E\ \epsilon_m} + x_c \quad ; \quad \epsilon_m = \frac{L - 0.5\,h'}{L}$$

E = effective modulus of elasticity of masonry mortar unit
f'_c = ultimate compressive stress of masonry mortar
a_m = hollow block flange thickness

Fig. 4 Resistance Function for Unreinforced Hollow Masonry Panel with Clearance at a Rigid Support.

almost entirely on the vertical load from the floor system and the wall above the ground floor.

Comparison with Experimental Results

Figures 5 and 6 show the comparison of the resistance function prepared by Mr. McDowell, et al. and that described herein with the MIT test beams described by Mr. McDowell.

It should be noted that the comparisons shown in Figures 5 and 6 are based upon strong direction spanning. Both laboratory and full scale tests have shown that the flexural capacity of masonry walls subjected to transverse loads when supported in the weak direction is considerably less than the flexural capacity when supported in the strong direction since for the former the path of cracking is not affected by the strength of the brick and is subsequently far more susceptible to the influence of flaws. However, the ultimate strength of masonry walls with rigid supports apparently is not affected by the direction of spanning.

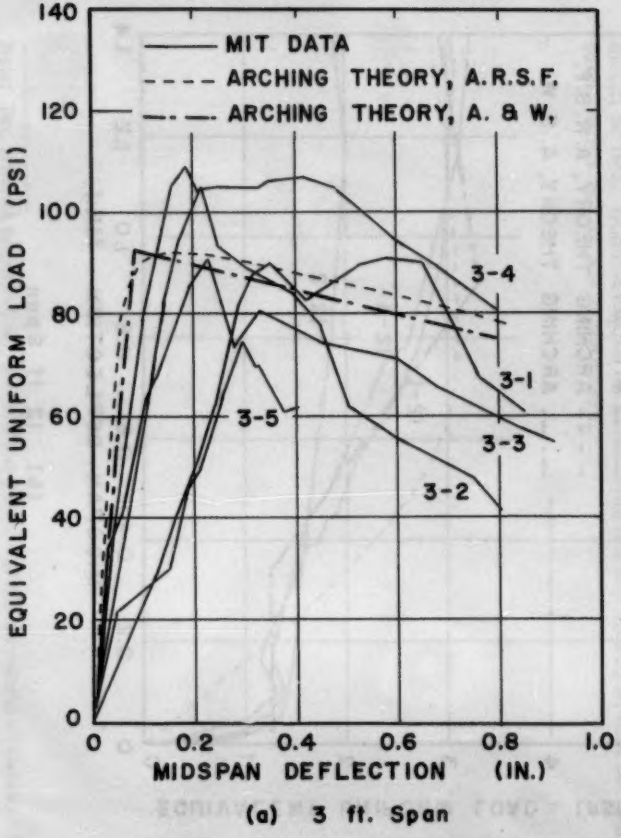

(a) 3 ft. Span

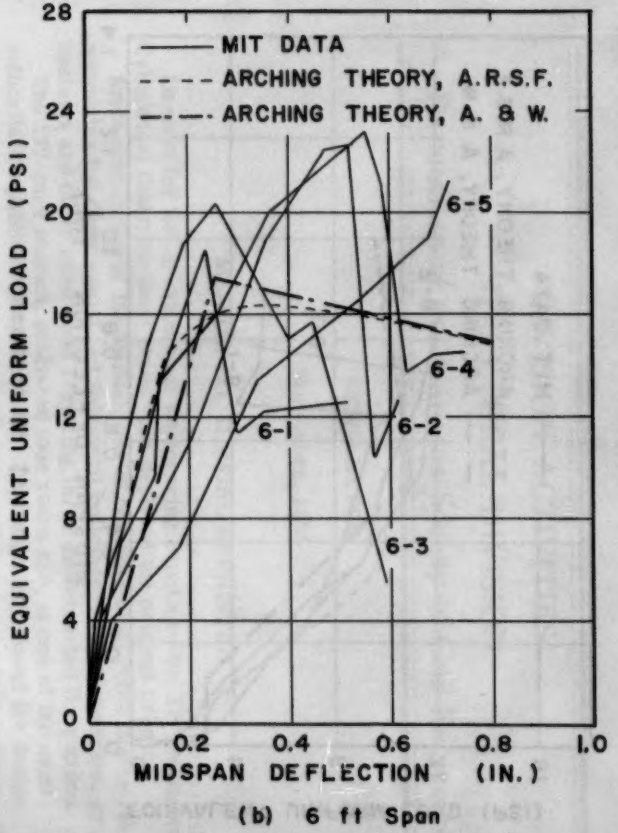

(b) 6 ft Span

Fig. 5 Load-Deflection Curves for 8-in Brick Beams, 3 and 6 ft Spans

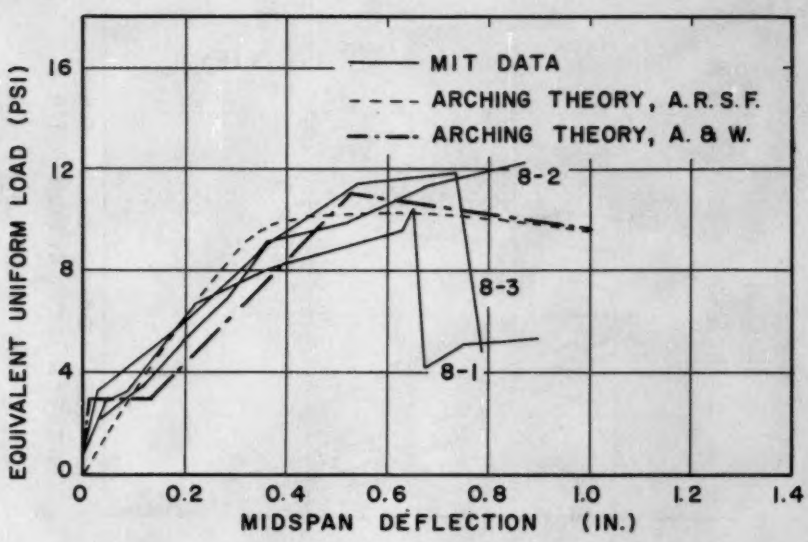

(a) 8 ft. Span

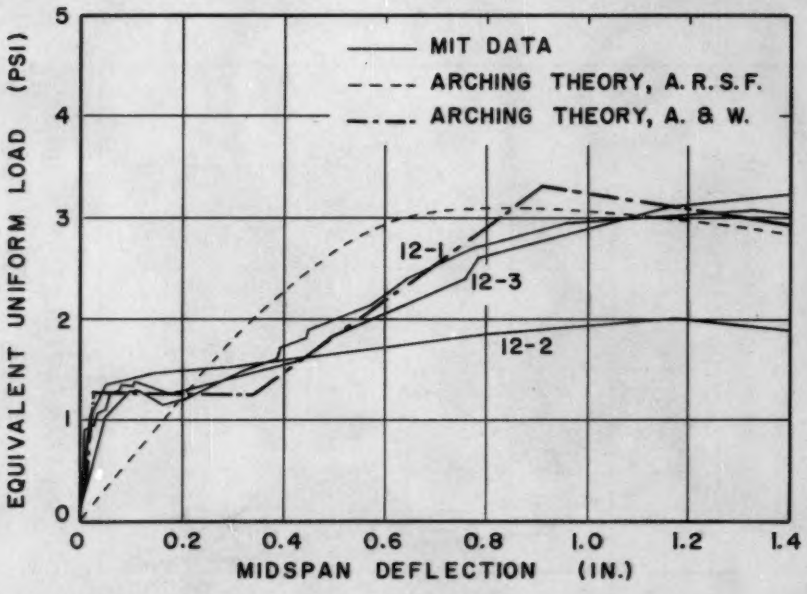

(b) 12 ft Span

Fig. 6 Load-Deflection Curves for 8-in. Brick Beams, 8 and 12 ft. Spans

DIVISION ACTIVITIES
STRUCTURAL DIVISION
Proceedings of the American Society of Civil Engineers

NEWSLETTER

September, 1956

MANUAL NO. 31 BEING REPRINTED

Demand for ASCE—Manual of Engineering Practice—No. 31 "Design of Cylindrical Concrete Shell Roofs" has depleted the original printing.

Since publication of the Manual, use of concrete shell roofs has increased noticeably for commercial and industrial buildings, aircraft hangars, gymnasiums and other structures requiring large unobstructed floor areas.

The 177-page manual, published four years ago, is one of the most authoritative publications in its field. Engineers have found the design tables invaluable in minimizing and systematizing design calculations. The Manual is being corrected and reprinted and will be available in the next month or two. Copies may be obtained from Society Headquarters for $5.00 each, with a 50% to ASCE members.

Note: No. 1956-22 is part of the copyrighted Journal of the Structural Division of the American Society of Civil Engineers, Vol. 82, ST 5, September, 1956.

PROCEEDINGS PAPERS

The technical papers published in the past year are identified by number below. Technical-division sponsorship is indicated by an abbreviation at the end of each Paper Number, the symbols referring to: Air Transport (AT), City Planning (CP), Construction (CO), Engineering Mechanics (EM), Highway (HW), Hydraulics (HY), Irrigation and Drainage (IR), Power (PO), Sanitary Engineering (SA), Soil Mechanics and Foundations (SM), Structural (ST), Surveying and Mapping (SU), and Waterways and Harbors (WW) divisions. Papers sponsored by the Board of Direction are identified by the symbols (BD). For titles and order coupons, refer to the appropriate issue of "Civil Engineering." Beginning with Volume 82 (January 1956) papers were published in Journals of the various Technical Divisions. To locate papers in the Journals, the symbols after the paper numbers are followed by a numeral designating the issue of a particular Journal in which the paper appeared. For example, Paper 861 is identified as 861 (SM1) which indicates that the paper is contained in issue 1 of the Journal of the Soil Mechanics and Foundations Division.

VOLUME 81 (1955)

SEPTEMBER: 787(PO), 788(IR), 789(HY), 790(HY), 791(HY), 792(HY), 793(HY), 794(HY)[c], 795(EM), 796(EM), 797(EM), 798(EM), 799(EM)[c], 800(WW), 801(WW), 802(WW), 803(WW), 804(WW), 805(WW), 806(HY), 807(PO)[c], 808(IR)[c].

OCTOBER: 809(ST), 810(HW)[c], 811(ST), 812(ST)[c], 813(ST)[c], 814(EM), 815(EM), 816(EM), 817(EM), 818(EM), 819(EM)[c], 820(SA), 821(SA), 822(SA)[c], 823(HW), 824(HW).

NOVEMBER: 825(ST), 826(HY), 827(ST), 828(ST), 829(ST), 830(ST), 831(ST)[c], 832(CP), 833(CP), 834(CP), 835(CP)[c], 836(HY), 837(HY), 838(HY), 839(HY), 840(HY), 841(HY)[c].

DECEMBER: 842(SM), 843(SM)[c], 844(SU), 845(SU)[c], 846(SA), 847(SA), 848(SA)[c], 849(ST)[c], 850(ST), 851(ST), 852(ST), 853(ST), 854(CO), 855(CO), 856(CO)[c], 857(SU), 858(BD), 859(BD), 860(BD).

VOLUME 82 (1956)

JANUARY: 861(SM1), 862(SM1), 863(EM1), 864(SM1), 865(SM1), 866(SM1), 867(SM1), 868(HW1) 869(ST1), 870(EM1), 871(HW1), 872(HW1), 873(HW1), 874(HW1), 875(HW1), 876(EM1)[c], 877 (HW1)[c], 878(ST1)[c].

FEBRUARY: 879(CP1), 880(HY1), 881(HY1)[c], 882(HY1), 883(HY1), 884(IR1), 885(SA1), 886(CP1), 887(SA1), 888(SA1), 889(SA1). 890(SA1), 891(SA1), 892(SA1), 893(CP1), 894(CP1), 895(PO1) 896(PO1), 897(PO1), 898(PO1), 899(PO1), 900(PO1), 901(PO1), 902(AT1)[c], 903(IR1)[c], 904 (PO1)[c], 905(SA1)[c].

MARCH: 906(WW1), 907(WW1), 908(WW1), 909(WW1), 910(WW1), 911(WW1), 912(WW1), 913 (WW1)[c], 914(ST2), 915(ST2), 916(ST2), 917(ST2), 918(ST2), 919(ST2), 920(ST2), 921(SU1), 922(SU1), 923(SU1), 924(ST2)[c].

APRIL: 925(WW2), 926(WW2), 927(WW2), 928(SA2), 929(SA2), 930(SA2), 931(SA2), 932(SA2)[c], 933(SM2), 934(SM2), 935(WW2), 936(WW2), 937(WW2), 938(WW2), 939(WW2), 940(SM2), 941 (SM2), 942(SM2)[c], 943(EM2), 944(EM2), 945(EM2), 946(EM2)[c], 947(PO2), 948(PO2), 949(PO2), 950(PO2), 951(PO2), 952(PO2)[c], 953(HY2), 954(HY2), 955(HY2)[c], 956(HY2), 957(HY2), 958 (SA2), 959(PO2), 960(PO2).

MAY: 961(IR2), 962(IR2), 963(CP2), 964(CP2), 965(WW3), 966(WW3), 967(WW3), 968(WW3), 969 (WW3), 970(ST3), 971(ST3), 972(ST3)[c], 973(ST3), 974(ST3), 975(WW3), 976(WW3), 977(IR2), 978(AT2), 979(AT2), 980(AT2), 981(IR2), 982(IR2)[c], 983(HW2), 984(HW2), 985(HW2)[c], 986(ST3), 987(AT2), 988(CP2), 989(AT2).

JUNE: 990(PO3), 991(PO3), 992(PO3), 993(PO3), 994(PO3), 995(PO3), 996(PO3), 997(PO3), 998 (SA3), 999(SA3), 1000(SA3), 1001(SA3), 1002(SA3), 1003(SA3)[c], 1004(HY3), 1005(HY3), 1006 (HY3), 1007(HY3), 1008(HY3), 1009(HY3), 1010(HY3)[c], 1011(PO3)[c], 1012(SA3), 1013(SA3), 1014(SA3), 1015(HY3), 1016(SA3), 1017(PO3), 1018(PO3).

JULY: 1019(ST4), 1020(ST4), 1021(ST4), 1022(ST4), 1023(ST4), 1024(ST4)[c], 1025(SM3), 1026 (SM3), 1027(SM3), 1028(SM3)[c], 1029(EM3), 1030(EM3), 1031(EM3), 1032(EM3), 1033(EM3)[c].

AUGUST: 1034(HY4), 1035(HY4), 1036(HY4), 1037(HY4), 1038(HY4), 1039(HY4), 1040(HY4), 1041(HY4)[c], 1042(PO4), 1043(PO4), 1044(PO4), 1045(PO4), 1046(PO4)[c], 1047(SA4), 1048 (SA4)[c], 1049(SA4), 1050(SA4), 1051(SA4), 1052(HY4), 1053(SA4).

SEPTEMBER: 1054(ST5), 1055(ST5), 1056(ST5), 1057(ST5), 1058(ST5), 1059(WW4), 1060(WW4), 1061(WW4), 1062(WW4), 1063(WW4), 1064(SU2), 1065(SU2), 1066(SU2)[c], 1067(ST5)[c], 1068 (WW4)[c], 1069(WW4).

---

c. Discussion of several papers, grouped by Divisions.

AMERICAN SOCIETY OF CIVIL ENGINEERS

OFFICERS FOR 1956

PRESIDENT

ENOCH RAY NEEDLES

VICE-PRESIDENTS

Term expires October, 1956:
FRANK L. WEAVER
LOUIS R. HOWSON

Term expires October, 1957:
FRANK A. MARSTON
GLENN W. HOLCOMB

DIRECTORS

Term expires October, 1956:
WILLIAM S. LaLONDE, JR.
OLIVER W. HARTWELL
THOMAS C. SHEDD
SAMUEL B. MORRIS
ERNEST W. CARLTON
RAYMOND F. DAWSON

Term expires October, 1957:
JEWELL M. GARRELTS
FREDERICK H. PAULSON
GEORGE S. RICHARDSON
DON M. CORBETT
GRAHAM P. WILLOUGHBY
LAWRENCE A. ELSENER

Term expires October, 1958
JOHN P. RILEY
CAREY H. BROWN
MASON C. PRICHARD
ROBERT H. SHERLOCK
R. ROBINSON ROWE
LOUIS E. RYDELL
CLARENCE L. ECKEL

PAST-PRESIDENTS

Members of the Board

DANIEL V. TERRELL
WILLIAM R. GLIDDEN

EXECUTIVE SECRETARY
WILLIAM H. WISELY

TREASURER
CHARLES E. TROUT

ASSISTANT SECRETARY
E. L. CHANDLER

ASSISTANT TREASURER
CARLTON S. PROCTOR

PROCEEDINGS OF THE SOCIETY

HAROLD T. LARSEN
Manager of Technical Publications

PAUL A. PARISI
Editor of Technical Publications

COMMITTEE ON PUBLICATIONS

SAMUEL B. MORRIS, *Chairman*

JEWELL M. GARRELTS, *Vice-Chairman*

ERNEST W. CARLTON
MASON C. PRICHARD
R. ROBINSON ROWE
LOUIS E. RYDELL